ChemInform Abstract: Computational Chemistry of Polyatomic Reaction Kinetics and Dynamics: The Quest for an Accurate CH5 Potential Energy Surface

ARTICLE *in* CHEMICAL REVIEWS · DECEMBER 2007

Impact Factor: 46.57 · DOI: 10.1021/cr078026x · Source: PubMed

3 AUTHORS, INCLUDING:

Joaquin Espinosa-Garcia
Universidad de Extremadura
141 PUBLICATIONS **2,157** CITATIONS
SEE PROFILE

Donald Truhlar
University of Minnesota Twin Cities
1,342 PUBLICATIONS **79,450** CITATIONS
SEE PROFILE

Computational Chemistry of Polyatomic Reaction Kinetics and Dynamics: The Quest for an Accurate CH_5 Potential Energy Surface

Titus V. Albu

Department of Chemistry, Box 5055, Tennessee Technological University, Cookeville, Tennessee 38505

Joaquín Espinosa-García

Departamento de Química Física, Universidad de Extremadura, 06071 Badajoz, Spain

Donald G. Truhlar*

Department of Chemistry and Supercomputer Institute, University of Minnesota, Minneapolis, Minnesota 55455-0431

Received May 9, 2007

Contents

* To whom correspondence should be addressed. E-mail address: truhlar@umn.edu.

1. Introduction

The $H + CH_4$ reaction is a prototype for gas-phase polyatomic reactions, just as the $H + H_2$ reaction[1,2] is a prototype for triatomic reactions, and it is an important reaction in combustion chemistry. The reaction between hydrogen atom and methane ($H + CH_4$) and the reverse reaction between methyl and hydrogen molecule ($CH_3 + H_2$) have been widely studied both experimentally and theoretically.

The complete construction of the potential energy surface represents a very important challenge in theoretical chemistry, and the quality and accuracy of the kinetic and dynamic description of a chemical reaction is strongly dependent on the quality of this surface. This review concerns the development of a multidimensional potential energy surface for the CH_5 system and how dynamics calculations on the various approximate surfaces that have been developed compare with experimentally determined kinetic and dynamic parameters. An older review[3] of potential energy surfaces for general polyatomic reactions included CH_5 as a special case. A recent review[4] of bimolecular reaction dynamics may also be consulted for a broader perspective than is afforded by the scope of the present review.

Throughout the review, we make an important distinction between explicit and interpolated surfaces on the one hand and direct dynamics on the other. As defined elsewhere,[5] in direct dynamics, "instead of using a pre-defined potential energy function, all required energies and forces for each geometry that is important for evaluating dynamical proper-

10.1021/cr078026x CCC: $65.00
Published on Web 10/31/2007

Titus V. Albu was born in Medgidia, Romania, in 1970. He received his License and M.S. degrees in Chemistry from the University of Bucharest in 1994 and 1995, respectively, under the guidance of Eugen Segal. He earned his Ph.D. in Chemistry from Case Western Reserve University in 2000 under the direction of Alfred B. Anderson. He worked for 2 years, as postdoctoral research associate, with Donald G. Truhlar at the University of Minnesota. In 2002, he joined the faculty in the Department of Chemistry at Tennessee Tech University, where he is allowed to pursue his research interests in theoretical and computational chemistry. He was promoted to Associate Professor in 2007. He has been married to Jisook Kim since 2000.

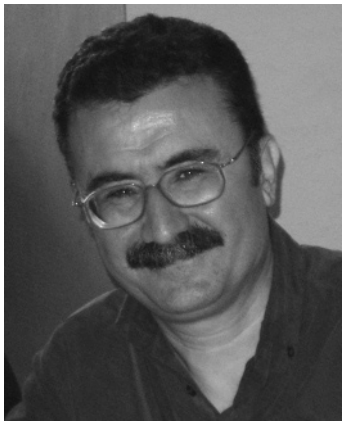

Joaquín Espinosa-García was born in Zafra (Badajoz), Spain, in 1956. He received his B.A. in Chemistry in 1978 and his Ph.D. in 1985 from the Universidad de Extremadura. He started his postdoctoral training as visiting fellow of the Laboratoire de Chimie Quantique of the Université Catholique de Louvain (Belgium) in 1988/89, working in collaboration with George Leroy and Michel Sana in the theoretical study of the reactivity of free radicals. In 1997 he worked with Donald G. Truhlar in the University of Minnesota, as visiting researcher, in the application of density functional theory to rate constants calculations of systems including heavy metals. Since then he has been regularly collaborating with Donald G. Truhlar in applications of the variational transition-state theory. Since 1990 he is Associate Professor in the Universidad de Extremadura. His research interests are computational chemistry, theoretical thermochemistry, and kinetics and dynamics studies based on the potential energy surface construction of polyatomic systems. He has been married to Esperanza Lozano since 1980. They have two twin daughters, Ana and Maria, both of whom are industrial engineers.

ties are obtained directly from electronic structure calculations." As further elaborated in the rest of the review, this corresponds to using an implicit potential energy surface rather than an explicit analytic one. Interpolated surfaces represent an intermediate level of representation that—depending on the precise implementation—might be called either direct or analytic or both. An important aspect of our review is that it includes these (modern) implicit potential energy surfaces as well as (older-style) analytic surfaces.

Donald G. Truhlar was born in Chicago in 1944. He received a B.A. in Chemistry from St. Mary's College of Minnesota in 1965 and a Ph.D. from Caltech in 1970 where his adviser was Aron Kuppermannn. He has been on the faculty of the University of Minnesota since 1969, where he is currently Regents Professor of Chemistry, Chemical Physics, Nanoparticle Science and Engineering, and Scientific Computation. His research interests are theoretical and computational chemical dynamics and molecular structure and energetics. He is the author of over 850 scientific publications, and he has received several awards for his research, including a Sloan Fellowship, Fellowship in the American Physical Society and the American Association for the Advancement of Science, an NSF Creativity Award, the ACS Award for Computers in Chemical and Pharmaceutical Research, the Minnesota Award, the National Academy of Sciences Award for Scientific Reviewing, the ACS Peter Debye Award for Physical Chemistry, the Lise Meitner Lectureship Award, the Schrödinger Medal of The World Association of Theoretical and Computational Chemists, and membership in the International Academy of Quantum Molecular Science. He has been married to Jane Truhlar since 1965, and he has two children, Sara Elizabeth Truhlar and Stephanie Marie Eaton Truhlar.

The review is structured as follow. Section 2 gives a general description of the CH_5 surface and describes the possible reaction mechanisms. Section 3 is devoted to presenting the available experimental data for this reactive system. The kinetics and dynamics data allow the testing of the quality of various potential energy surfaces. Section 4 presents methods of *constructing* potential energy surfaces, with a special focus on the methods used for the CH_5 system. Section 5 is focused entirely on describing methods for *investigating* potential energy surfaces (with the purpose of extracting kinetics and dynamics data), again with a special focus on the methods used for the CH_5 system. Section 6 presents the results of various theoretical investigations on the CH_5 system, including investigations carried out on the potential energy surfaces presented in section 4 using the methods described in section 5. Section 7 is devoted to comparing the results of theoretical studies with the available experimental data, and it therefore includes only the studies relevant to determining the current status, that is, the studies carried out on the most accurate surfaces with the most accurate dynamics methods. Section 8 gives the main conclusions of the review. Section 9 is a glossary of acronyms.

2. General Description of the CH_5 Potential Energy Surface

The existence of a potential energy surface (PES) is a result of the Born−Oppenheimer approximation,[6] i.e., the separation of electronic and nuclear motions. The PES is the electronic energy of the ground state as a function of geometry, where electronic energy is defined to include nuclear repulsion as well as electronic kinetic and Coulomb energy.[7]

The electronic energy of each of the electronically adiabatic states is a function of the positions of the nuclei and can be considered as a hypersurface in the coordinate-energy space. Each hypersurface or PES is then the effective potential energy for the nuclear motion when the system is in that electronic state. The PESs for the various electronic states are independent of isotopic substitutions. Most thermally activated chemical reactions involve only one potential energy surface, namely, the lowest-energy one. The chemical transformations discussed in this paper are assumed to follow the electronically adiabatic approximation and to occur in the lowest-energy electronic state. The electronic spin multiplicity of the ground-state PES for CH_5 is 2.

For the purpose of discussing the characteristics of the PES, we need to label the five hydrogen atoms, and we will denote them as H_a, H_b, H_c, H_d, and H_e. Once the hydrogen atoms are labeled, one can see that, because of the tetrahedral geometry of the carbon atom in CH_4, there are two distinctive pseudoconfigurations of a methane molecule in which the carbon atom is bonded to the identically labeled hydrogen atoms. These two pseudoconfigurations are mirror images of each other, similar to the enantiomers of an optically active organic compound with a chiral carbon center. In order to distinguish between these two pseudoconfigurations, we will use a rule similar to the widely used R-S system proposed by Cahn et al.[8,9] To do so, we consider that the priorities of the labeled hydrogen atoms decrease in the order $H_a > H_b > H_c > H_d > H_e$, and we labeled the pseudo-isomers as *r* and *s*. For example, in the case of $CH_bH_cH_dH_e$, the two pseudoconfigurations are shown below:

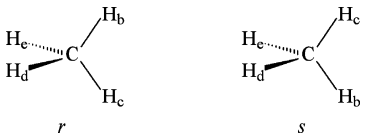

With distinguishable atoms, the PES has 10 energetically equivalent $H + CH_4$ asymptotes and 10 energetically equivalent $CH_3 + H_2$ asymptotes. On the basis of the label of the hydrogen atom and the rule of labeling the methane molecule as *r* or *s*, the 10 $H + CH_4$ asymptotes can be labeled as *ar*, *as*, *br*, *bs*, *cr*, *cs*, *dr*, *ds*, *er*, and *es*. The 10 $CH_3 + H_2$ asymptotes can be labeled, based on the two labels of the hydrogen atoms in the H_2 molecule, as *ab*, *ac*, *ad*, *ae*, *bc*, *bd*, *be*, *cd*, *ce*, and *de*.

The chemical reaction between methane and hydrogen atom has two main reactive branches, which can be generically denoted as follows:

(i) Abstraction reaction

$$H' + CH_4 \rightarrow H'H + CH_3 \quad (1)$$

(ii) Exchange (or substitution) reaction

$$H' + CH_4 \rightarrow H + CH_3H' \quad (2)$$

One can see that the abstraction reaction connects a $H + CH_4$ asymptote with a $CH_3 + H_2$ asymptote, while the exchange reaction connects two different $H + CH_4$ asymptotes.

Although the discussion above concerns the case where all hydrogens are protium, experimental information about the exchange reaction has been provided only for the case where one or more of the protiums is isotopically substituted, which can make the exchange observable, as in $T + CH_4 \rightarrow CH_3T + H$. Wolfgang[10] discussed the experimental results concerning the mechanisms and stereochemistry of reactions 1 and 2 for the case when the reagent hydrogen atom is translationally hot. Both abstraction and exchange reactions can occur through two mechanisms that are represented in Figure 1. In the rebound abstraction mechanism,[11] also called

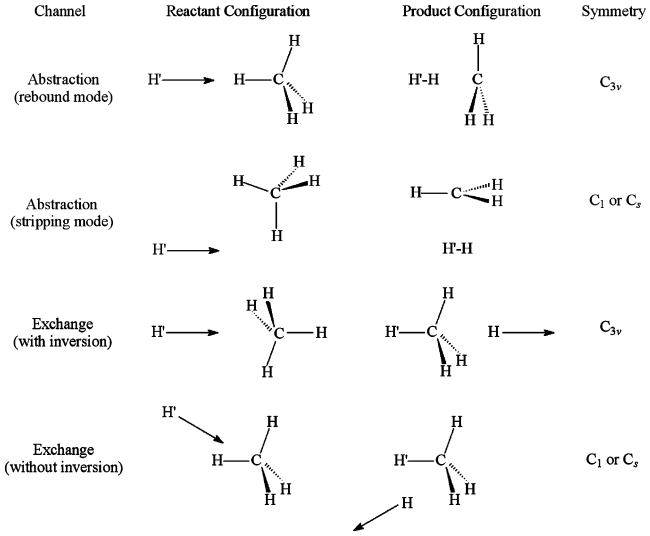

Figure 1. Stereochemistry of abstraction and exchange transformations.

the axial mechanism, the incoming hydrogen atom (H′) approaches along a C−H bond of methane, and H−H′ departs in the opposite direction along this axis, maintaining C_{3v} symmetry along the minimum energy path (MEP) for this mechanism. The stripping mechanism of the abstraction process involves the approach of the H′ atom to the methane molecule in C_1 symmetry (i.e., with no symmetry) or C_s symmetry (i.e., with a plane of symmetry). Stripping is expected to be less favorable at low energies or under thermal conditions, but we note that the border between the rebound and stripping mechanisms for abstraction is not well-defined; the distinction depends mainly on impact parameter, and the observable consequences are mainly confined to molecular beam experiments where the scattering angles of the product are measured. However, for exchange, there are two mechanisms that are more readily distinguishable. In the exchange reaction with inversion (also known as Walden inversion by analogy to the widely studied[12,13] Walden inversion mode of S_N2 reactions), the incoming H′ atom attacks the carbon atom from behind one of the C−H bonds with the MEP having the reactants H collinear to a C−H bond. The direction of attack is opposite to that for rebound abstraction, but similar to that, the C_{3v} symmetry is conserved along the MEP for this process. The saddle point will have trigonal bipyramidal geometry and D_{3h} symmetry. The inversion exchange mechanism was shown to take place for reaction $H + CD_4 \rightarrow CD_3H + D$,[14] but this result is in contradiction with the experimental evidence for related hydrogen exchange reactions with substituted alkanes that shows almost complete retention of configuration.[15] The retention of configuration would suggest an alternative mechanism, the noninversion exchange, in which the H′ atom approaches one of the C−H bonds from one side, with the system having C_1 symmetry. Another possible exchange mechanism that leads to racemization, not shown in Figure 1, was theoretically investigated by Weston and Ehrenson[16] and by Morokuma and Davis;[17] this mechanism involves an intermediate

of C_{4v} symmetry and was found to be energetically less favorable than the inversion mechanism.

Another transformation occurring on the CH_5 surface, along each of the $H + CH_4$ asymptotes, is the one in which the stereochemistry of methane is modified without any or with a minimal effect from the hydrogen atom, for example, the transformation *ar* → *as*. This transformation occurs through the intermediacy of a tetravalent planar carbon. Other than being mentioned here as a possible transformation, this process will not be further discussed in this paper. (The reader is referred to a recent article[18] for further discussion of the planar tetravalent carbon.)

On the CH_5 potential energy surface, an abstraction reaction, in either rebound or stripping mode, starting from one $H + CH_4$ asymptote, for example, the one labeled *ar*, leads to four $CH_3 + H_2$ asymptotes, the ones labeled *ab*, *ac*, *ad*, and *ae*. An exchange reaction, starting also from the $H + CH_4$ asymptote labeled *ar*, leads, in the inversion mode, to the $H + CH_4$ asymptotes labeled *bs*, *cr*, *ds*, and *er* and, in the noninversion exchange, to the $H + CH_4$ asymptotes labeled *br*, *cs*, *dr*, and *es*. Each of these transformations occurs either through a unique C_{3v} reaction path, as in the case of the rebound abstraction or inversion exchange, or through multiple equivalent paths (three C_s paths or six C_1 paths in the cases discussed here), as is the case of stripping abstraction and the noninversion exchange. Along each of the paths described above there is a saddle point, although the saddle point is the same for stripping abstraction and rebound abstraction.

It can be seen that each $H + CH_4$ asymptote can transform to eight of the other nine $H + CH_4$ asymptotes through an exchange reaction, to the ninth such asymptote through an internal isomerization of methane, and to four $CH_3 + H_2$ asymptotes through an abstraction reaction.

Similarly, the reverse of an abstraction reaction starting from one $CH_3 + H_2$ asymptote, for example, the one labeled *ab*, leads to four $H + CH_4$ asymptotes, the ones labeled *ar*, *as*, *br*, and *bs*. Each one of these transformations follows the same path or paths as the forward process, and each path has a saddle point.

In this paper, we will focus on the transformations occurring in the lower range of energies, i.e., the abstraction reaction (and its reverse hydrogen transfer reaction) and the inversion exchange reaction. On the CH_5 potential energy surface, there are 20 equivalent MEPs for the abstraction reaction and 20 equivalent MEPs for the inversion exchange reaction. We will explicitly discuss the characteristics of the saddle points for only one of these paths for each transformation, namely, *ar* → *ab* and *as* → *br*, respectively.

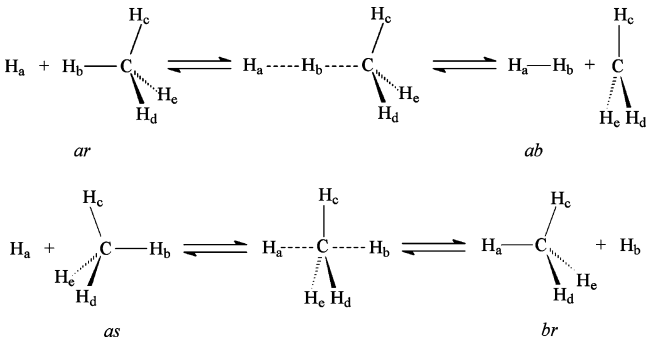

Other important features on the CH_5 potential energy surface that should be considered are the possible minima due to van der Waals interaction between methane and hydrogen atom or between methyl radical and hydrogen molecule. These minima will be located along all reaction paths for abstraction or exchange reactions. Experimentally their presence has not been detected, although they are surely present, and theoretical studies present controversies, as will be analyzed in section 6.2.

3. Experimental Data

The determination of the reaction dynamics, at least approximately, from an assumed PES is much more straightforward than the inverse problem of reconstructing the PES from experimental chemical rate data. The main foci of interest in the experimental studies are the kinetic determinations of accurate rate constants, activation energies, and kinetic isotope effects, the curvature in the Arrhenius representation for the forward and reverse reactions, the discrepancy in the value of the equilibrium constant depending on whether it was calculated from kinetic or thermochemical data, and a variety of issues in state-selected reaction dynamics. While the experimental activation energy provides information about the barrier height, the kinetic isotope effects are very sensitive to other features of the potential energy surface such as barrier width, zero-point energy of reactants and the transition state, and tunneling contributions. Furthermore, low-temperature curvature in Arrhenius plots is especially sensitive to tunneling.

3.1. Rate Constant for the $H + CH_4 \rightarrow H_2 + CH_3$ Reaction

Most of the relevant experimental data consist of rate constants, which have been determined for both perprotio and isotopically substituted cases over several temperature ranges with various experimental techniques: catalytic H atom recombination,[19] photochemical,[20] flame,[21−24] flow discharge,[25,26] flow technique using electron spin resonance (ESR) measurements of the atom concentration,[27−29] shock tube-resonance fluorescence,[30] flow photolysis-shock tube,[31] discharge flow-resonance fluorescence,[32] or laser photolysis-shock tube.[33] This extensive experimental literature on the thermal rate constants has been reviewed and evaluated by several authors.[26,33−40] Experimental results and compilations[33,35−40] are listed in Table 1.

Arrhenius fits of the experimental rate constants give activation energies between 4.5 and 15.1 kcal/mol. The Arrhenius activation energy and preexponential factor obtained by Berlie and LeRoy,[19] 4.5 kcal/mol and 1.7×10^{-14} cm^3 $molecule^{-1}$ s^{-1}, respectively, are the lowest experimental values. The authors admitted uncertainties and experimental difficulties, especially at low temperature, and therefore, these values can be discarded. The experimental values at moderate temperatures (500−900 K)[26−28] show a good agreement, with activation energies in the range 11.6−12.9 kcal/mol. The high-temperature values[21,24,30,31] show good agreement of the preexponential factor but very different activation energies. According to the compilations of Walker[34] and Sepehrad et al.,[26] the direct experimental measurements show linear Arrhenius plots, at least within experimental error limits. However, other compilations show small curvature in the Arrhenius representations and propose three-term expressions of the usual form, namely,

$$k = AT^m \exp(-B/T) \qquad (3)$$

Table 1. Experimental Rate Constants (cm^3 $molecule^{-1}$ s^{-1}) for the $H + CH_4 \rightarrow H_2 + CH_3$ Reaction Fitted to $k = AT^m \exp(-B/T)$ Expression[a]

T (K)	A	m	B	k_{300}	k_{600}	k_{1500}	experimental technique	year	ref
372−463	1.7(−14)[b]	0	2265	8.9(−18)	3.9(−16)	3.8(−15)	catalytic	1954	19
1159−1900	3.3(−10)	0	5915	9.0(−19)	1.7(−14)	6.4(−12)	flame	1961	21
426−747	1.15(−10)	0	6069	1.9(−19)	4.7(−15)	2.0(−12)	flow	1969	27
500−732	1.0(−10)	0	5967	2.3(−19)	4.8(−15)	1.9(−12)	flow	1970	28
1700−2300	1.2(−9)	0	7580	1.3(−20)	3.9(−15)	7.7(−12)	shock tube	1975	30
1300−1700	2.49(−19)	3.0	8300	6.5(−24)	5.3(−17)	3.3(−12)	flame	1976	24
640−818	3.02(−10)	0	6627	7.7(−20)	4.8(−15)	3.6(−12)	flow	1979	26
897−1729	1.78(−10)	0	6440	8.5(−20)	3.9(−15)	2.4(−12)	flash photolysis	1991	31
897−1729	1.6(−19)	2.57	3340	5.4(−18)	8.4(−15)	2.5(−12)	flash photolysis	1991	31
748−1054	2.55(−10)	0	6874	2.9(−20)	2.7(−15)	2.6(−12)	flow	2001	32
913−1697	2.935(−10)	0	6934	2.7(−20)	2.8(−15)	2.9(−12)	shock tube	2001	33
370−1800	2.09(−10)	0	5990	4.5(−19)	9.6(−15)	3.9(−12)	review	1968	34
300−1800	3.73(−20)	3	4405	4.2(−19)	5.2(−15)	6.7(−12)	review	1973	35
370−1800	2.35(−17)	2	4449	7.7(−19)	5.1(−15)	2.7(−12)	review	1978	36
400−1800	1.26(−10)	0	6002	2.6(−19)	5.7(−15)	2.3(−12)	review	1979	26
300−2500	3.73(−20)	3	4405	4.2(−19)	5.2(−15)	6.7(−12)	review	1984	37
300−2000	3.73(−20)	3	4405	4.2(−19)	5.2(−15)	6.7(−12)	review	1986	38
300−2000	2.18(−20)	3	4045	8.2(−19)	5.6(−15)	5.0(−12)	review	1992	39
1000−2500	1.09(−15)	1.6	5455	1.3(−19)	3.4(−15)	3.5(−12)	review	1994	40
298−3000	7.45(−19)	2.59	5057	9.3(−20)	2.6(−15)	4.3(−12)	review	2001	32
348−1950	6.78(−21)	3.156	4406	1.9(−19)	2.6(−15)	3.8(−12)	review	2001	33

[a] T in K. [b] $1.7(-14) \equiv 1.7 \times 10^{-14}$.

Table 2. Experimental Rate Constants (cm^3 $molecule^{-1}$ s^{-1}) for the $CH_3 + H_2 \rightarrow CH_4 + H$ Reaction Fitted to $k = AT^m \exp(-B/T)$ Expression[a]

T (K)	A	m	B	k_{300}	k_{600}	k_{1500}	experimental technique	year	ref
372−580	5.2(−13)[b]	0	5124	2.0(−20)	1.0(−16)	1.7(−14)	photolysis	1956	52
372−1370	1.32(−18)	2	4810	1.3(−20)	1.6(−16)	1.2(−13)	pyrolysis	1974	41
584−671	8.3(−13)	0	5290	1.8(−20)	1.2(−16)	2.4(−14)	pyrolysis	1981	42
1066−2166	3.31(−11)	0	7200	1.2(−21)	2.0(−16)	2.7(−13)	shock-tube	1986	43
897−1729	5.2(−12)	0	5940	1.3(−20)	2.6(−16)	9.9(−14)	flash photolysis and K	1991	31
897−1729	2.3(−23)	3.22	2050	2.3(−18)	6.7(−16)	9.9(−14)	flash photolysis and K	1991	31
1250−1950	2.1(−13)	0	7780	1.1(−24)	4.9(−19)	1.2(−15)	shock tube	1995	44
646−1104	1.45(−11)	0	6810	2.0(−21)	1.7(−16)	1.5(−13)	photolysis	1996	54
1269−1806	1.90(−10)	0	10814	4.2(−26)	2.8(−18)	1.4(−13)	shock tube	2001	33
1200−2000	2.57(−11)	0	7801	1.3(−22)	5.8(−17)	1.4(−13)	review	1973	35
370−700	1.4(−12)	0	5490	1.6(−20)	1.5(−16)	3.6(−14)	review	1976	56
300−2500	1.1(−21)	3.0	3900	6.7(−20)	3.6(−16)	2.8(−13)	review	1984	37
300−2500	4.8(−22)	3.12	4384	1.2(−20)	1.5(−16)	2.1(−13)	review	1986	38
300−2500	1.14(−20)	2.74	4740	9.6(−21)	1.7(−16)	2.4(−13)	review	1992	39
298−3000	1.06(−20)	2.70	4451	1.9(−20)	2.0(−16)	2.1(−13)	review	2001	32

[a] T in K. [b] $5.2(-13) \equiv 5.2 \times 10^{-13}$.

Sometimes Arrhenius curvature is an indication of a reaction exhibiting significant tunneling contributions, but any reaction shows a curved Arrhenius plot if studied with enough precision over a wide enough temperature range. The most recent recommended expression for the thermal rate constant over a wide temperature range (348−1950 K) is[33]

$$k(T) = 6.78 \times 10^{-21} T^{3.156} \exp(-4406/T)\ \mathrm{cm^3\ molecule^{-1}\ s^{-1}} \quad (4)$$

which gives rate constants that are lower than the ones obtained using the expression of Baulch et al.[39] recommended for the 300−2000 K temperature range:

$$k(T) = 2.18 \times 10^{-20} T^{3} \exp(-4045/T)\ \mathrm{cm^3\ molecule^{-1}\ s^{-1}} \quad (5)$$

3.2. Rate Constant for the $CH_3 + H_2 \rightarrow CH_4 + H$ Reaction

The reverse reaction $CH_3 + H_2 \rightarrow CH_4 + H$ has also been widely investigated over several temperature ranges and with several experimental techniques: pyrolysis−H_2 flow,[41,42] shock-tube,[33,43,44] or pyrolysis,[45−54] and this extensive experimental work on the thermal rate constant has been reviewed and compiled by several authors.[35,37−39,55,56] Key data are listed in Table 2.

The rate constants at lower temperatures (350−700 K) agree well with each other,[42,52] and a similar situation is found at higher temperatures (1000−2000 K).[43,44] The work of Knyazev et al.[54] covers the intermediate temperature range (600−1000 K). Each of these three temperature ranges allows for a linear Arrhenius representation, but when the rate constants are plotted over the entire temperature range (350−2000 K), the Arrhenius representation is curved, according to the latest compilations.[37−39] The rate constant expressions

$$k(T) = 3.31 \times 10^{-11} \exp(-7200/T)\ \mathrm{cm^3\ molecule^{-1}\ s^{-1}} \quad (6)$$

and

$$k(T) = 2.3 \times 10^{-23} T^{3.22} \exp(-2050/T)\ \mathrm{cm^3\ molecule^{-1}\ s^{-1}} \quad (7)$$

reported by Möller et al.[43] and Rabinowitz et al.,[31] respectively, were obtained from the spectroscopic observation of CH_3 at 216.5 nm and by converting the results for the $H + CH_4 \rightarrow H_2 + CH_3$ reaction using the equilibrium constant calculated from the JANAF thermochemical tables, respectively.

The most recent recommended expression for the thermal rate constant of the $CH_3 + H_2 \rightarrow CH_4 + H$ reaction, in the 200−2000 K temperature range, is[39]

$$k(T) = 1.14 \times 10^{-20} T^{2.74} \exp(-4740/T)\ \mathrm{cm^3\ molecule^{-1}\ s^{-1}} \quad (8)$$

3.3. Equilibrium Constant

When the usual phenomenological rate constant expressions are assumed to hold, the ratio of the forward to reverse rate constant is equal to the equilibrium constant.[57,58] However, this relation is not satisfied precisely when the rate constants are obtained from experimental data, because of errors in the kinetics measurements. In a number of early studies,[26,38,39,42,56,59] it was pointed out that there is a discrepancy in the value of the equilibrium constant depending on whether it was calculated from kinetic data (as the ratio of forward and reverse rate constants) or from thermodynamic data (using the change in enthalpy and entropy determined from thermodynamics tables). In 1990, Furue and Pacey[59] assembled experimental data on the temperature dependence of the forward (52 data points in the 372−2300 K temperature range) and reverse (38 data points in the 372−2166 K temperature range) reactions and concluded that the reaction at 0 K should be 1.3 ± 0.4 kcal/mol exothermic because the enthalpies of activation for the forward and reverse reactions extrapolated to 0 K are 13.3 ± 0.4 and 14.6 ± 0.4 kcal/mol, respectively. This result from experimental kinetic data differs from the value obtained from thermochemical data, which yields a practically thermoneutral reaction with an enthalpy of reaction of −0.02 kcal/mol at 0 K. (Note that, for a bimolecular reactions with two products, the enthalpy of reaction at 0 K is the same as the change in potential energy plus the change in the zero-point energy (ZPE); this sum is sometimes called the zero-point-inclusive energy of reaction.) Later, Pacey and co-workers[29] resolved this controversy in the equilibrium constant by determining forward rate constants by ESR-discharge flow method in the 348−421 K temperature range and obtaining rate constants much smaller than previously reported. Discarding the old data for the forward reaction and including only these new results[29] and the ones from the shock-tube study of Rabinowitz et al.,[31] the authors found a forward enthalpy of activation at 0 K of 14.9 ± 0.4 kcal/mol (compared to the old value of 13.3 ± 0.4 kcal/mol) and an enthalpy of reaction at 0 K of −0.3 ± 0.4 kcal/mol, in much better agreement with the thermodynamic value. With this information, the reverse enthalpy of activation is 15.2 ± 0.4 kcal/mol (compared to the old value of 14.6 ± 0.4 kcal/mol). The authors also concluded that the measurements of the forward rate constant should be made extra cautiously with special attention to stoichiometric factors and possible impurity effects.

The most recent expression for the equilibrium constant of the $H + CH_4 \rightleftharpoons H_2 + CH_3$ reaction is that proposed by Sutherland et al.:[33]

$$K = -18.356 + (6.5749 \times 10^{-2})T - (3.5127 \times 10^{-5})T^2 + (6.4082 \times 10^{-9})T^3 \quad (9)$$

3.4. Kinetic Isotope Effects

While the experimentally determined absolute rate constants are the best data for estimating the barrier heights on the PES, kinetic isotope effects are very sensitive to other features of the PES such as the width of the barrier, the zero-point energy of the reactants and the transition state, and the tunneling contributions. A kinetic isotope effect is the ratio of the rate constant with one isotopic substitution pattern (or with no substitution) to that with another. By convention, one always puts the lighter isotopic case in the numerator. Then a kinetic isotope effect larger than unity is called normal, and a kinetic isotope effect smaller than unity is called inverse.

As noted by Schatz et al.,[60] in the case of the $H + CH_4 \rightarrow H_2 + CH_3$ reaction, there are 16 deuterium-substituted variants:

$$H + CH_4 \xrightarrow{k_1} H_2 + CH_3 \quad (10)$$

$$H + CHD_3 \xrightarrow{k_2} H_2 + CD_3 \quad (11)$$

$$D + CH_4 \xrightarrow{k_3} DH + CH_3 \quad (12)$$

$$H + CH_3D \xrightarrow{k_4} HD + CH_3 \quad (13)$$

$$D + CHD_3 \xrightarrow{k_5} DH + CD_3 \quad (14)$$

$$H + CD_4 \xrightarrow{k_6} HD + CD_3 \quad (15)$$

$$D + CH_3D \xrightarrow{k_7} D_2 + CH_3 \quad (16)$$

$$D + CD_4 \xrightarrow{k_8} D_2 + CD_3 \quad (17)$$

$$H + CH_3D \xrightarrow{k_9} H_2 + CH_2D \quad (18)$$

$$H + CH_2D_2 \xrightarrow{k_{10}} H_2 + CHD_2 \quad (19)$$

$$H + CH_2D_2 \xrightarrow{k_{11}} HD + CH_2D \quad (20)$$

$$D + CH_3D \xrightarrow{k_{12}} DH + CH_2D \quad (21)$$

$$H + CHD_3 \xrightarrow{k_{13}} HD + CHD_2 \quad (22)$$

$$D + CH_2D_2 \xrightarrow{k_{14}} DH + CHD_2 \quad (23)$$

$$D + CH_2D_2 \xrightarrow{k_{15}} D_2 + CH_2D \quad (24)$$

$$D + CHD_3 \xrightarrow{k_{16}} D_2 + CHD_2 \quad (25)$$

There are also 16 possible deuterium isotopic variants for the reverse reaction, $CH_3 + H_2 \rightarrow CH_4 + H$, with the rate constants being denoted k_{-1}−k_{-16}. For the reverse reaction, of these 16 possible isotopic reactions, experimental results were determined only for k_{-1}−k_{-8},[35,41,42,47−49,52,53,61−64] while for the forward reaction, the kinetic isotope effects are even

Table 3. Kinetic Isotope Effects for Some Deuterated Reactions[a]

T (K)	$H + CH_4/D + CH_4$	$CH_3 + H_2/CH_3 + D_2$	$CD_3 + H_2/CD_3 + D_2$	$CH_3 + HD/CH_3 + DH$	$CD_3 + HD/CD_3 + DH$
400	0.74	4.8	3.3	3.2	1.8
500	0.84	3.5	2.9	2.0	1.6
600	0.91	2.8	2.6	1.4	1.5
700	0.97	2.4	2.4	1.1	1.4
780		2.1[62]			
829		2.0[41,64]			
930		1.6[41,64]			
ref	28	53	53	53	53

[a] The convention for the last two columns is that $CH_3 + XY$ denotes the reaction to produce $CH_3X + Y$, not $CH_3Y + X$.

less well-characterized, and only k_1, k_3, and k_6 have been experimentally determined.[20,28,65−67]

Using the photolysis of acetone and acetone-d_6 as a source of CH_3 and CD_3 radicals, Davison and Burton[48] studied k_{-7} in the 423−723 K temperature range, Whittle and Steacie[49] studied $k_{-2}-k_{-7}$ in the 403−693 K temperature range, and Shapiro and Weston[53] studied $k_{-2}-k_{-8}$ in the 398−718 K temperature range. Some experimental results are listed in Table 3. One can see that, for the reverse reactions, the kinetic isotope effects shown in Table 3 are all larger than 1 in the studied temperature range of 398−723 K.

Another isotopic reaction of relevance is the hot-atom reaction between methane and tritium, $T^* + CH_4$.[68−70] Chou and Rowland[68−70] formed tritium atoms with kinetic energies of 2.8 eV (~65 kcal/mol) by 185 nm photolysis of TBr and concluded that the abstraction/exchange ratio is ~4 for this high energy. Ting and Weston[71] formed hot methyl radicals by 135 nm photolysis of CH_3Br and CD_3Br and investigated the hot methyl reaction, $CH_3^* + H_2$ (or D_2).

3.5. Low-Temperature Tunneling Effects

The reaction between CD_3 and H_2 as well as other isotopic combinations of CD_3 were investigated at 5 K in solid parahydrogen by Momose and co-workers.[72,73] At this low temperature, the reaction occurs essentially exclusively by tunneling. The tunneling rates (3.3×10^{-6} s^{-1}, 2.0×10^{-6} s^{-1}, and 1.0×10^{-6} s^{-1} for CD_3, CD_2H, and CDH_2, respectively) depend on the degree of deuteration in the methyl radicals.[73] Because the reaction between CH_3 and H_2 did not proceed in a week, an upper limit of the tunneling rate of 8×10^{-8} s^{-1} was estimated for the unsubstituted case.

3.6. State-Selected Reaction Dynamics

Experimental studies of the detailed reaction dynamics have been less frequent than kinetics experiments. The original studies involving hot T atoms from nuclear recoil experiments[74,75] and photolytic sources[68] established the existence of abstraction and exchange channels. Bersohn and co-workers[14] investigated the exchange reaction by detecting the D-atom product from the $H + CD_4 \rightarrow D + CHD_3$ reaction at an average relative translational energy of ~2.17 eV (50 kcal/mol). The absolute reaction cross section for H exchanging D was determined to be 0.084 ± 0.014 Å^2 compared to 0.040 ± 0.014 Å^2 for the $H + CH_3D$ reaction. Around 80% of the initial H atom kinetic energy is released as D atom kinetic energy, implying that the reaction is nearly vibrationally adiabatic. They found that the reaction takes place by an S_N2-type inversion mechanism and suggested that trajectories with small impact parameter lead to either exchange or abstraction depending on the orientation of the incoming H atom with respect to the C−D bond.

Valentini and co-workers[67,76,77] examined the abstraction channel by measuring the rovibrational distributions of the HD product from the $H + CD_4$ reaction using coherent anti-Stokes Raman spectroscopy. It was found that, at a collision energy of 1.5−1.6 eV (35−37 kcal/mol), the rotational energy of HD in the first vibrationally excited state is significantly greater than the rotational energy of the ground vibrational state. There is an unusual positive correlation between the product rotational and vibrational excitations. Only very little of the 1.5 eV (35 kcal/mol) available energy appears as internal excitation of the HD product molecule: 7% in vibration and 9% in rotation. The total reaction cross section was found to be very small, in particular, 0.14 ± 0.03 Å,^{2} so the maximum impact parameter is <1 Å.[67]

The most recent experimental work is that of Zare and co-workers,[78−81] and it focuses on understanding the reaction dynamics. An initial study looked at the nascent CD_3 products from the $H + CD_4$ reaction.[78] At a collision energy of 1.95 eV (45 kcal/mol), the CD_3 products are produced mainly in their ground vibrational state with some CD_3 produced in their first vibrationally excited state in the low-frequency umbrella-bending mode. It was found that the CD_3 products are backward scattered with respect to the incident H-atom direction; this eliminates the rebound mechanism that was found to occur in the $H + D_2 \rightarrow HD + D$ reaction.[82,83] The authors proposed two possible explanations for the angular distribution of the CD_3 products: (1) a stripping mechanism is favored over a rebound mechanism at the energy studied, and (2) a competition between abstraction and exchange diminishes the probability for abstraction at small impact parameters. The later possible explanation was rejected when experiments carried out at a lower collision energy, 27.8 kcal/mol, where the exchange channel is not open, led to similar results.[79] Further investigation of the reaction in a collision energy range of 0.5−3.0 eV (12−69 kcal/mol) showed that the stripping mechanism applies even at energies slightly above the threshold.[80,81]

Another aspect of the reaction dynamics that has been under recent investigation is the effect of the chemical reactivity of vibrationally excited reactant molecules. The effects of C−H stretching excitation on the $H + CH_4 \rightarrow H_2 + CH_3$ abstraction reaction have been investigated using a photo law-of-cosines (photo-LOC) technique.[84] The reaction of fast H atoms with methane excited in either the antisymmetric stretching fundamental or first overtone with collision energies between 1.52 and 2.20 eV (35 and 51 kcal/mol) was investigated by measuring the vibrational and angular distribution of the CH_3 product.[84] It was found that methane excited in the antisymmetric stretching fundamental increases the overall reaction cross section by a factor of 3.0 ± 1.5 over the whole collision energy range. Considering that the reaction cross section of the $H + CD_4$ abstraction reaction

actually decreases by a factor of 2 over the collision energy range of 1.48−2.36 eV (34−54 kcal/mol), it is clear that vibrational excitation is much more effective than an equivalent amount of translational energy in promoting the reaction at the energies considered. The vibration excitation rather than translational energy also controls the product-state distribution. The product distribution of the reaction between H and vibrationally excited CHD_3 at a collision energy of 1.53 eV (35 kcal/mol) has shown that the reaction mechanism is close to the pure spectator model.[85] This result is slightly different than the one for the similar reaction between Cl and vibrationally excited CHD_3 at a collision energy of 0.18 eV (4 kcal/mol), for which a greater extent of intramolecular vibrational redistribution was suggested.[85]

In sum, the state-to-state dynamics studies are difficult to perform at low energies for this reaction, because the H atoms, which are produced in a photolysis process, are hot. Moreover, even in the case of high energies (1−2 eV), the reaction cross section is small.[67] As a result, there have only been a few recent experimental dynamics studies on this system.[67,78−81] For example, there is considerably more experimental work for the Cl + CH_4 reaction than for the H + CH_4 reaction.

4. Methods for Constructing Potential Energy Surfaces

Some methods for calculating dynamical properties of a reaction require full-dimensional potential energy surfaces, while other methods require information in only a limited region of the surface. In general, one can obtain this information either from an analytic potential energy surface or from electronic structure calculations carried out on the fly; the latter approach is called direct dynamics.[86−89] Intermediate between fitting potential energy surfaces and direct dynamics methods are methods based on interpolating potential energy surfaces. Since these do not involve a fit, they are a form of direct dynamics, but as the interpolation becomes more global, they can resemble a fit. Sometimes direct dynamics methods that involve no fitting at all are called straight direct dynamics. This section presents several general methods used to construct potential energy surfaces, with the focus being on methods that have been applied to the CH_5 potential energy surface.

The potential energy surfaces for reactive systems will be divided into three large categories: analytic, implicit (defined by a level of electronic structure theory), and interpolated. These three types of potential energy surfaces are reviewed below. This section only considers methods; results are presented in sections 6 and 7.

4.1. Analytic Surfaces, Mainly VB/MM

Valence bond (VB) potential energy surfaces include any approach that involves the London equation,[90] which is a two-configuration VB treatment of a three-atom system with one active *s* orbital on each center.[91] The London equation and its various extensions are, however, used much more broadly than just for such three-atom systems because they lead to a convenient three-dimensional analytic form for a PES with a simple reaction barrier.[92] In order to treat a system with more than three or four atoms, the London equation can be combined with analytic functions for the potential energy of nonreactive degrees of freedom; the latter are usually called molecular mechanics (MM). For example, Raff's work[93] can be considered one of the first examples of combining VB with MM; he used VB (i.e., a London−Eyring−Polanyi−Sato surface, which is defined later) for three-body reactive parts, and he added force-field terms (i.e., MM) for the rest. Most of the analytic surfaces for atom + methane are modifications of Raff's original combined VB and MM method (such combinations will be denoted VB/MM). If there are additional elements, we may designate the method as VB/MM + corrections. But the corrections, if analytic, could be considered to be more MM, so we prefer to say just VB/MM. More generally, one could consider systematic ways to use different MM parameters for products than for reactants, with intermediate values in between; this strategy[94] has been applied to H + C_2H_6 but not H + CH_4.

The full potential energy surface for the CH_5 system is 12-dimensional, but the first analytic surfaces developed and employed in studying the system were 3- or 4-dimensional surfaces. Gorin et al.[95] developed the first surface for the abstraction and inversion reaction channels using a three-electron VB model with empirical parameters. This 3-dimensional PES had reasonable barrier heights for both reaction channels but also had an unphysical CH_3−H−H well of 8 kcal/mol depth. A recalibrated version of the surface of Gorin et al. was used by Polanyi[96,97] for the reaction between methyl and hydrogen. This calibrated three-body surface was designed to give, for the functional form used, the lowest barrier height compatible with a surface with no energy basins. This surface was based on a semiempirical VB treatment in which the geometry of the methyl portion was frozen.

In 1963, Johnston and Parr[98] obtained a three-body, reduced-dimensionality surface by applying the bond-energy-bond-order (BEBO) method.[99,100] Later, Arthur and co-workers also used the original BEBO method and modifications of it in a series of studies.[101−103] The BEBO method provides the PES only along the reaction path, but it was later extended[104] to provide a more complete PES for H + CH_4 and other reactions. It is now known that the BEBO method is very sensitive to the input data and should be used only for qualitative correlations, not for quantitative work.

In 1970, Polanyi and co-workers[105] developed a London−Eyring−Polanyi−Sato (LEPS) surface[90,106−108] to study the reaction of hot tritium with methane, T + CH_4, as a linear three-atom model refined from a series of three-body surfaces developed previously.[109] The CH_3 fragment was treated as a pseudoatom in this surface. Other early studies using both LEPS and BEBO surfaces include the work of Kurylo et al.,[28] who examined H + CH_4 abstraction reaction, and the study of Shapiro and Weston,[53] who investigated the CH_3 + H_2 reaction.

At this point, it is relevant to make some points about the LEPS approach. London's work[90] may be considered to be an extension of the quantum mechanical Heitler−London method of H_2 to the triatomic H_3 system. As mentioned above, his treatment involves only *s* orbitals. In 1931, Eyring and Polanyi[106] proposed a semiempirical way to calculate the Coulomb and exchange integrals appearing in London's equation. The resulting London−Eyring−Polanyi (LEP) surface is a convenient empirical functional form.[110] Later, Sato[107,108] added flexibility (one more parameter) to the functional form, creating the LEPS model. The LEPS model introduced a more reasonable way to obtain the required Coulomb and exchange integrals from diatomic data; the method was first applied to triatomic atom−diatom systems

but soon was also used as a starting point to construct the surfaces of polyatomic systems, often with more parameters. Thus, for polyatomic systems, we can speak of LEPS-type surfaces, to distinguish them from the "pure" LEPS surfaces used for triatomic systems, and in all cases, these surfaces must be considered as semiempirical because they use theoretical and/or experimental information in building the complete PES of the reacting system. The LEPS model with the extra parameter set equal to zero is identical to the diatomics-in-molecules method.[111,112] The diatomics-in-molecules method has been extended to CH_3 and CH_4 but, to the best of our knowledge, not to CH_5.

The first full-dimensional analytic surfaces were proposed by Bunker and co-workers and by Raff; however, their approaches in constructing the analytic surfaces were quite different. In 1969−1975, Bunker and co-workers[113−117] proposed a series of three many-body, purely empirical surfaces[114,116,117] that were used in trajectory calculations to describe the tritium hot-atom abstraction and exchange reactions. Their method did not involve the London equation. The initial surface was created by Bunker and Pattengill[114] and was used to describe both the abstraction and substitution reactions. This surface[114] was written as a sum of a reactive potential, which included the interaction of the carbon, the incoming tritium, and only one hydrogen reactive, and a nonreactive potential, which included the rest of the nonreactive hydrogens in methane. The two hydrogens that form H_2 were not treated as identical to the methyl hydrogens, and thus, the symmetry of the methane molecule was not treated properly. By using Monte Carlo classical trajectory calculations, it was shown that considering only one H in CH_4 to be reactive is unjustified and a severe defect.[114] Valencich and Bunker[116] removed this restriction so that all hydrogen atoms were treated equivalently and designed a new surface that contains a different functional form than the initial surface. This new surface, which is similar to the surface described below, was calibrated so that the classical trajectory studies would agree with the experimental results for the hot-atom abstraction and substitution reactions. The third surface was presented by Chapman and Bunker[117] and, because it involves minor modifications of the Valencich and Bunker[116] surface as described below, will be called the Valencich−Bunker−Chapman (VBC) surface.

The VBC potential energy surface is given by a sum of terms

$$V_{\mathrm{VBC}} = \sum_{i=1}^{4}\sum_{j>i}^{5} S_i S_j F(\phi_{ij}) + D(\xi)\sum_{i=i}^{5} M_i + U_{\mathrm{A}}U_{\phi} + U_{\mathrm{H}} \tag{26}$$

where indices i and j in the double sum correspond to the five C−H bonds; S is a switching function,

$$S_i = S(r_i) = 1, \quad r_i < r_0 \tag{27}$$

$$S_i = S(r_i) = -M(r_i), \quad r_i > r_0 \tag{28}$$

where $M(r_i)$ is a Morse function and $r_0 = 1.09$ Å, which is the length of a C−H bond in methane on this surface; and $F(\phi_{ij})$ is a tabular function depending upon the angle ϕ_{ij} between the C−H_i and C−H_j bonds. The terms containing $F(\phi_{ij})$ include the dependence on the H−C−H bond angles that do not disappear in the $CH_3 + H_2$ asymptotic limit and are responsible for maintaining the correct local geometry at carbon as it changes from tetrahedral to planar. The second term in eq 26 is a product of a tabular function $D(\xi)$ and a sum of five reduced Morse functions corresponding to each of the C−H bonds. The tabular function is used to attenuate the Morse curve and to calibrate the overall thermochemistry. The variable ξ of the tabular function is the effective number of hydrogens near to the carbon and is defined as

$$\xi = \sum_{i=i}^{5} S(r_i) \tag{29}$$

The second-to-last term in eq 26 controls the abstraction channel in the product valley. It consists of a product of two functions, U_{A}, which is the potential for collinear orientations of the C−H−H moiety primarily involved in the abstraction, and U_{ϕ}, which is the bend potential for deviation from the collinear orientation. The last term, U_{H}, gives a quadratic repulsion between methyl hydrogens and the hydrogens atoms in H_2. The differences between the Valencich and Bunker[116] surface and the VBC surface are in the form of U_{A} and in the inclusion of U_{H}. In later years, reactive potential energy surfaces like this (not based on VB theory) have been relatively infrequently employed, but it is possible that some of the non-London functional forms that have been introduced[118−123] could be applied fruitfully to CH_5.

Raff's approach to construct the CH_5 surface[93] was different than the one employed by Bunker and co-workers, and it was based on an earlier study in which Raff et al.[124] showed that the two-body parameters of a semiempirical, two-configuration valence bond surface were approximately transferable from one three-body system to another. Later, Raff generalized those three-body semiempirical, two-configuration valence bond surfaces to generate a CH_5 surface.[93] This surface will be called the R surface. His potential consists of a sum of four valence bond three-body terms (giving a stretching potential) plus a bend potential,

$$\begin{aligned} V &= V_{\mathrm{stretch}} + V_{\mathrm{bend}} \\ &= V_3(R_{\mathrm{CH}_1}, R_{\mathrm{CH}_b}, R_{\mathrm{H}_1\mathrm{H}_b}) + V_3(R_{\mathrm{CH}_2}, R_{\mathrm{CH}_b}, R_{\mathrm{H}_2\mathrm{H}_b}) + \\ &\quad V_3(R_{\mathrm{CH}_3}, R_{\mathrm{CH}_b}, R_{\mathrm{H}_3\mathrm{H}_b}) + V_3(R_{\mathrm{CH}_a}, R_{\mathrm{CH}_b}, R_{\mathrm{H}_a\mathrm{H}_b}) + \\ &\quad V_{\mathrm{bend}} \end{aligned} \tag{30}$$

where H_b is the hydrogen farthest from the carbon (i.e., the incoming H atom), H_a is the hydrogen closest to H_b, and H_i ($1 \le i \le 3$) are the remaining hydrogens, which are spectators.

The function $V_3(R_{\mathrm{AB}}, R_{\mathrm{AC}}, R_{\mathrm{BC}})$ is a three-body potential obtained from a London equation, and it is a combination of triplet and singlet two-body potentials given by

$$\begin{aligned} V_3(R_{\mathrm{AB}}, R_{\mathrm{AC}}, \mathrm{R}_{\mathrm{BC}}) &= Q_{\mathrm{AB}} + Q_{\mathrm{AC}} + Q_{\mathrm{BC}} - \\ &\quad \left\{\frac{1}{2}\left[(J_{\mathrm{AB}} - J_{\mathrm{BC}})^2 + (J_{\mathrm{BC}} - J_{\mathrm{AC}})^2 + (J_{\mathrm{AC}} - J_{\mathrm{AB}})^2\right]\right\}^{1/2} \end{aligned} \tag{31}$$

with

$$Q_{\mathrm{XY}}(R_{\mathrm{XY}}) = [{}^1E_{\mathrm{XY}}(R_{\mathrm{XY}}) + {}^3E_{\mathrm{XY}}(R_{\mathrm{XY}})]/2 \tag{32}$$

$$J_{\mathrm{XY}}(R_{\mathrm{XY}}) = [{}^1E_{\mathrm{XY}}(R_{\mathrm{XY}}) - {}^3E_{\mathrm{XY}}(R_{\mathrm{XY}})]/2 \tag{33}$$

where ${}^1E_{\mathrm{XY}}$ and ${}^3E_{\mathrm{XY}}$ are the singlet and triplet potentials for each of the X−Y interactions, with X−Y corresponding

to A−B, B−C, or A−C. The singlet potential is expressed by a Morse potential of the form

$$^1E_{XY}(R_{XY}) = D_{XY}^{(1)}\{\exp[-2\alpha_{XY}(R_{XY} - R_{XY}^e)] - 2\exp[-\alpha_{XY}(R_{XY} - R_{XY}^e)]\} \quad (34)$$

and the triplet potential (in the original Raff surface) is given by

$$^3E_{XY}(R_{XY}) = D_{XY}^{(3)}\{\exp[-2\beta_{XY}(R_{XY} - R_{XY}^e)] + 2\exp[-\beta_{XY}(R_{XY} - R_{XY}^e)]\} \quad \text{for } R_{XY} < R^* \quad (35)$$

and

$$^3E_{XY}(R_{XY}) = C_{XY}[R_{XY} + A_{XY}]\exp(-\sigma_{XY}R_{XY}) \quad \text{for } R_{XY} > R^* \quad (36)$$

where R_{XY} is the distance between X and Y atoms, R_{XY}^e is the equilibrium value of the distance, and $D_{XY}^{(1)}$, $D_{XY}^{(3)}$, α_{XY}, β_{XY}, C_{XY}, σ_{XY}, and R^* are adjustable parameters.

The bend potential is a sum of six harmonic terms that can be written explicitly as

$$V_{bend} = \frac{1}{2}\sum_{j=1}^{3} k_j(\theta_j - \theta_j^0)^2 + \frac{1}{2}\sum_{j=1}^{3} k_j(\alpha_j - \alpha_j^0)^2 \quad (37)$$

where the first sum is over the three H−C−H_t angles θ_j between the methyl hydrogens and H_t (where H_t is the H atom in CH_4 that is the closest to the incoming H) and the second sum is over the three H−C−H angles α_j involving two methyl hydrogens. The calibration process for the R surface was based on semiempirical molecular orbital methods (intermediate neglect of differential overlap, INDO,[125] calculations) and ab initio quantum calculations, but, unfortunately, neither the geometry of the saddle point nor its energy agreed with the best available ab initio results at the time.[17]

Steckler et al.[126] analyzed the VBC and R surfaces and found that they are not appropriate for use in reaction-path analysis or in variational transition-state theory (VTST) rate constant calculations. One requirement for the use of these dynamics methods is that the potential energy surface has continuous first and second derivatives, and neither the VBC nor the R surface fulfills this condition. Steckler et al.[126] modified these two surfaces, which will be called modified VBC or MVBC in the one case and will be called modified R or MR in the other. Most of the modifications were designed to have a minimal effect on the topology of the surfaces. For the MVBC surface, the tabulated $F(\phi_{ij})$ and $D(\xi)$ functions were replaced by some functions that fit the tabulated values in the important regions of the surface. In addition, the switching function S (eqs 27 and 28) presented discontinuous second derivatives in the original VBC surface and was modified with a patch centered just beyond the location of discontinuity. Another modified version of the VBC surface was used by Huang et al.[127] in a quasiclassical trajectory study of the abstraction reaction.

The MR surface differs from the original R surface in three respects. First, the discontinuities in the first derivative of the R surface at equilibrium methane were removed by using an average of the four shortest C−H bond lengths as a variable and by introducing a polynomial fit to the $\theta_j^0(R)$ function between R_e and $R_e + \delta$, where δ is a small distance. Second, an out-of-plane bend potential V_{op}, especially important in the $CH_3 + H_2$ asymptotic limit, was added. The functional form used for this potential is the same as the harmonic term used by Duchovic et al.[128] in their surface for the dissociation of methane,

$$V_{op} = f_\Delta(R_{C-H_t})\sum_{i=1}^{3}\Delta_i^2 \quad (38)$$

where

$$\Delta_i = \cos^{-1}\left[\frac{(\mathbf{r}_2 - \mathbf{r}_1)(\mathbf{r}_3 - \mathbf{r}_1)}{|(\mathbf{r}_2 - \mathbf{r}_1)(\mathbf{r}_3 - \mathbf{r}_1)|}\cdot\frac{\mathbf{r}_i}{|\mathbf{r}_i|}\right] - \phi_0(R_{C-H_t}) \quad (39)$$

where $\mathbf{r}_1$, $\mathbf{r}_2$, and $\mathbf{r}_3$ are the vectors between the carbon and the methyl hydrogens and ϕ_0 is the reference angle. Finally, the discontinuity in the second derivative in the C−H triplet interaction in the three-body valence bond terms, ^3E, was removed by replacing the functional by a cubic spline fit. Steckler et al.[126] also concluded that the R surface was physically more reasonable and provided a more logical starting point for designing new potential energy surfaces for this reaction than the VBC surface.

In a study accompanying the one by Steckler et al.,[126] Joseph et al.[129] presented four new analytic surfaces that were calibrated against the ab initio[60,130−132] and experimental information (thermochemical data, vibrational frequencies, reaction rate constants, Arrhenius parameters, and kinetic isotope effects) available at the time. All of these four surfaces, named as J1, J2, J2A, and J3, were constructed starting from the MR surface, with the difference between them being mainly in the way in which the new calibration is made. Besides the calibrations, a few small changes were made to the functional forms in these surfaces. The reason for these changes is that the way in which the singlet and triplet curves were defined in both R and MR surfaces (the triplet repulsion decays faster than the singlet attraction) leads to the presence of some spurious wells. The wells were removed on the J1, J2, J2A, and J3 surfaces by replacing the triplet potential in eqs 35−36 by a functional form of Sato for all R_{XY},

$$^3E_{XY}(R_{XY}) = D_{XY}^{(3)}\{\exp[-2\alpha_{XY}(R_{XY} - R_{XY}^e)] + 2\exp[-\alpha_{XY}(R_{XY} - R_{XY}^e)]\} \quad (40)$$

where α_{XY} and $D_{XY}^{(3)}$ are adjustable parameters and R_{XY}^e is the equilibrium XY singlet bond length on the R and MR surfaces. The out-of-plane bending potential added in the MR surface also includes a quartic term and is given by

$$V_{op} = f_\Delta(R_{C-H_t})\sum_{i=1}^{3}\Delta_i^2 + h_\Delta(R_{C-H_t})\sum_{i=1}^{3}\Delta_i^4 \quad (41)$$

The original bend potential for the Raff surface and the Morse range parameters α_{XY} were also slightly altered. The Morse parameter α_{XY} was allowed to relax from the methane limit to the methyl limit by using a switching function,

$$\alpha_{CH} = a_{CH} + b_{CH}\left(\frac{\tanh[c_{CH}(\bar{R} - R^0)] + 1}{2}\right) \quad (42)$$

where $\bar{R}$ is the average of the four shortest C−H bond lengths

in the system. In addition, for surfaces J2A and J3, a more complicated expression for the $D^{(3)}_{XY}$, depending on the R_{CH_t}, was considered. The J1 surface is illustrated in Figure 2.

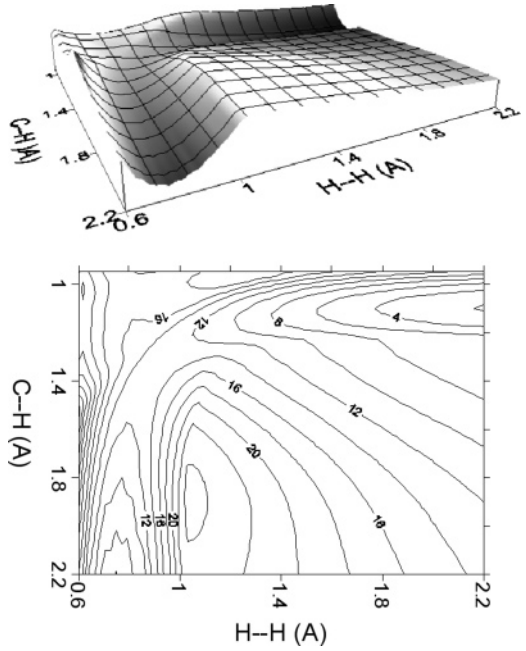

Figure 2. Three-dimensional representation (upper plot) and two-dimensional contour representation (lower plot) for the J1 surface.[129] Contours are equally spaced by 2 kcal/mol. The broken C−H and formed H−H bonds are in Å, and the rest of the internal coordinates are relaxed.

Jordan and Gilbert[133] further refined the surfaces proposed by Joseph et al.[129] and developed a symmetric potential energy surface that was suitable for use in trajectory calculations. Jordan and Gilbert took account of the fact that the hydrogen atom closest to the incoming hydrogen at any point during the reaction is not necessarily the same hydrogen atom that ultimately transfers during the reaction. To include this aspect, they constructed a potential energy surface that treats the four hydrogen atoms in methane identically. Ideally, the potential energy surface should treat all five hydrogens identically, and this is expected to be especially important in the treatment of the exchange reaction. Because the exchange reaction requires very high energies, it should not be important at thermally accessible energies, and it was not considered. The stretching and the out-of-plane bending potentials of Joseph et al. are symmetric to interchange of the four methane hydrogens and were used unchanged. The harmonic bending term was symmetrized using the original functional suggested by Raff:[93]

$$V_{\text{harm}} = \frac{1}{2}\sum_{i=1}^{3}\sum_{j=i+1}^{4} k^0 k_i k_j (\theta_{ij} - \theta^0_{ij})^2 \qquad (43)$$

The force constant k^0 must be attenuated so it will provide the correct asymptotic values, and Jordan and Gilbert considered two ways to do this. The first choice, utilized in the JG1 surface, was to use the form of Joseph et al.[129] but to make it symmetric with respect to all four methane hydrogens, while the second choice, utilized in the JG2 surface, was based on the attenuation function proposed by Duchovic et al.[128] for the dissociation of methane. It was concluded that the second surface provides a better description for the reaction, so the JG2 surface was used in their quasiclassical trajectory dynamical calculations. The JG2 surface is illustrated in Figure 3.

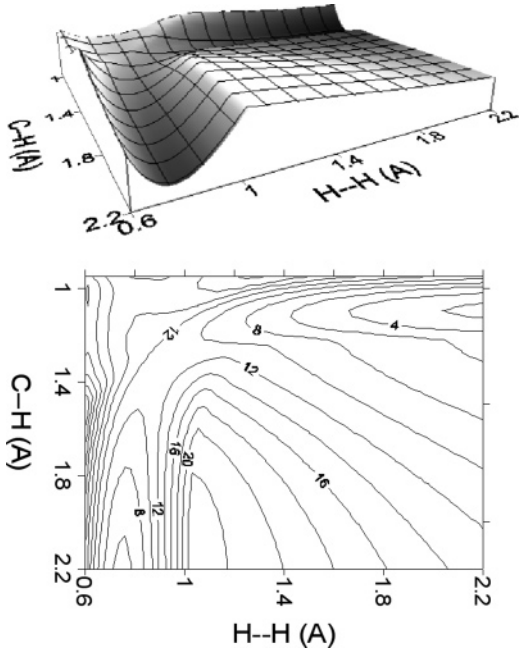

Figure 3. Same as Figure 2, but for the JG2 surface.[133]

The J2 and JG2 surfaces were calibrated based on ab initio results from the 1980s, so, in 1996, Espinosa-García and Corchado[134] recalibrated these surfaces in the light of more recent and more accurate theoretical and experimental data. The new surfaces that resulted were called MJ2 and MJG2, and they were used in dynamics calculations employing VTST. Yu[135] also reparameterized the JG2 surface; he increased the classical (i.e., zero-point-exclusive) barrier height from 10.9 to 15.0 kcal/mol, and he used the surface in time-independent quantum mechanical scattering calculations. Yu attributed the low barrier on previous surfaces to the fact that they were constructed by trajectory or VTST calculations, which he claimed provided an incomplete description of quantum effects; this criticism was repeated by Kerkeni and Clary.[136] This is true for trajectory calculations, as will be discussed in section 5.4, but not for VTST. VTST with a transmission coefficient based on optimized multidimensional tunneling includes quantum effects in all degrees of freedom and is quite accurate,[137,138] as discussed in section 7.1. Thus, VTST calculations provide a much more reliable way to calibrate barrier heights than do reduced-dimensionality calculations. Nevertheless, Yu's barrier height of 15.0 kcal/mol is quite close to our current best estimate (14.8 kcal/mol), which is discussed below.

Recently Varandas et al.[139] questioned the use of VTST for fine-tuning potential energy surfaces for reactions like the H + CH_4 reaction. They pointed out that VTST calculations[140] and multiconfiguration time-dependent Hartree quantum dynamical calculations[141,142] often give quite different results from reduced-dimensionality calculations. They argue that the reduced-dimensionality calculations involve larger regions of the potential energy surface and are, therefore, more reliable. They also state that accurate quantum dynamics is unavailable for more than four atoms.

This argument and this statement are incorrect, and they deserve a critical review. The H + CH_4 multiconfiguration time-dependent Hartree calculations,[141−143] based on the flux correlation function approach of Miller and co-workers,[144,145] represent converged quantum dynamical calculations of the thermal rate constant of a six-atom system for a given potential energy surface; they involve a limited region of the potential energy surface not because of any approximation but rather because they are efficiently formulated to take advantage of the observation[145] that thermal rate constants of simple barrier reactions are dominated by short-time dynamics in the vicinity of the dynamical bottleneck. The demonstration that VTST plus multidimensional tunneling calculations[140,146] agree with the multiconfiguration time-dependent Hartree calculations shows that they too give accurate results, as do earlier tests[147] for simpler reactions. Therefore, comparison of the results of either converged multiconfiguration time-dependent Hartree calculations[142] or VTST plus multidimensional tunneling calculations[140,146] to experiment does provide a way to tune a potential energy surface at least for the regions of the surface that are important for thermal rate constants. It should go without saying that calculations of thermal rate constants by any method do not provide a way to tune regions of the potential energy surface that do not have a significant effect on the thermal rate constant. These dynamical methods are discussed more fully in sections 5.3 and 5.5, but here we simply anticipate that one can test and tune potential energy surfaces by the following two-step process:[137,138] first, one verifies the accuracy of the very efficient VTST plus multidimensional tunneling method by comparison to accurate quantum dynamics for a given realistic (although not necessarily quantitatively accurate) surface; then, one compares VTST plus multidimensional tunneling to the experiment for a variety of surfaces or for a set of surfaces containing parameters. In this process, one should be very careful. One could use an inaccurate or unreliable functional form for the potential energy surface and adjust one parameter to get the rate constant right at one temperature. This would probably not yield an accurate surface, although it would be a step in the right direction. If instead one uses a realistic functional form (such as the implicit potential energy surface implied by a high-level electronic structure method with one or more parameters), and one checks that a particular set of reasonable parameters can yield the rate constant (and perhaps other experimental observables) for the all-protium reaction and various isotopologs as functions of temperature, one can expect that the surface under consideration is probably quite accurate, at least in the regions that have a significant effect on the rate constant. (The reader should also be wary of other aspects of the article by Varandas et al.[139] that are too far from the main subject of this review for full analysis, but which deserve a few comments. For example, one should be careful to note that the fact that trajectory calculations, which are not reliable for thermal rate constant, depend on the whole low-energy part of the surface does not mean that the thermal rate constant depends significantly on the whole surface. Furthermore, trajectory calculations may well show more recrossing than quantal dynamics because of their failure to account for local zero-point energy at the dynamical bottleneck and because they involve overbarrier reaction even when the accurate dynamics is dominated by tunneling. Varandas et al. also assert that one should doubt the statistical equilibrium aspects of the treatments of the flux autocorrelation function formalism and VTST, but these are well-justified theoretically[120,141,144,148] and there is generally no reason to doubt their usefulness.)

In 1999,[149] Espinosa-García pointed out that the JG2 surface involves an out-of-plane potential that is not completely symmetric with respect to the permutations of the four hydrogens atoms in methane, i.e., the surface depends on the permutations among the four hydrogens and, therefore, depends on the order in which the hydrogen atoms are listed in the input data. Espinosa-García[150] corrected this problem by modifying the original JG2 surface, and he recalibrated this new surface based on more recent theoretical calculations. This surface was denoted PES-2002 in recent studies[151−153] but is called EG here. The EG surface is illustrated in Figure 4. The EG surface is independent of

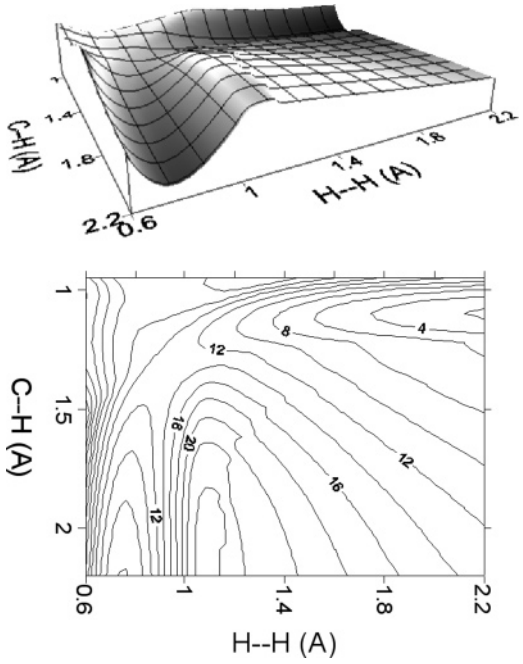

Figure 4. Same as Figure 2, but for the EG surface.[150]

permutations of the four hydrogen atoms of methane. In a first phase, one of us had applied the same methodology as the starting point in developing other surfaces for similar symmetrically substituted hydrogen abstraction reactions of the type A + CX_4 → CX_3 + AX, where A is the acceptor atom and the X substituents have the same atomic number. So, one of us constructed surfaces for several six-body systems, H + SiH_4,[154] H + GeH_4,[149] O(^{3}P) + CH_4,[155] F($^2P_{3/2}$,$^2P_{1/2}$) + CH_4,[156,157] Cl + CH_4,[158,159] Br + CH_4,[160] and H + CCl_4,[161] and one seven-atom system, HO + CH_4.[162] Recently, in a second phase, this strategy was extended to gas-phase asymmetrically substituted polyatomic reactions, beginning with the A + CYX_3 reactive system[163] and following with the A + CWXYZ reactive system,[164] where the W, X, Y, and Z substituents can be the same or different. Note that, in the symmetrically as in the asymmetrically substituted PESs, the surface is symmetric with respect to the permutation of equivalent atoms in systems of type CW_2X_2 or CYX_3, which is very important for dynamic studies. These surfaces provide generally excellent kinetics and dynamics results. Various methods of creating and exploring global analytic potential energy surfaces have been reviewed recently by Espinosa-García and co-workers[165,166] and others.[167,168]

4.2. Implicit Surfaces Defined by a Level of Electronic Structure Theory

At the beginning of section 4, we made the distinction between analytic surfaces and direct dynamics. We have seen, however, that many of the CH_5 analytic surfaces have been based on the London equation or extensions thereof. When we recall that the London equation is the approximate solution to a two-configuration valence bond configuration interaction calculation, we begin to appreciate that the distinction between analytic fits and electronic structure calculations is a slippery slope. However, much of the interest in direct dynamics stems from using higher levels of electronic structure theory, either ab initio calculations or generally parametrized methods with more predictive value than the London equation. This distinction, too, is slippery, since one may start with a general parametrization and introduce specific reaction parameters.[88,137,169] Nevertheless, the more accurate the general parametrization is, the more likely it is that a specific parametrization will yield an accurate surface over a broad range of geometries on the basis of limited input. Consider, for example, the difference between reparameterizing a generally parametrized MM method and reparameterizing a generally parametrized semiempirical molecular orbital theory (like AM1 or most versions of density functional theory). In MM, if one wants to include, for example, bend−stretch coupling, one must explicitly include it. In molecular orbital theory, however, it is there automatically. One should mention, though, that although electronic structure calculations allow a full investigation of reactive potential energy surfaces, many studies are devoted to only a few aspects of the surface. For example, most of the studies of CH_5 examine only one or more stationary points and possibly the reaction path or reaction swath. (A reaction swath, as defined elsewhere,[87,170] is the union of the valley around the MEP with the additional set of geometries on the concave side of the MEP that may be sampled by wave packets or semiclassical tunneling paths describing corner-cutting tunneling. This region is illustrated for the $CH_3 + HT$ reaction in ref 170.)

Molecular orbital (MO) based surfaces include Hartree−Fock (HF), density functional theory (DFT), and hybrid density functional theory (HDFT). (Note that HDFT is the name given to versions of DFT in which some or all of the local approximation to the exchange energy, based on the local spin densities and their gradients, is replaced by HF nonlocal exchange energy.[171] The latter is sometimes called exact exchange, but it is not exact if the Kohn−Sham orbitals are not obtained using an exact density functional. "Hybrid" is actually an unfortunate choice of adjective for HDFT because it seems to make some readers think that HDFT is not actually DFT, and such readers label nonhybrid methods as "pure". A better way to distinguish nonhybrid and hybrid methods is to call them "local" and "nonlocal". Since the unknown exact density functional must be nonlocal, it is hardly "fair" to call other nonlocal functionals "impure". Nevertheless, the adjective hybrid is well-established jargon in the field, and so we shall use it here.) Post−Hartree−Fock correlated wave function methods include perturbation theory,[172−174] configuration interaction (CI),[175−178] and coupled cluster theory.[179−186] These methods usually begin by calculating delocalized MOs such as one obtains by restricted or unrestricted HF (RHF or UHF), but they can also[183,187] start from orbitals generated by DFT or HDFT (in either restricted or unrestricted form). In addition to these methods, a special class of electronic structure theory methods includes Pople and co-workers' Gaussian methods (G2, G3, and G4)[188−191] and multicoefficient correlation methods (MCCM).[192−196] These multiparameter and multicoefficient methods try to reduce the main sources of error in an ab initio calculation that are due to the truncation of the one-electron basis set and the truncation of the number of excitations or configurations used for treating correlation energies.[192] In these methods, the electronic energy (extrapolated to full configuration interaction, FCI, and a complete one-electron basis set, CBS) is obtained as a parametrized combination of contributions from various ab initio levels of theory. We will not review here all electronic structure theory methods applied to the CH_5 system,[17,60,130,131,197−207] just those that have yielded significant results.

An MCCM simultaneously extrapolates both the various components of the correlation energy to FCI and the one-electron basis set to the limit of CBS. The combination of FCI with CBS is called complete configuration interaction (CCI). CCI is, therefore, equivalent to the exact solution of the electronic Schrödinger equation. (We should not forget, though, that extrapolating to the CCI limit is still approximate because the extrapolation itself is imperfect.) The extrapolation is carried out by using a set of coefficients optimized to minimize the errors against a large database of thermodynamic quantities, and several parametrizations are available.[193,194,196,208,209] Each MCCM is associated with a coefficient tree that is a geometric representation of the electronic energy expression (with methods of increasing accuracy from top to bottom and basis sets increasing in size from left to right). The coefficient tree for the multicoefficient QCISD

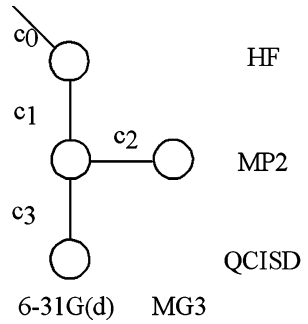

Figure 5. Coefficient tree for the MC-QCISD method.

(MC-QCISD) method[196] is given in Figure 5, and the electronic energy expression is

$$E(\text{MC-QCISD}) = c_0\,E[\text{HF/6-31G(d)}] + c_1\,\Delta E[\text{MP2}|\text{HF/6-31G(d)}] + c_2\,\Delta E[\text{MP2/MG3}|\text{6-31G(d)}] + c3\,\Delta E[\text{QCISD}|\text{MP2/6-31G(d)}] \quad (44)$$

where MP2 denotes Møller−Plesset second-order perturbation theory[172,173] and the pipe "|" notation is defined by

$$\Delta E(\text{L/B2}|\text{B1}) = E(\text{L/B2}) - E(\text{L/B1}) \quad (45)$$

and

$$\Delta E(\text{L2}|\text{L1/B}) = E(\text{L2/B}) - E(\text{L1/B})\ (46) \quad (46)$$

where L1 and L2 denote levels and B1 and B2 denote basis sets.

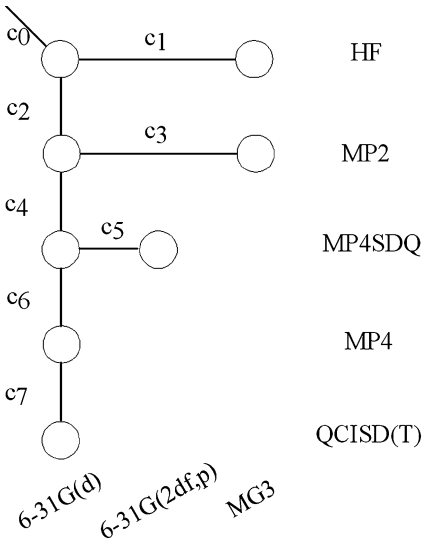

Figure 6. Coefficient tree for the MCG3 method.

Similarly, the coefficient tree for the multicoefficient G3 (MCG3) method[194] in given in Figure 6, and the electronic energy expression is

$$\begin{aligned} E(\mathrm{MCG3}) = {} & c_0\, E[\mathrm{HF/6\text{-}31G(d)}] + \\ & c_1\, \Delta E[\mathrm{HF/MG3|6\text{-}31G(d)}] + \\ & c_2\, \Delta E[\mathrm{MP2|HF/6\text{-}31G(d)}] + \\ & c_3\, \Delta E[\mathrm{MP2|HF/MG3|6\text{-}31G(d)}] + \\ & c_4\, \Delta E[\mathrm{MP4SDQ|MP2/6\text{-}31G(d)}] + \\ & c_5\, \Delta E(\mathrm{MP4SDQ|MP2/6\text{-}31G(2df,p)|6\text{-}31G(d)}] + \\ & c_6\, \Delta E[\mathrm{MP4|MP4SDQ/6\text{-}31G(d)}] + \\ & c_7\, \Delta E[\mathrm{QCISD(T)|MP4/6\text{-}31G(d)}] + E_{\mathrm{SO}} + E_{\mathrm{CC}} \end{aligned} \quad (47)$$

where E_{SO} is the spin-orbit energy, E_{CC} is the core correlation energy, and

$$\Delta E(\mathrm{L2|L1/B2|B1}) = \Delta E(\mathrm{L2|L1/B2}) - \Delta E(\mathrm{L2|L1/B1}) \quad (48)$$

Applications of the MC-QCISD and MCG3 methods to the CH_5 system have been carried out[137,138] in conjunction with the specific reaction parameter[88,169] (SRP) methodology. Here, a subset of the MCCM coefficients was specifically optimized for the hydrogen abstraction reaction, while the other parameters retained their value from the general parametrizations. The MC-QCISD-SRP and MCG3-SRP potential energy surfaces have been constructed so the classical barrier height has a value of 14.8 kcal/mol, which was the best estimate[137] of the barrier height. These surfaces, along with other SRP surfaces, were used in conjunction with variational transition-state theory with multidimensional tunneling contributions to calculate the rate constants[137] and the kinetic isotope effects[138] that should be quite accurate over a wide temperature range.

Until recently, density functional theory was not reliable for barrier height prediction. Local functionals tend to seriously underestimate barrier heights, and even many hybrid functionals systematically underestimate them.[210] However, some modern functionals do much better, and they may be used either for semiquantitative predictions on their own or as a starting point for SRP calculations. Thus, the SRP procedure has also been applied to HDFT calculations for CH_5.[137] The version of HDFT used for the DFT−SRP implicit potential energy surface of CH_5 is based on a combination of modified[211] Perdew−Wang[212] and HF exchange energy with Perdew−Wang[212] correlation energy. This combination was previously parametrized in a general way for thermochemical kinetics applications, yielding the MPW1K density functional,[213] which has 42.8% HF exchange. Since the MPW1K functional is already a reasonably accurate general parametrization for reactive potential energy surfaces, only one parameter was changed for CH_5, namely, the percentage of HF exchange, which was raised to 60%.[137] The resulting density functional, which defines another implicit potential energy surface for CH_5, is called MPW60. All three of these SRP potential energy surfaces for CH_5, namely, the MCG3-SRP, the MC-QCISD-SRP, and the MPW60 (which could also be called MPW1K-SRP), are expected to be quite accurate; although the MPW60 surface is not expected to be as accurate as the MCG3-SRP one, it is very much less expensive to evaluate. Studies on implicit surfaces and the results of these investigations are presented in section 6.2.

4.3. Interpolated Surfaces

The development of interpolated surfaces is driven by the need for an accurate and global potential energy surface to be used in conjunction with dynamics methods that require global information about the surface. The use of direct dynamics (as explained in the introduction, this refers to methods in which the information needed for dynamics is calculated on-the-fly by electronic structure theory without the intermediacy of an analytic potential energy fit), although possible, is computationally prohibited in some cases (especially for systems with many more electrons than CH_5) by the cost of using reliable electronic structure methods.[4] So the use of an interpolated surface that maintains the accuracy of the electronic structure theory PES with the affordability of an analytic potential energy surface still has uses, at least for very small systems where fitting surfaces is still not impractical.

Collins and co-workers have developed a method for generating molecular potential energy surfaces by interpolation.[214−220] The initial applications of the method involved generating surfaces for four-atom reactive systems, and these studies were extended to include some larger systems including the CH_5 system.[221] In this method, the potential energy at any configuration is given by Shepard interpolation, i.e., a weighted average of Taylor series around data points where the potential energy and its derivatives are known

$$V(\mathbf{Z}) = \sum_{g \in G} \sum_{i=1}^{N_d} w_{g \circ i}(\mathbf{Z}) T_{g \circ i}(\zeta) \quad (49)$$

where N_d is the number of molecular configurations, data points, or reference points where the energy and its derivatives have been evaluated; ζ is a set of internal coordinates; $\mathbf{Z}$ is the matrix of inverse distances ($Z_k \equiv 1/R_k$), which are preferred to the internuclear distances; G denotes the symmetry group of the molecule, and $g \circ i$ denotes that the ith data point, $\mathbf{Z}(i)$, is replaced by a data point transformed by the group element g. Each Taylor expansion T_i, defined by

$$T_i(\zeta) = V[\zeta(i)] + \sum_{k=1}^{3N-6} [\zeta_k - \zeta_k(i)] \left.\frac{\partial V}{\partial \zeta_k}\right|_{\zeta=\zeta(i)} + \frac{1}{2!} \sum_{k=1}^{3N-6} \sum_{j=1}^{3N-6} [\zeta_k - \zeta_k(i)][\zeta_j - \zeta_j(i)] \left.\frac{\partial^2 V}{\partial \zeta_k \partial \zeta_j}\right|_{\zeta=\zeta(i)} \quad (50)$$

where N is the number of atoms in the system, has an associated normalized weight function w_i, which weights the contribution of the Taylor expansion about each of the $\mathbf{Z}(i)$ data points to the total potential energy at the configuration $\mathbf{Z}$. The form of the weight function assigns a larger weight to the data points that are closer to $\mathbf{Z}$, and various forms of the weight function have been proposed.[217,221−223]

The initial data set is typically located along the MEP. Successive improvement of the PES is achieved by addition of new data points whose locations must depend on the properties of the PES and the dynamical process being considered. These locations are chosen in the regions of the configuration space that are important for the dynamical process of interest, in particular in regions identified by running a large number of classical trajectory calculations. (The method could also be applied with quasiclassical trajectories.) Collins and co-workers[221] found that energy, gradient, and Hessian calculations at 1000−1300 geometries are necessary to build an accurate surface (relative to the analytic surface that provided the data points in that study); this is about five times more data points than are necessary to construct an accurate OH_3 surface (where OH_3 is a the system composed of one oxygen atom and three hydrogen atoms).[215−217]

The interpolated surface of Collins and co-workers[221] is a extension of this method to polyatomic systems. The interpolation of the local Taylor expansions is done in internal coordinates. The interpolated CH_5 surface was compared with the analytic surface used to get the grid-point information, which is a modification of the original JG2 surface[133] that is completely symmetrized and is invariant with respect to inversion. Upon the modification, the modified JG2 surface has a slightly higher barrier and a slightly higher $CH_3 + H_2$ asymptote than the original JG2 surface. No comparison with experimental rate constants was made.

Another interpolated CH_5 surface was created by Takata et al.,[222] who modified Collins' method[214−220] by using a modified Shepard interpolation method.[224,225] Takata et al.[222] constructed a 4-dimensional surface with C_{3v} symmetry and used it in investigating the abstraction reaction. The authors used 400 data points at a low level of theory, UHF/6-31G-(d,p), to construct this surface.

Wu and Manthe[223] created a series of interpolated surfaces employing Shepard interpolation.[216,221] They used a statistical approach to select the geometries at which input data are specified and added data until they obtained reasonable convergence, which required about 40−60 Hessians. Manthe and co-workers[226,227] later developed a highly accurate interpolated PES based on about 50 data points obtained using coupled-cluster theory with single and double excitations and with a quasi-perturbative treatment of triple excitations, CCSD(T), methodology.

Kerkeni and Clary developed surfaces from a minimal number of grid points using a fitting procedure in hyperspherical coordinates.[136] More recently, Bowman and co-workers used invariant polynomial methods[228,229] to develop two interpolated CH_5 surfaces by a fit to 20 728 energies at the RCCSD(T)/aug-cc-pVTZ level of theory.[230,231] Xie and Bowman further improved these surfaces in a follow-up study.[232] Note that the 20 728 energy points used by Bowman and co-workers cannot be directly compared to the 40−60 Hessians employed by Wu and Manthe.[223] In fact, it requires approximately 324 energies (324 is 18 squared, and 18 is 3 coordinates per atom times 6 atoms) to compute a Cartesian-coordinate Hessian, and 324 times 60 equals 19 440. Therefore, the efforts are comparable.

Note added in proof: Very recently, Minkoff, Thompson, Wagner, and co-workers[440,441] reported major progress in using interpolating moving least squares for fitting potential energy surfaces sytematically.

4.4. Multiconfiguration Molecular Mechanics

Multiconfiguration molecular mechanics (MCMM)[233−235] is a dual-level method that combines molecular mechanics potentials and their simplicity with electronic structure information and its accuracy to create a semiglobal potential energy surface. The Born−Oppenheimer potential energy at a geometry defined in internal coordinates $\mathbf{q}$ is given by the lowest eigenvalue of a 2×2 electronically nonadiabatic Hamiltonian matrix $\mathbf{V}$:

$$\mathbf{V} = \begin{pmatrix} V_{11}(\mathbf{q}) & V_{12}(\mathbf{q}) \\ V_{12}(\mathbf{q}) & V_{22}(\mathbf{q}) \end{pmatrix} \quad (51)$$

The diagonal elements, V_{11} and V_{22}, of the matrix are given by molecular mechanics potentials for the reactant and the product configuration, respectively. The V_{12} element is called the resonance energy function or the resonance integral and is obtained by Shepard interpolation of quadratic expansions at a small number of points where electronic structure data are available. The lowest eigenvalue of matrix $\mathbf{V}$ is

$$V(\mathbf{q}) = \frac{V_{11}(\mathbf{q}) + V_{22}(\mathbf{q}) - \sqrt{[V_{11}(\mathbf{q}) - V_{22}(\mathbf{q})]^2 + 4V_{12}(\mathbf{q})^2}}{2} \quad (52)$$

MCMM is essentially a combination of elements drawn from five computational techniques: (i) the combined quantum mechanics−molecular mechanics (QM/MM) method,[93,126,236,237] (ii) semiempirical valence bond theory,[1,90,238−247] (iii) Chang and co-workers' method of estimating V_{12} in empirical valence bond calculations,[248,249] (iv) the use of redundant internal coordinates[250−252] to represent low-order expansions of potential energy surfaces in internal coordinates,[233] and (v) the Shepard interpolation method.[214,253] The method has been applied in conjunction with variational transition state theory calculations that included multidimensional tunneling contributions for a number of unimolecular and bimolecular hydrogen transfer reactions.[233−235,254−256] MCMM may be considered to be an extension of molecular mechanics to chemical reactions. It has been compared elsewhere[257] to other methods (for example, the methods of Raff[93] and Warshel and Weiss[243]) that share some of the same elements.

The relationship of MCMM to the combined QM/MM method may be illustrated by writing

$$V_{jj}(\mathbf{q}) = V_j^{\text{Reactive}}(\mathbf{q}) + V_{\text{MM}}^{\text{Spectator}}(\mathbf{q}) \quad (53)$$

where $V_j^{\text{Reactive}}(\mathbf{q})$ is the part that depends on j and $V_{\text{MM}}^{\text{Spectator}}(\mathbf{q})$ is the rest. Then, eq 51 becomes

$$\mathbf{V} = \begin{pmatrix} V_1^{\text{Reactive}}(\mathbf{q}) & V_{12}(\mathbf{q}) \\ V_{12}(\mathbf{q}) & V_2^{\text{Reactive}}(\mathbf{q}) \end{pmatrix} + V_{\text{MM}}^{\text{Spectator}}(\mathbf{q}) \quad (54)$$

The first term in eq 54 may be considered a two-configuration VB treatment (of which London's method is a special case) of the reactive subsystem. Thus, MCMM, given by eq 51, is closely related to the combined QM/MM method of eq 54.

One difference between the Shepard interpolation scheme of Collins and co-workers, as employed by Manthe and co-workers,[223,227] and the MCMM scheme[233−235,254−256] that also uses Shepard interpolation is that Collins' scheme interpolates $V_{11}(\mathbf{q})$, in the notation of eq 51, whereas MCMM interpolates $V_{12}(\mathbf{q})$, which makes it much more efficient.[255]

5. Methods for Applying Potential Energy Surfaces to Chemical Reactions, Especially as a Means for Investigating the Performance of the Surfaces

This section presents several methods used to investigate reactive potential energy surfaces in general and the CH_5 potential energy surface in particular.

5.1. Stationary Points

The investigation of potential energy surfaces is almost always initiated by locating stationary points (i.e., determining their geometries and their relative energies), in particular local minima, which correspond to optimal molecular structures, and saddle points, which correspond to structures with zero gradient but with a negative force constant in one direction. In the case of the CH_5 surface, the stationary points of interest are the saddle points for the abstraction and exchange or substitution channels and the van der Waals wells corresponding to H and CH_4 or to CH_3 and H_2.

5.2. Reaction Paths and Reaction-Path Dynamics

The simplest picture of the reaction process is that of motion along a "reaction path", usually taken as the "minimum energy path" linking the reactants, the saddle point, and the products. The MEP is a path that traces out a valley floor on the PES, along a valley that rises to the saddle point and is continued by another valley down to the products. Useful dynamics calculations may be based on knowledge of the PES in these valleys, and, e.g., one may use variational TST or methods based on the reaction-path Hamiltonian. Such methods also form a starting point for more sophisticated methods to evaluate tunneling contributions.

These methods begin with the definition of the path variously known as the MEP or intrinsic reaction path or intrinsic reaction coordinate (IRC),[258−260] which are all names for the path of steepest descents in mass-weighted or mass-scaled coordinates.[261−265] Mass scaling or mass weighting the coordinates is done to make the reduced mass independent of the direction of motion with no cross terms in the kinetic energy; any coordinate system where this has been accomplished is called isoinertial. The original paper that used the language of IRC[266] did not contain the mass scaling and does not correspond to the current universally accepted definition. We prefer the abbreviation MEP[120,264,265] for the isoinertial path of steepest descent. The MEP is especially suited to dynamics calculations based on reaction-path potentials.[92,120,261,262,264,265,267−272] Several different schemes for locating such paths have been developed,[264,120,267,273,86,274−277] with some of these methods being applied to investigate CH_5 surfaces.[86,274,276,277] The great advances in this field, and therefore the possibility to study more and more complex systems, were due to the development of analytical gradients of the potential energy surface initiated by Pulay's pioneering work[278] and continued by McIver and Komornicki,[279,280] and later by the development of analytical second derivatives.[281−285] All current work employing reaction paths owes a debt to the pioneering work of Hofacker and co-workers[269,286] and Marcus.[270]

Modern variational transition state theory (considered below) is usually based on a curvilinear reaction-path formalism,[250,252] because the original polyatomic generalizations[268,287] are based on rectilinear coordinates, which are not as physical as curvilinear coordinates and sometimes lead to unphysical (even imaginary) frequencies.

Taketsugu and Gordon[288] introduced a reaction-path Hamiltonian that is based on a reaction coordinate and a curvature coordinate. A two-dimensional "reaction plane" is determined by the path tangent and curvature vectors. This scheme was proposed for the case where a reaction path has a sharply curved region. The authors applied their new scheme to the $CH_3 + H_2 \rightarrow CH_4 + H$ reaction.

More recently, Konkoli et al.[289] investigated the mechanism of the $CH_3 + H_2 \rightarrow CH_4 + H$ reaction using the unified reaction valley analysis (URVA)[289,290] based on the reaction-path Hamiltonian of Miller et al.[268] and the generalization of the adiabatic mode concept introduced by Konkoli and co-workers.[291−294] The authors distinguished five reaction phases: the reactant, the reactant preparation, the transition state, the product preparation, and the product. The strength of this method is that it combines the analysis of properties that were previously only separately or not at all investigated in connection with the original reaction-path Hamiltonian, namely, energies, geometries, internal forces, electron density distribution, vibrational modes, reaction-path vector, and curvature vector.

Okuno and co-workers[295,296] proposed a reaction-path Hamiltonian described with a reaction coordinate and quasirectilinear vibrational coordinates that are constructed from a nonlinear combination of curvilinear internal coordinates. This method was expected to be more useful for reaction-path dynamics under the zero-angular momentum assumption and was used to investigate the $F + CH_4 \rightarrow FH + CH_3$ reaction. Natanson,[297] however, pointed out the explicit relations between Okuno's projected covariant Hessian matrix[295,296] and the projected Cartesian force constant matrix utilized in the Cartesian[268,287] formulation.

Billing[298] applied the reaction-path method for the CH_5 system to investigate dynamics quantities for the $H + CH_4 \rightarrow H_2 + CH_3$ reaction based on information along the reaction path.

5.3. Transition State Theory and Variational Transition State Theory with Multidimensional Tunneling Contributions

Variational transition state theory with multidimensional tunneling contributions (VTST/MT) is a powerful method for investigating chemical reaction dynamics.[106,120,148,265,271,299−306] The average errors for the VTST/MT-calculated rate constants as compared with accurate quantum data for triatomic reactive systems were shown to

be ~30%.[147] Similar or smaller errors were found also for the $H + CH_4 \rightarrow H_2 + CH_3$ reaction when comparing the VTST/MT rate constant to accurate full-dimensional quantum mechanical results on the same potential energy surface.[140,146]

The canonical variational transition-state theory (CVT) rate constant, k^{CVT}, is obtained by variationally minimizing the generalized transition-state (GT) rate constant, k^{GT}, with respect to the position s of the generalized transition state along the reaction coordinate[106,120,148,265,301−305]

$$k^{CVT}(T) = \min_s k^{GT}(T,s) \quad (55)$$

where the reaction coordinate s is the signed distance along the MEP in the isoinertial coordinate system[271] in which all coordinates are scaled to a common reduced mass. The conventional transition-state theory[307] (TST) rate constant, k^{TST}, is obtained by locating the transition state normal to the imaginary-frequency normal mode at the saddle point ($s = 0$). The CVT rate constant including tunneling is then given by

$$k^{CVT/MT} = \kappa^{CVT/MT} k^{CVT} \quad (56)$$

where $\kappa^{CVT/MT}$ is the transmission coefficient and is given by[304]

$$\kappa^{CVT/MT} = \int_{V_a^{HG}}^{\infty} d(E/RT) P^{MT}(E) \exp\{-[E - V_a^G(s_*^{CVT}(T))]/RT\} \quad (57)$$

where $P^{MT}(E)$ is the ground-state multidimensional tunneling (MT) probability at energy E, $s_*^{CVT}(T)$ is the location of the dynamical bottleneck at T, and R is the gas constant. V_a^G is the vibrationally adiabatic ground-state potential energy curve and is the sum of the potential energy along the MEP, $V_{MEP}(s)$, and the zero-point energies for the normal coordinates perpendicular to the reaction coordinate. For a nonlinear system, this is given in the harmonic approximation by

$$V_a^G(s) = V_{MEP}(s) + \sum_{m=1}^{3N_{atoms}-7} \frac{1}{2}\hbar\omega_m(s) \quad (58)$$

where $\omega_m(s)$ is the frequency of generalized normal mode m at location s along the MEP and N_{atoms} is the total number of atoms in the reactive system. Finally, V_a^{HG} is the higher of the V_a^G at the reactants and that at the products. In principle, we should include anharmonicity,[170,308] and in practice, one often does this for simple reactions[104] and for torsions in complicated reactions;[309−312] however, the inclusion of full anharmonicity in polyatomic reaction dynamics is still mainly a subject for future study. We note, though, that anharmonicity in the reactants often largely cancels anharmonicity at the transition state for reactions without torsions, such as $H + CH_4$.

The ground-state tunneling probability and, therefore, the transmission coefficient can be calculated using various semiclassical approximations: the zero-curvature tunneling (ZCT) approximation,[147,264,304,313] the centrifugal-dominant small-curvature semiclassical adiabatic ground-state tunneling (called small-curvature tunneling or SCT) approximation,[313,314] version 4 of the large-curvature tunneling (LCT) approximation,[5,147,313,315,316] and the microcanonically optimized multidimensional tunneling (μOMT) approximation.[5,147] Note that the SCT, LCT, and μOMT approximations are multidimensional and that the tunneling coefficients also include the nonclassical reflection contributions at energies above the classical barrier.[317] The ZCT and SCT approximations only require PES information in the valley around the MEP, whereas the LCT and μOMT approximations require data in a more extended part of the reaction swath. There are a large number of studies on the $H + CH_4 \rightarrow H_2 + CH_3$ reaction and the reverse reaction employing VTST/MT,[126,129,134,137,138,140,146,150,199,200,318] and these studies are reviewed in sections 6 and 7.

5.4. Classical Dynamics and Quasiclassical Trajectories

A quasiclassical trajectory[319] (QCT) is a classical trajectory that is initiated with a quantized value for the rovibrational energy, but the propagation is treated classically; after collision, the rovibrational levels of the products (which form a continuous distribution because of the classical propagation) are determined by comparing the unquantized classical action variables to the set of allowed (quantized) values.[320−323] Several procedures to include the quantization of the polyatomic vibrations in combination with quasiclassical trajectory calculations on various PESs have been presented and analyzed.[324−330]

QCT calculations are a powerful tool for the dynamical simulation of reactive systems, although they usually provide less accurate rates than VTST/MT because of the loss of vibrational quantization during propagation. The QCT method has been widely used in the study of triatomic and tetratomic systems and less widely used to study larger systems, because of the quantization difficulty for both final and initial states,[231,325,328] the expected low accuracy-to-cost ratio, and the scarcity of reliable potential energy surfaces.

On CH_5 analytic surfaces, classical trajectory studies were carried out by Kuntz et al.[105] and by Bunker and coworkers.[114−117] In one of these studies, Chapman and Bunker[117] introduced some quantization in the reactant vibrational energy by performing a quasiclassical trajectory study for the reverse $CH_3 + H_2$ reaction. QCT studies were also carried out by Raff,[93] Jordan and Gilbert,[133] and Huang et al.[127]

More recently, QCT calculations[79−81,230] have been used to understand various aspects of the stripping mechanism observed for the $H + CD_4$ reaction and the state-to-state dynamics properties at various collision energies,[78] and to analyze the product energy partition and rovibrational distribution[151] or the product angular distribution[153] for the $H + CD_4$ reaction.

Two other QCT studies[152,231] were carried out to quantify the role of the C−H antisymmetric stretch mode in methane on the reactivity and state-to-state dynamics for the $H + CH_4$ reaction. In spite of very different surfaces used, both studies[152,231] found similar enhancement of reactivity with respect to the methane ground state, results also in agreement with experimental observations.[84] This is encouraging because quasiclassical trajectories suffer from unphysical loss of initial state-specific quantization. As an example, after 25 fs, only 80% of the energy initially deposited in the asymmetric stretch of CH_4 remains in the mode excited, even in the absence of a collision;[231] this unphysical decay is due to approximation of classical propagation.

5.5. Quantum Dynamics

Quantum reactive scattering calculations can be classified as involving time-independent and time-dependent meth-

ods.[331] One time-independent approach is based on coupled-channel representations of the wave function that leads to coupled, second-order differential equations.[332] The solutions of these equations give the entire state-to-state scattering matrix at a given total energy. Another effective alternative to coupled channel methods for reactive scattering problems is the use of variational theory in which the scattering matrix is obtained directly from the wave function.[333] In the time-dependent methods, the scattering matrix is obtained by the use of wave packets for a range of energies, from a single initial energy.[334]

Both time-independent and time-dependent methods scale exponentially with the number of degrees of freedom and, in addition, become more expensive as the total angular momentum increases.[335] Because of this impediment, a number of approximate methods called reduced-dimensionality methods have been developed.[336] These methods scale much less drastically with the number of degrees of freedom and the quantum number *J*. The basic premise in these methods is to treat a subset of all degrees of freedom (i.e., the most coupled ones) by rigorous quantum methods and to treat the remaining, weakly coupled degrees of freedom by a variety of approximate methods. These approximate methods apply to all observables, but the emphasis in the present review is on the thermal rate constant.[337,338]

Quantum dynamics methods employing flux correlation functions are a powerful theoretical tool because the flux correlation functions allow a direct calculation of rate constants without requiring the solution of a full scattering problem. The rate constant of a chemical reaction can be calculated from flux correlation functions[339,340] as well as from state-to-state reaction probabilities, cumulative reaction probabilities, or reaction cross sections.[340−342]

A number of quantum dynamics studies, both accurate and approximate, have been reported for the $H + CH_4 \rightarrow H_2 + CH_3$ reaction and some of its isotopic variants. Earlier quantum dynamics studies on the CH_5 system were reduced-dimensionality studies in which the system was treated as a linear four-atom system $H + HCX \rightarrow H_2 + CX$. Takayanagi[343] carried out a three-dimensional scattering calculation in which the CH_3 moiety was treated as a pseudodiatom CX in which X is a pseudoatom with the mass of H_3 located at the center of mass of this three-atom subsystem. The effect of all degrees of freedom was included by an energy-shifting approximation. The rotating bond umbrella approximation was used in four-dimensional studies[135,344] of the abstraction reaction employing time-independent quantum scattering calculations. The four internal motions included in this model were the H−C and H−H reactive bond stretches, the umbrella-type mode of the CH_3 or CH_4 fragment, and the rotational mode of CH_3 (bending mode in CH_4).

Another model, the semirigid vibrating rotor target model,[345] was used in time-dependent wavepacket calculations. Four-dimensional,[345−347] five-dimensional (which includes one additional vibrational mode, i.e., the umbrella mode),[348,349] and six-dimensional[350,351] studies were reported. In the six-dimensional study of Wang and Bowman,[350] the system was treated as a rotating-atom triatom reaction system, and a full dimensional quantum calculation was carried out for this pseudoatom−triatom reaction. The approximate reduced-dimensionality quantum approaches used by these workers and others in the investigation of the $H + CH_4 \rightarrow H_2 + CH_3$ reaction were reviewed by Bowman.[352] In these methods, some degrees of freedom are included only as an effective potential, in a way similar to earlier treatments of atom−diatom reactions.[264,353−356]

The generalized reduced-dimensionality method, developed originally for reactions of type $X + YCZ_3 \rightarrow XY + CZ_3$ by Palma and Clary,[337] was used, for the $H + CH_4 \rightarrow H_2 + CH_3$ reaction, in a four-dimensional study by Palma et al.[357] and in a seven-dimensional study by Yang et al.[358] The seven-dimensional study assumes that nonreacting CH_3 maintains a C_{3v} symmetry during the reaction. Kerkeni and Clary[136,359] developed another reduced-dimensionality procedure to calculate approximate rate constants for chemical reactions from hyperspherical quantum scattering using a minimal number of electronic structure calculations and quantum-dynamical computations. This method utilizes a smooth interpolating functional developed in the hyperspherical representation. The methodology was applied to the $H + CH_4 \rightarrow H_2 + CH_3$ reaction,[136,338] the $D + CH_4 \rightarrow DH + CH_3$ reaction,[360] and the $Mu + CH_4 \rightarrow MuH + CH_3$ reaction,[361] where Mu represents muonium, an ultralight isotope of hydrogen.

Szichman and Baer[362] used a different approximate approach, i.e., a five-dimensional quantum mechanical method that employs the infinite-order-sudden-approximation method for the methane rotations. (It is known from earlier work on simpler reactions[363] that this is usually less accurate than the vibrationally adiabatic approximation.)

The first full-dimensional quantum-mechanical calculation of the thermal rate constant for the $H + CH_4 \rightarrow H_2 + CH_3$ reaction was reported by Huarte-Larrañaga and Manthe.[143] This initial report was subsequently followed by other studies,[141,142,226,364,365] including a correction[142] to the original calculation. Huarte-Larrañaga and Manthe used flux correlation functions to calculate the rate constant from dynamics only in the strong interaction region of the PES without including the asymptotic regions. Time propagation was achieved by using the multiconfigurational time-dependent Hartree approach[366−368] in which the wave functions are expanded as a direct product basis of single-variable time-dependent functions. The equations of motion are obtained from the Dirac−Frenkel variational principle to guarantee the optimal choice of those single-particle functions. More details can be found in a review of the method.[369]

Wang also studied the $CH_3 + H_2 \rightarrow CH_4 + H$ reaction[370] and two isotopic reactions[371] using time-dependent wavepacket propagation calculation. In these six-dimensional studies, the system is treated as a diatom−diatom reaction, and a full-dimensional quantum dynamics calculation is carried out for this pseudodiatom−diatom reaction.

5.6. Other Dynamics Methods

Transition-state theory with temperature-dependent effective potential energy functions derived from a quantum mechanical path integral analysis was used by Goodson et al.[372] to calculate the rate constant for the $H + CH_4 \rightarrow H_2 + CH_3$ reaction. More recently, Zhao et al.[373] carried out a path integral calculation of thermal rate constants within the quantum instanton approximation[374] for the $H + CH_4 \rightarrow H_2 + CH_3$ reaction.

6. Theoretical Investigations of the CH_5 Potential Energy Surfaces

The quality and accuracy of calculations of chemical reaction dynamics is strongly dependent on the quality of

Table 4. Saddle Point Geometries and Energetic Parameters for the Forward, $H + CH_4 \rightarrow H_2 + CH_3$, and the Reverse, $CH_3 + H_2 \rightarrow CH_4 + H$, Abstraction Reactions[a]

surface	R_{HH_t}[b]	R_{CH_t}	R_{CH}	θ_{HCH_t}	$\nu^{\ddagger}$	ZPE‡	$V_f^{\ddagger}$	$V_r^{\ddagger}$	ΔE	$\Delta H_{0,f}^{\ddagger}$	$\Delta H_{0,r}^{\ddagger}$	ΔH_0	ref
R	0.783	1.598	1.094	113.6			5.6						93
MR	0.783	1.61	1.10		1395	26.7	6.8	10.6	−3.8	5.9	12.8	−6.8	126
MVBC	0.905	1.84	1.10		3672	28.6	10.2	8.0	2.1	10.8	13.7	−2.9	126
J1	0.900	1.346	1.096	106.6	989	26.5	13.0	10.2	2.8	12.2	12.2	0.0	129,431
J2	0.896	1.353	1.097	106.4	966	26.2	12.7	9.9	2.8	11.6	11.6	0.0	129,431
J2A	0.910	1.34	1.10		1302	26.1	13.3	10.5	2.8	12.1	12.1	0.0	129
J3	0.900	1.35	1.10		1088	26.2	12.9	10.1	2.8	11.8	11.8	0.0	129
JG1	0.916	1.327	1.094	107.4	1093	26.2	10.9	8.2	2.8	9.8	9.9	−0.1	133
JG2	0.916	1.327	1.094	107.4	1092	27.3	10.9	8.2	2.8	10.9	11.0	−0.1	133
MJ2	0.948	1.328	1.096	107.4	1390	26.1	13.8	11.0	2.8	12.7	12.6	0.1	134
MJG2	0.939	1.335	1.094	107.2	1363	26.5	14.3	10.9	3.4	12.5	12.9	−0.4	134
EG[c]	0.931	1.331	1.095		1293	26.5	12.9	10.1	2.8	12.1	12.1	0.0	150

[a] Distances in Å; angles in degrees; $\nu^{\ddagger}$ in cm^{-1}; ZPE‡, $V_f^{\ddagger}$, $V_r^{\ddagger}$, $\Delta H_{0,f}^{\ddagger}$, $\Delta H_{0,r}^{\ddagger}$, ΔE, and ΔH_0 are in kcal/mol. $V_f^{\ddagger}$ and $V_r^{\ddagger}$ are the classical barrier heights for the forward and the reverse reactions, respectively; $\Delta H_{0,f}^{\ddagger}$ and $\Delta H_{0,r}^{\ddagger}$ are the enthalpy of activation at 0 K for the forward and the reverse reactions, respectively; ΔE is the classical energy of reaction; ΔH_0 is the enthalpy of reaction at 0 K. [b] H_t is the transferring hydrogen atom. [c] Note that the R_{HH_t} and R_{CH_t} bond lengths are in error in the original paper.[150]

the potential energy surface. Furthermore, the feasibility of different kinds of dynamics calculations depends on the amount of PES data available. Thus, if only the most relevant stationary points (reactants, products, and saddle point) are available, conventional transition-state theory[375,376] can be used, and it gives a qualitative description of the rate constants and their temperature variation. However, conventional TST is unreliable. If such a comparison is made with a good outcome, it may result from cancellation of errors. To ease the task of using more reliable methods, several algorithms have been developed to obtain kinetic information with the minimum of electronic structure calculations. Thus, Gray et al.[377] and Carrington et al.[378] employed quadratic interpolation on unimolecular reactions, and several interpolation methods have been developed to ameliorate the cost for triatomic[379] and polyatomic bimolecular reactions.[273,380]

More accurate information can be obtained from the knowledge of the PES in the reaction valleys (defined above), and this permits one to use reaction-path methods,[268,381] variational TST,[301,382,383] and zero-curvature and small-curvature multidimensional methods to evaluate the tunneling effect.[5,147,313−316] These reaction-valley methods can be very accurate in many cases, and since their requirements for PES information are intermediate between only knowing stationary points and knowing a full PES, reaction-valley approaches are particularly practical methodologies for polyatomic reactions.

If one also knows the PES in the more extended reaction swath, one can also carry out μOMT calculations,[5,147] which are more reliable when tunneling is important and the MEP is very curved. The direct dynamics approach was originally employed for classical mechanical dynamics calculations,[237,384−388] and, since then, it has received a great amount of attention.[86,389−392] Finally, if a global surface is available as an analytic function of the coordinates of the system, classical or quasiclassical trajectory calculations or quantum dynamics calculations can be carried out to provide detailed dynamics information.

6.1. Analytic Surfaces

Several laboratories have constructed global surfaces for the $H + CH_4 \rightleftharpoons H_2 + CH_3$ reaction using functional forms or fitting techniques based on a variety of electronic structure calculations. Usually, these surfaces are semitheoretical or semiempirical in nature, or both, because they include parameters that are chosen either on the basis of other theoretical studies or to reproduce some experimental kinetics and/or dynamics data, or both. A characteristic parameter of a potential energy surface, easy to calculate and practical for direct comparisons between various surfaces, is the classical barrier height. Table 4 lists the classical barrier height and some other saddle point characteristics on various analytic potential energy surfaces.

Gorin et al.[95] developed the first global surface for the abstraction and inversion reaction channels. The barrier heights of 9.5 and 37 kcal/mol, respectively, were in fair agreement with experimental data, but the PES also had an unphysical CH_3-H-H well with a depth of 8 kcal/mol.

The BEBO PES of Johnston and Parr[98] was used to study the abstraction reaction, obtaining an activation energy of 11 kcal/mol. Arthur and co-workers[101−103] also used BEBO and concluded that the original BEBO method gives rate constants smaller than the experimental values, and this disagreement was corrected by introducing a modification. Their results suggested that tunneling contributions do not appear to play a significant role for this reaction.

LEPS and BEBO surfaces were used in the work of Kurylo et al.[28] and Shapiro and Weston,[53] who calculated rate constants using TST. Kurylo et al.[28] determined the $H + CH_4/D + CH_4$ kinetic isotope effect, while Shapiro and Weston[53] looked at $CH_3 + H_2/CH_3 + D_2$, $CD_3 + H_2/CH_3 + D_2$, and $CH_3 + HD/CH_3 + DH$ kinetic isotope effects. Both studies compared the theoretical results with experimentally determined ones. Both methods lead to similar predictions and slightly underestimated the experimental results. When the one-dimensional Eckart tunneling correction[393] is applied, the agreement becomes poorer. The surfaces gave geometric and energetic saddle point properties that compared poorly with the best ab initio calculation at that time,[17] so the poor agreement with the experimental results could have been foreseen.

Bunker and co-workers[114−117] performed classical trajectory studies on the $H + CH_4$ reaction and some isotope variants, using a series of improved surfaces that culminated in the VBC surface. Using the VBC surface, Chapman and Bunker[117] performed a quasiclassical trajectory study of the reverse $CH_3 + H_2$ reaction. They found an abstraction/exchange ratio in agreement with the ratio to be between 3 and 4 found experimentally by Chou and Rowland.[68−70] At approximately the same time, Raff[93] studied the same abstraction and exchange mechanisms of hot tritium atom with methane using quasiclassical trajectory calculations on the R surface.

In 1987, Truhlar and co-workers[126] reviewed the VBC and R surfaces for the abstraction mechanism and concluded that neither of these surfaces was realistic enough for quantitative studies of the dynamics, especially for calculating forward and reverse rate constants using VTST. New surfaces, MVBC and MR, were proposed and were used in VTST/MT calculations. In a second paper,[129] Joseph et al. presented a series of improved semiempirical surfaces, the J1, J2, J2A, and J3 surfaces. These surfaces have classical barrier heights for the abstraction reaction of ~13 kcal/mol, which is higher than the values for MR and MVBC surfaces (Table 4). The J1, J2, J2A, and J3 surfaces were used, in conjunction with VTST/MT calculations, to investigate the abstraction mechanism. The best surface of the series, J3, was found to reproduce quite well experimental data available at the time: rate constants for the forward and reverse reactions, activation energies, and kinetic isotope effects.

The J1 surface proposed by Joseph et al.[129] was later employed in a study of the $CH_3 + H_2 \rightarrow CH_4 + H$ reaction by Fernandez-Ramos et al.[318] In this study, QCT, using a linearized semiclassical initial-value representation method, and VTST/MT calculations of the rate constants and the kinetic isotope effects were carried out to compare the two theoretical methods. The rate constants were similar at low temperatures but show some differences at higher temperatures.

In 1995, Jordan and Gilbert[133] introduced two new surfaces, JG1 and JG2, and performed quasiclassical trajectory calculations on their new surfaces. As shown in Table 4, the properties of the saddle points on the two surfaces are very similar. The authors considered JG2 to be the better of the two surfaces, and this surface was used in QCT calculations. In these calculations, it was found that only the methane symmetric stretch mode couples to the reaction coordinate.

As pointed out in most of the studies to be discussed, the JG2 surface is not accurate enough (i.e., it has too low of a barrier height) to allow for a direct comparison between the rate constants determined on this surface and the experimental values. (The calculated rate constants are consistently larger that the experimental ones.) These quantum dynamics studies were, therefore, mostly focused on introducing and testing the accuracy of various reduced-dimensionality methods, which were compared to the full-dimensional quantum dynamics calculations of Huarte-Larrañaga and Manthe,[141,143,364] which were also carried out with the inaccurate surface.

Takayanagi[343] carried out a three-dimensional scattering calculation in which rotationally averaged cross sections and thermal rate constants were calculated. The effect of excitation of the symmetric stretch and bending modes of CH_4 on reactivity and the vibrational distribution of H_2 and CH_3 products were investigated, and it was found that excitation of the methane symmetric stretching mode significantly enhances the reactivity. Yu and Nyman[344] performed time-independent four-dimensional quantum scattering calculations on the forward reaction. They found that the vibrational excitation of the C−H stretching mode and/or the bending modes of CH_4 enhance the reactivity, and that the tunneling effect is pronounced.

Wang et al.[345] carried out four-dimensional, time-dependent wavepacket calculations using the semirigid vibrating rotor target model to investigate the $H + CH_4 \rightarrow H_2 + CH_3$ reaction. A subsequent study by Wang and Zhang[346,347] further investigated the stereodynamics and the effect of rotational and vibrational excitation of the reactants on the reactivity. Furthermore, Wang and Zhang[348,349] used a generalized version of the semirigid vibrating rotor target model that includes one additional vibrational mode, i.e., the umbrella mode. Wang and Bowman[350] used also the JG2 surface to carry out a six-dimensional time-dependent quantum calculation for the $H + CH_4 \rightarrow H_2 + CH_3$ reaction and for the zero total angular momentum. In this study, initial state-selected reaction probabilities, the cumulative reaction probability, and the thermal rate constant were determined. Wang[370] reported six-dimensional, time-dependent wavepacket propagation calculations for the reverse $CH_3 + H_2 \rightarrow CH_4 + H$ reaction. The initial state-selected reaction probability, cumulative reaction probabilities, and thermal rate constant were calculated. A follow-up study determined the same dynamics quantities for the isotopic reactions $CH_3 + HD$ and $CH_3 + D_2$.[371]

Palma et al.[357] carried out a quantum dynamics study using a generalized reduced-dimensionality method. Two methods of converting the reduced-dimensionality reaction probabilities into rate constants were considered, one in which an energy-shifting correction is performed using the vibrational frequencies of the reaction complex at the classical transition state and the other in which the correction is done using the frequencies at the vibrationally adiabatic transition state. The rate constants obtained using generalized-transition-state frequencies were found to be in much better agreement with the full-dimensional results of Huarte-Larrañaga and Manthe.[141,143,364] Another reduced-dimensional approach was used by Szichman and Baer.[362] In this five-dimensional quantum mechanical study, total reaction probabilities, cross sections, and temperature-dependent rate constants were calculated and strong non-Arrhenius dependence and pronounced tunneling effects were found at low temperature.

Yang et al.[358] carried out a seven-dimensional quantum study for the $H + CH_4 \rightarrow H_2 + CH_3$ reaction. It was found that the umbrella mode of the CH_3 group should be treated accurately for this reaction. The authors found that calculated rate constants agree well with the experimental values, which suggested that the barrier height on the JG2 surface may be reasonable. Other theoretical studies using the JG2 surface include the study by Billing,[298] who employed the reaction-path method, and two studies by Truhlar and co-workers,[140,146] who carried out VTST/MT calculations. In these later studies, Truhlar and co-workers[140,146] found that VTST/MT results are within 25% of the full-dimensional quantum dynamics results of Huarte-Larrañaga and Manthe,[141,143,364] although they are several orders of magnitude less expensive.

In 1996, Espinosa-Garcia and Corchado[134] proposed two new surfaces, MJ2 and MJG2, which are recalibrations of the J2 and JG2 surfaces, respectively. These surfaces have classical barrier heights of 13.8 and 14.3 kcal/mol, respectively. The rate constants were calculated in the 300−1500 K temperature range using VTST with semiclassical tunneling contributions. The Arrhenius plot was found to be curved. Yu[135] further reparameterized the JG2 surface to a classical barrier height of 15.0 kcal/mol[135] and carried out four-dimensional time-independent quantum mechanical scattering calculations similar to the one performed by Yu and Nyman.[344]

A more recent analytic surface is the EG surface, which is fully symmetric with respect to the permutations of the

Table 5. Saddle Point Geometries and Energetic Parameters for the Forward, $H + CH_4 \rightarrow H_2 + CH_3$, and the Reverse, $CH_3 + H_2 \rightarrow CH_4 + H$, Abstraction Reactions[a]

method	R_{HH_t}[b]	R_{CH_t}	θ_{H_tCH}	R_{CH}	$\nu^{\ddagger}$	ZPE‡	$V_f^{\ddagger}$	$V_r^{\ddagger}$	ΔE	$\Delta H_{0,f}^{\ddagger}$	$\Delta H_{0,r}^{\ddagger}$	ΔH_0	ref
Pol-CI	0.919	1.469	102.4	1.080	974	27.9	15.9[c]	10.7	5.2	15.6	13.3	2.2	60,130,131
BH&HLYP/6-311G(d,p)	0.896	1.387	103.4	1.079	1411	27.3	12.6	11.2	1.4	11.1	13.0	−1.9	200
B3LYP/6-311G(2d,2p)	0.890	1.414	103.0	1.083	1127		9.9			8.6			204
BLYP/6-311G(2d,2p)	0.888	1.441	102.7	1.089	943		8.1			7.0			204
MPW1K/6-31+G(d,p)	0.885	1.401	103.0		1302	27.5	13.3	9.8	3.6	12.0	11.5	0.5	137
MPW60/6-31+G(d,p)	0.889	1.388	103.1		1458	27.9	14.8	11.1	3.6	13.4	13.0	0.4	137
MP2/DZ+P[d]	0.876	1.396	103.6	1.084	1776	27.6	21.8	15.3	6.5	20.4	17.1	3.3	201
MP2/TZ+2P+F[d]	0.872	1.405	103.0	1.080	1662	27.2	20.6	13.3	7.4	19.2	15.0	4.2	201
MP2/6-311G(d,p)	0.873	1.409	103.2	1.086	1639	27.2	17.6	11.6	6.0	16.3	11.6	2.9	199
MP2/cc-pVDZ	0.882	1.426	102.7	1.094			16.8	10.1	6.7				199
MP2/cc-pVTZ	0.869	1.409	102.7	1.077	1604	27.4	20.3	12.5	7.7	19.0	14.3	4.6	205,206
QCISD/6-311G(d,p)	0.899	1.390	103.7	1.089	1529	26.8	16.3	13.8	2.5	14.8	15.5	−0.7	199
QCISD/cc-pVDZ	0.910	1.407	103.2	1.097			15.0	12.2	2.7				199
PMP4(SDTQ)/6-311G(d,p)[e]	0.931	1.363	104.3	1.079	1744	27.9	15.5	12.3	3.3	14.2	14.3	−0.1	197
CCSD(T)/cc-VQZ	0.897	1.393	103.2	1.082	1500	26.6	15.4	12.6	2.8	13.7	14.1	−0.4	198
CCSD(T)/aug-cc-pVTZ	0.897	1.399	103.1	1.085	1437		14.8	12.0	2.8				230
MCOMP2	0.874	1.380	102.9		1547	26.8	15.5	10.8	4.6	14.0	12.5	1.5	137
MC-QCISD	0.899	1.385	103.2		1480	26.4	15.4	13.4	2.1	13.8	14.7	−0.9	137
MG3	0.905	1.387	103.3		1397	26.4	14.9	13.1	1.7	13.3	14.6	−1.3	137
MG3-CHO-SGP	0.901	1.394	103.1		1406	26.5	15.1	12.0	3.1	13.4	13.4	0.0	137
MG2	0.888	1.409	103.0		1352	26.4	14.7	11.2	3.5	13.2	12.8	0.4	137
MCOMP2-SRP	0.880	1.368	103.0		1559	26.6	14.8	11.5	3.3	13.2	12.9	0.3	137
MC-QCISD-SRP	0.882	1.409	103.1		1332	26.2	14.8	11.5	3.3	13.4	12.9	0.5	137
MG3-SRP	0.896	1.398	103.0		1372	26.5	14.8	11.5	3.3	13.2	13.0	0.2	137

[a] Distances in Å; angles in degrees; $\nu^{\ddagger}$ in cm^{-1}; ZPE‡, $V_f^{\ddagger}$, $V_r^{\ddagger}$, $\Delta H_{0,f}^{\ddagger}$, $\Delta H_{0,r}^{\ddagger}$, ΔE, and ΔH_0 are in kcal/mol. $V_f^{\ddagger}$ and $V_r^{\ddagger}$ are the classical barrier heights for the forward and the reverse reactions, respectively; $\Delta H_{0,f}^{\ddagger}$ and $\Delta H_{0,r}^{\ddagger}$ are the enthalpy of activation at 0 K for the forward and the reverse reactions, respectively; ΔE is the classical energy of reaction; ΔH_0 is the enthalpy of reaction at 0 K. [b] H_t is the transferring hydrogen atom. [c] A value of 13.5 kcal/mol was found by Walsh through extrapolation to account for the inexactness of the POLCI wave function. [d] DZ + P is a polarized double-ζ basis set, TZ + 2P + F is a triple-ζ basis set augmented by two sets of polarization functions and by a set of f functions on the C. [e] The barrier height was calculated including spin projection; the geometry of the saddle point and the frequencies were determined at the UMP2/6-31G(d,p) level.

four hydrogens atoms in methane. This surface was used by Espinosa-Garcia and co-workers in VTST/MT studies,[150] in QCT studies,[151−153] and in reduced-dimensionality quantum studies.[153] Although the surface has a classical barrier height (12.9 kcal/mol) that is much smaller that the best estimate (14.8 kcal/mol), the VTST calculations[150] and quasiclassical trajectory studies[151] on the EG surface showed better agreement with the experimental data than might have been expected based on the low barrier height. The EG surface was also used by Zare, Schatz, and co-workers[79−81] in their recent QCT studies, showing good correlation with the experimental data, and by Zhao et al.,[373] who carried out a path integral calculation of thermal rate constants.

6.2. Electronic Structure Theory Surfaces

Minimal objectives for theoretical investigations of PESs by electronic structure theory include determination of the geometries and relative energies of the stationary points (minima and saddle points). Characteristic features of the saddle point on various implicit PESs discussed in this section are listed in Table 5. More elaborate theoretical studies focus not only on the stationary points but also on determining more features of the CH_5 surface, specifically, the reaction path and the regions surrounding it that are important in the dynamics. Even if it is not known which features are important for the dynamics, implicit PESs defined by a level of electronic structure theory may be used in conjunction with direct dynamics methods.

From a historical perspective, a few very early semiempirical theoretical calculations are worth mentioning. In 1960, Hartmann et al.[394] obtained the energy of CH_5 by treating it as a pseudo-sodium atom with hydrogen-like orbitals; in 1967 Kaufman et al.[395] performed extended Hückel calculations for a limited number of configurations of the rebound-attack abstraction model; and in 1971, Weston and Ehrenson[16] calculated the energies of several configurations of the CH_5 radical (including those of D_{3h}, C_{4v}, and C_s symmetry) using a modified complete-neglect-of-differential-overlap (CNDO) semiempirical molecular orbital method. In 1971, Lathan et al.[396] performed ab initio calculations with small basis sets for XH_n molecules. For CH_5, the configurations with D_{3h}, C_{4v}, and C_s symmetries were analyzed, and they did not find any stable configuration of CH_5. Two local minima were described, which represent loose complexes between CH_4 and H in the entry valley of the abstraction reaction and between CH_3 and H_2 on the exit channel.

In 1972 and practically simultaneously, Morokuma and Davies[17] and Ehrenson and Newton[397] reported ab initio calculations directed toward elucidating the details of intermediate structures along likely reaction pathways; they considered both stereochemical and energetic factors. The C_{3v} symmetry for the rebound abstraction model and the D_{3h}, C_{4v}, and C_s symmetries for the exchange process (with or without inversion) were analyzed. Ehrenson and Newton[397] used UHF calculations with a Gaussian basis set of polarized double-ζ quality, while Morokuma and Davis[17] included correlation effects, although polarization functions were not included in the basis set. Both studies yielded similar results with respect to the possible mechanisms at different energies. They concluded that the abstraction reaction is the only possible one at thermal energies (this was already known from experiment), and that all transformations are possible at higher energies (also already known).

Three important theoretical papers appeared in 1977. Botschwina and Meyer[398] reported electronic structure calculations of the barrier height of the inversion exchange (D_{3h} symmetry) based on the coupled electron pair approximation and configuration interaction (CI) with pseudo-

natural orbitals (PNO-CEPA) calculations; Nieblaeus et al.[399] performed UHF−CI calculations using a polarized double-ζ basis set to predict barriers of the abstraction and inversion exchange reactions; and Siegbahn[400] reported CI calculations that gave an inversion exchange barrier similar to the previous results. All of these three studies yield similar results to those of Morokuma and Davis,[17] confirming the proposed transformations and the temperature ranges.

Cársky and Zahradnik[401] calculated rate constants by conventional TST using ab initio information from Nieblaeus et al.[399] and Botschwina and Meyer[398] for the abstraction and exchange reactions, respectively. They concluded that the 16.1 kcal/mol barrier height of Nieblaeus et al.[399] was too high by ∼2 kcal/mol (which is a quite reasonable assessment since we shall see below that the accurate forward barrier height is ∼14.8 kcal/mol).

In the 1980s, the most complete ab initio study of this surface was reported in a series of papers by Schatz, Walch, and others.[60,130,131] In the first paper, Walch[130] determined saddle point geometries and barrier heights for abstraction and inversion exchange reactions using polarization configuration interaction (Pol-CI) with a polarized triple-ζ basis set. The barrier heights and the geometries of the saddle points for both reactions were similar to previous calculations that include correlation energy.[17,398,399] Schatz et al.[131] performed a normal-mode analysis of the saddle point. Later Schatz et al.[60] used this normal mode information to calculate thermal rate constants using conventional TST for the abstraction and exchange mechanisms, for the forward and reverse reactions, and for all the deuterium isotopic counterparts associated with them. This study estimated the forward barrier for the $H + CH_4$ abstraction reaction to be 12.5 kcal/mol, a value smaller than the current best estimate of 14.8 kcal/mol. Schatz et al.[60] also included tunneling contributions calculated using the Wigner lowest-order transmission coefficient[402] and found small curvature of the Arrhenius plot over the 400−2000 K temperature range. The calculated kinetic isotope effects show differences from the experimental values, but these differences could not be traced to the limitations in the available surface information or to the dynamics methodology used. In 1984, Sana et al.[132] studied a series of five hydrogen abstractions reactions from methane ($R + CH_4 \rightarrow RH + CH_3$) using ab initio methods, and the energetic and geometry of the saddle point agrees with previous calculations. The results of Walch et al.[60,130,131] and those of Sana et al.[132] were used as the basis for the calibration of Joseph et al.'s analytic surfaces.[129]

Truhlar and co-workers[86] used the direct dynamics method with ab initio calculations to study the efficiency of several methods for generating the reaction path, using the $CH_3 + H_2 \rightarrow CH_4 + H$ reaction as the model. In fact, as this was the main objective, only the abstraction mechanism was considered using a very low ab initio level (UHF/STO-3G), and therefore, the final rate constants should not be compared to the experiment. However, the dynamic description is very interesting. The analysis of the curvature of the reaction path (contained in the Hamiltonian reaction path) shows the typical two sharp peaks, one on the reactant side of the barrier, related to the H−H stretching motion, and another on the exit side, related to the C−H stretching mode. This analysis indicates two features: first, the nonadiabatic flow of energy between the reaction coordinate and the orthogonal bound modes and, second, the fact that the reaction-path curvature must be taken into account in order to correctly calculate the tunneling contributions. This fact could not be taken into account with the information at the stationary points only, as in previous work. In a follow-up study, Boatz and Gordon[403] computed vibrational energy distributions and intrinsic frequencies to provide a clear and intuitive picture of the evolution of generalized normal coordinates along the reaction path.

In these reaction-path studies,[86,403] as well as in other similar ones,[134,250−252,289] knowledge of the vibrational frequencies along the reaction path is necessary, and various underlying coordinate systems have been used for this analysis.[404−412] The choice of the coordinate system is very important for making such calculations practical and accurate. $H + CH_4 \rightarrow H_2 + CH_3$ and another reactive system[252] were used[250,409,413] to test a general formulation that allows physically intuitive curvilinear internal coordinates (that are nonlinear functions of Cartesian coordinates) to be used for the calculation of generalized normal-mode vibrational frequencies in the reaction valley. For the $H + CH_4 \rightarrow H_2 + CH_3$ system, the authors demonstrated that the lowest frequencies obtained using curvilinear coordinates are real over the whole reaction path, whereas the frequencies obtained with rectilinear coordinates (which may be expressed as a linear combination of Cartesian coordinates) have unphysical imaginary values over a wide range of the reaction coordinate, and the unphysical imaginary value in this case is not an indication of the existence of a ridge or branching point on the PES along the reaction coordinate.

In the 1990s, the CH_5 reactive system was investigated with higher levels of electronic structure methods (both for the correlation energy treatment and for basis sets). González et al.[197] optimized the saddle point geometry at the unrestricted second-order Møller−Plesset perturbation theory (UMP2) level of theory with small basis sets and calculated the barrier heights with the fourth-order Møller-Plesset perturbation theory with spin projection (PMP4). González et al.[197] also calculated rate constants for the $H + CH_4$ abstraction reaction using conventional TST plus the Wigner lowest-order transmission coefficient (which neglects the reaction-path curvature, the change in vibrational frequencies along the reaction path, and all effects higher than order $\hbar^2$) and found small curvature of the Arrhenius plot in the 300−2000 K temperature range. They concluded that the calculated forward barrier height of 15.5 kcal/mol is overestimated by about 1−2 kcal/mol.

Later, Kraka et al.[198] reported higher-level ab initio calculations, in particular CCSD(T) with basis sets of polarized quadruple-ζ quality, in a study of a series of reactions $X + H_2 \rightarrow XH + H$, where X = F, OH, NH_2, and CH_3. The geometry of the saddle point and the barrier height agree with earlier results (Table 5), and the authors remarked that "this is the best agreement between experiment and theory that has been obtained from ab initio calculations not including any empirical based corrections". The authors obtained classical forward and reverse barrier heights of 15.4 and 12.6 kcal/mol and zero-point-inclusive forward and reverse barrier heights of 13.7 and 14.1 kcal/mol. Additional CCSD(T) single-point calculations with a better basis set give somewhat smaller barrier heights. In probably the most complete "double slash" calculation available, CCSD(T)/cc-pVQZ//CCSD(T)/cc-VQZ (the energies calculated using CCSD(T)/cc-pVQZ methods for geometries optimized using CCSD(T)/cc-VQZ method), the classical barrier height for

the $H + CH_4 \rightarrow H_2 + CH_3$ reaction was determined to be 15.3 kcal/mol.

Dobbs and Dixon[201] studied both the abstraction and exchange reactions at high ab initio levels with large basis sets. The optimization of the saddle point using MP2 with two different basis sets was followed by single-point energy calculations at increasingly higher levels of theory. The results are given in Table 5. It was found that both improvement of the basis set and improvement of the level of correlation reduce the barrier height. Dobbs and Dixon[201] calculated abstraction rate constants with the conventional TST and the Wigner lowest-order transmission coefficient in the 300−2000 K temperature range, and they concluded that the forward barrier height of 15.1 kcal/mol used in their rate constant calculations might be overestimated by about 1−2 kcal/mol. Unfortunately their calculations involve an incorrect symmetry factor. Their estimation actually agrees with the calculations of Kraka et al.[198] and shows the importance of a correct treatment of the correlation energy and the basis-set extension for describing the barrier heights. It was found that, in general, lower-level ab initio calculations tend to overestimate the barrier height and that very high level ab initio calculations are necessary to yield better agreement with the experiment.

Truong[199] reported geometries of the saddle point for the $H + CH_4$ abstraction reaction and relative energies calculated at the QCISD/6-311G(d,p) level of theory. The classical barrier height of 16.3 kcal/mol was found to be similar with previous ab initio calculations, and it was concluded that both forward and reverse classical barrier heights are overestimated by about 1 kcal/mol. Direct dynamics calculations were carried out on the QCISD/6-311G(d,p) surface, and variational TST with multidimensional semiclassical tunneling methods (i.e., CVT/SCT) were used to determine the rate constants. Truong obtained agreement with available experimental rate constants for both the forward and reverse reactions in the 300−1500 K temperature range, after scaling the energy along the MEP by a factor of 0.86.

In the same year, Truong and Duncan[200] carried out similar calculations using HDFT methods. They found that classical barrier heights were underestimated by about 2.7 and 0.6 kcal/mol for the forward and reverse reactions, respectively, compared to the values of Kraka et al.[198] The fact that DFT methods underestimate the barrier height for this reaction was also found by Jursic[203,204] in two reports in which the results of a number of DFT and HDFT methods and ab initio methods were compared with respect to the barrier height of $H + CH_4 \rightarrow H_2 + CH_3$. Compared with the experimental activation energy, considered to be 11−12 kcal/mol in that study, Jursic found that the ab initio methods overestimate the barrier height while DFT and HDFT underestimate it. This poor performance of DFT (underestimating the barrier height or even yielding a negative barrier height for reactions with a small barrier) was found also for other systems[414−420] for which saddle points were "well-known" and is now known to be a general deficiency of the density functional methods available before 2000.

In 1996, Taketsugu and Gordon[288] investigated the $CH_3 + H_2 \rightarrow CH_4 + H$ reaction on two surfaces, namely, UHF and the full-valence complete active space self-consistent field (CASSCF) method (nine electrons in nine active orbitals), with the 6-31G(d,p) basis set. They proposed an alternative reaction-path Hamiltonian in terms of a reaction coordinate, a curvature coordinate, and the remaining $3N - 8$ normal coordinates plus momenta conjugate to these coordinates. This alternative permits an analysis of the reaction-path curvature and also a separation of the reaction path into regions that can be classified based on the degree of curvature. Interestingly, the main conclusions agree with the ones of Baldridge et al.,[86] who used the conventional (Cartesian) reaction-path Hamiltonian.

In 1997, Konkoli et al.[289] investigated the mechanism of the $CH_3 + H_2 \rightarrow CH_4 + H$ reaction on the UMP2/6-31G-(d,p) surface using the unified reaction valley analysis. In 1999, Kurosaki and Takayanagi[205,206] performed high-level ab initio calculations for the $CH_3 + H_2 \rightarrow CH_4 + H$ reaction similar to those of Kraka et al.,[198] but with a smaller basis set, and obtained similar geometric and energetic results. Their studies were more extensive because they looked at the van der Waals interactions between the reactants and between the products, carried out an investigation of the reaction path, and calculated the rate constants.

Among the more recent theoretical investigations that were focused only on the location and characterization of the stationary points on the CH_5 potential energy surfaces, there are a few more to be mentioned. Porezag and Pederson[202] determined the saddle point properties for both the abstraction and exchange reactions by using DFT. They compared a functional based on the local spin density approximation with a generalized gradient functional to determine if the over-bonding typically observed for hydrocarbons using the local density approximation (leading to underestimated barrier heights) is surmounted by using a generalized gradient approximation. They found an improvement in the relative energies of transition states but still an underestimation of the barrier height, with a value of 9.3 kcal/mol for the abstraction reaction and 28.6 kcal/mol for the exchange reaction. Patchkovskii and Ziegler[207] showed that the calculated barrier heights for some reactions, including the $CH_3 + H_2 \rightarrow CH_4 + H$ reaction, could be improved, although not significantly, by using self-interaction-corrected DFT. The $CH_3 + H_2 \rightarrow CH_4 + H$ reaction as part of the original multireaction data set developed for parametrizing a new hybrid density functional for kinetics.[213] The saddle point properties as well as the forward and reverse classical barrier heights were determined with a number of hybrid density functional methods.[213,421−426] This work led to the first reasonably accurate density functional for kinetics MPW1K,[213] followed by a series of successfully improved functionals for kinetics, including BB1K[427] and MC3BB.[428]

The B3LYP/6-31G(d,p) surface was used by Schatz and co-workers[79−81] in QCT calculations for the $H + CD_4$ reaction to explain experimental data on the stripping mechanism and state-to-state dynamics properties at high energies.[78]

In a pair of papers published in 2002, Pu and Truhlar[137,138] reported the most advanced theoretical study to date on the CH_5 system. In the first investigation,[137] four implicit potential energy surfaces were developed and tested for the $H + CH_4 \rightarrow H_2 + CH_3$ reaction. The stationary points on these surfaces were characterized, and the rate constants were calculated by means of CVT with the SCT approximation and the harmonic approximation in curvilinear coordinates for vibrations. In the second part of the study,[138] the kinetic isotope effects were calculated for a number of isotopic reactions. The four potential energy surfaces built in this study[137] were semiempirical, that is, SRP modifications of standard surfaces such that the classical barrier height for the abstraction reaction has the value of 14.8 kcal/mol, which

was chosen by empirical analysis as the best estimate for the forward barrier height. The first surface was called MPW60 and was based on the mPW1PW91 hybrid density functional method but with the percentage of HF exchange raised to 60%. The SRP parametrization for the MPW60 surface was carried out by varying only the percentage of the HF exchange. (The best prediction of the experimental rate constants was achieved, though, on the MPW58 surface, for which the percentage of HF exchange is 58%, with this surface having a barrier height of 14.6 kcal/mol as compared to 14.8 for MPW60.) The other three surfaces were constructed with multicoefficient correlation methods (MCCMs) and were labeled MCOMP2-SRP, MC-QCISD-SRP, and MCG3-SRP, respectively. In all of these cases, there are more parameters than can practically be modified. In each of the three SRP parametrizations, only two parameters (i.e., coefficients) were modified, in particular the most sensitive ones (the ones that required the least modification from the standard values). The coefficients were modified such that the $H + CH_4 \rightarrow H_2 + CH_3$ reaction has a classical barrier height of 14.8 kcal/mol and an endothermicity of 3.3 kcal/mol, which was considered the best estimate value based on a mixture of experimental and theoretical data. Properties of all these surfaces are given in Table 5. On the basis of the best two surfaces (MC-QCISD-SRP and MCG3-SRP), the $C-H_t$ and H_t-H internuclear distances at the saddle point (where H_t is the transferring H atom) were determined to be 1.39−1.41 and 0.88−0.90 Å, respectively, and the imaginary frequency at the saddle point was estimated to be between 1300*i* and 1500*i* cm^{-1}. These values can be used as references for discussing the accuracy of other accurate potential energy surfaces. The MCG3-SRP surface for CH_5 was, at the time it was published, the most accurate surface available for any reaction with more than four atoms.

Another important feature of the CH_5 surface that has, however, received relatively little attention is the existence of van der Waals complexes composed of the two reactants or the two products ($H\cdots CH_4$ and $CH_3\cdots H_2$, respectively). As was noted in section 2, their presence has not been detected experimentally, although they are surely present, and theoretically their existence depends on the theoretical method used. These complexes are expected to be important at low temperatures.

In 1939, Gorin et al.[95] theoretically found on their analytic surface a stabilized complex (8 kcal/mol) corresponding to a weak bond between methane and a hydrogen atom. The topic of van der Waals complexes arose again when Lathan et al.[396] performed low-quality ab initio calculations on this system and found very loose complexes, $H\cdots CH_4$ and $CH_3\cdot\cdot\cdot H_2$, whose existence in the calculations presumably resulted from basis-set superposition error. In 1996, Jursic,[203] using several ab initio and DFT calculations, reported that formation of a methane−hydrogen complex is not energetically favorable, but later Konkoli et al.,[289] on the basis of the unified reaction-valley approach, discuss the existence of a van der Waals region on the reactant and product side.

In 1999, Kurosaki and Takayanagi[205,206] investigated carefully the existence of these complexes, which could be produced in their reaction in solid *p*-H_2. (As a model for chemical reactions in condensed phases, Hancock et al.[429] investigated unimolecular rearrangements of similar $H\cdots H_2$ van der Waals complexes.) Kurosaki and Takayanagi determined the existence of both $H\cdots CH_4$ and $CH_3\cdots H_2$ van der Waals complexes on a PES calculated at the MP2/cc-pVTZ level (where cc-pVTZ is the correlation-consistent polarized-valence triple-ζ basis set proposed by Dunning[430]). Without including ZPE, one finds that these complexes are predicted to bound even when basis-set superposition error is included, although the binding is weak. The ZPE of the van der Waals complexes is greater than the ZPE of separated reagents, and any discussion of the possible observation of the van der Waals bound states must take account of this. More recently, Manthe and co-workers[227] used the CCSD(T) method with various basis sets to construct an interpolated surface, and they reported the presence of the van der Waals complexes in both the reactant and the product valleys.

6.3. Interpolated Surfaces

As was described in section 4.3, one of the first interpolated PESs for the CH_5 system was developed by Takata et al.[222] The surface was employed in conjunction with the dynamic reaction-path method, but the focus of the study was in constructing the interpolated surface in the region of the global CH_5 surface corresponding to the abstraction reaction. Because of the low level of theory, UHF/6-31G(d,p), used for the grid points, their results were not quantitative, and comparing the results with experimental results was not attempted.

Wu and Manthe[223] used their interpolated surface to reproduce the thermal rate constants calculated without interpolation with errors smaller than 20%. Using a similar procedure, highly accurate interpolated surfaces were created by Manthe and co-workers.[226,227] These surfaces have a classical barrier height of 14.93 kcal/mol, in excellent agreement with the earlier work of Pu and Truhlar,[137] which yielded a best estimate of 14.8 kcal/mol. In one of these studies,[227] the authors found that a quite accurate surface can be obtained with 23 Hessians located on the MEP. These interpolated surfaces were used in full-dimensional quantum dynamics calculations employing flux correlation functions and multiconfigurational time-dependent Hartree wavepacket propagation. In another recent study using one of these interpolated surfaces, the rate constant for the $D + CH_4$ reaction and kinetic isotope effects were calculated.[365]

The interpolated surface of Kerkeni and Clary was developed from a minimal number of grid points calculated at the CCSD(T)/cc-pVTZ level of theory using a fitting procedure in hyperspherical coordinates.[136] This surface has a zero-point-inclusive barrier height, $\Delta H^{\ddagger}_{0,f}$, of 14.2 kcal/mol. This surface was used in quantum reactive scattering calculations for the $H + CH_4$ reaction, and the calculated rate constants were similar to the ones reported by Pu and Truhlar[137] and by Wu et al.[226]

Bowman and co-workers[230−232] also obtained accurate interpolated CH_5 surfaces based on a large number of RCCSD(T)/aug-cc-pVTZ data points. These surfaces have a classical barrier height for the abstraction reaction of 14.8 kcal/mol, and $C-H_t$ and H_t-H distances at the saddle point of 1.399 and 0.897 Å, respectively. (The characteristics of the saddle point on this surface are essentially the same as those determined on the MG3-SRP surface developed by Pu and Truhlar.[137]) These values are very close to the saddle point characteristics on the actual RCCSD(T)/aug-cc-pVTZ surface.[230] The surfaces were used in QCT calculations for the $H + CH_4$ reaction[231] and the $H + CHD_3$ reaction.[232] The comparison of the results of these studies with the experimental data is presented in section 7.

7. Comparison to Experiment

Almost every theoretical investigation of the CH_5 surface invokes comparison with experimentally determined quantities. In order for this comparison to be meaningful, the theoretical studies should be based on an accurate PES and should employ a validated dynamics method. The focus of this section is to present comparisons between calculated and experimental data where these conditions are met or are close to being met. In addition, we will concentrate only on the most recent experimental data. By comparing calculated kinetics and dynamics quantities with experimental ones, one can determine characteristics and/or shortcomings of the potential energy surfaces used, of the dynamics methods employed, or of some combination of the two.

7.1. Rate Constants

The rate constant is probably the best macroscopic measure of the accuracy of a potential energy surface, at least in the thermal bottleneck region, because it is a well-defined observable that can often be measured with high precision and good reproducibility. Deducing rate constant values from surface information implies the use of a dynamics method. A reliable dynamics method should account for the quantum effects on nuclear motions and should include all degrees of freedom. Such a method was devised and applied for the $H + CH_4 \rightarrow H_2 + CH_3$ reaction by Manthe and co-workers.[141−143] The original application of this method was limited to an inaccurate surface (i.e., the JG2 analytic surface), and a meaningful comparison with experimental data was not attempted. More recently, accurate full-dimensional quantum dynamics calculations were carried out on a more accurate interpolated surface that was constructed based on CCSD(T)/cc-pVQZ and CCSD(T)/aug-cc-pVQZ ab initio data points.[226,227,365] (The classical barrier height for this surface is 14.93 kcal/mol, the $C-H_t$ and H_t-H distances at the saddle point are 1.401 and 0.895 Å, respectively, and the imaginary frequency is $1414i$ cm^{-1}; these data are very close to the best estimates of Pu and Truhlar.[137]) The rate constants calculated on this surface[226,227,365] using full-dimensional quantum dynamics calculations slightly underestimate (by ~25% at higher temperatures and by about a factor of 2 at lower temperatures) the experimental rate constants values obtained based on the fit of Sutherland et al.[33] A better agreement would be expected on a surface with a slightly smaller barrier height than 14.93 kcal/mol, which is the value on the surface used by Manthe and co-workers.[226,227,365] A representation of these and other calculated rate constants as well as experimental data is given in Figure 7.

A more affordable way to extract kinetic and dynamics information associated with a PES is to use a less exact but more affordable and still reliable dynamics method. Variational transition state theory with semiclassical multidimensional tunneling contributions is the most successful such method because of its relative simplicity (in terms of automatization and availability)[431] and its accuracy. Investigating a potential energy surface using VTST/MT and direct dynamics includes all degrees of freedom and includes quantum effects on nuclear motion and should be almost as accurate but much more affordable than full-dimensional quantum calculations. In fact, a direct comparison between the full-dimensional quantum calculations of Manthe and co-workers and the direct dynamics VTST/MT results for the $H + CH_4 \rightarrow H_2 + CH_3$ reaction with the same potential energy surface shows differences that are similar in magnitude to typical experimental errors.[140,146] Note that this comparison between the results from exact full-dimensional quantum calculations and VTST calculations is only meaningful as a test of the theoretical dynamics method when the calculations are performed on the same potential energy surface.

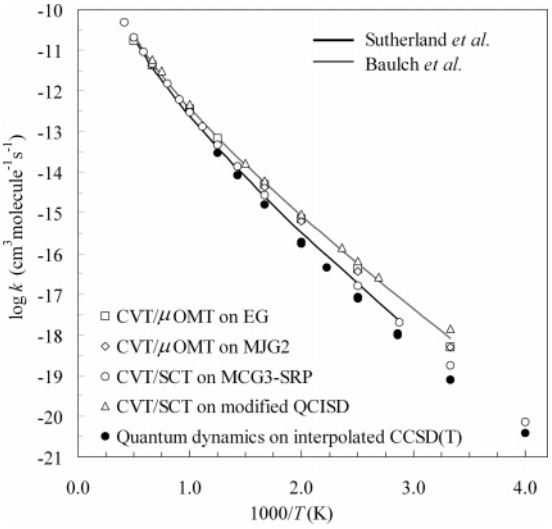

Figure 7. Calculated and experimental rate constants for the $H + CH_4 \rightarrow H_2 + CH_3$ reaction. The experimental data are based on the fits proposed by Sutherland et al.[33] and Baulch et al.[39] The calculated data are as follows: □ are CVT/μOMT rate constants on the EG surface with a barrier height of 12.9 kcal/mol,[150] ◇ are CVT/μOMT rate constants on the MJG2 surface with a barrier height of 14.3 kcal/mol,[134] ○ are CVT/SCT rate constants on the MCG3-SRP surface with a barrier height of 14.8 kcal/mol,[137] Δ are CVT/SCT rate constants on a modified QCISD/6-311G(d,p) surface with a barrier height of 14.0 kcal/mol,[199] and ● are full-dimensional quantum dynamics rate constants on an interpolated CCSD(T) surface with a barrier height of 14.93 kcal/mol.[226,227,365]

The best implicit potential energy surface for the $H + CH_4 \rightarrow H_2 + CH_3$ reaction is the MCG3-SRP PES of Pu and Truhlar,[137] which has a classical barrier height of 14.8 kcal/mol. Rate constants between 250 and 2400 K were calculated using CVT/SCT and the harmonic approximation in curvilinear coordinates for vibrations along the MEP. Excellent agreement (with errors of 25% or less) between the calculated rate constants and the most recent experimental values[33] was obtained over the whole temperature interval (Figure 7). The experimentally observed curvature in Arrhenius representation was also accurately predicted.

Other direct dynamics calculations using VTST/MT reporting good agreement with experimental rate constants are the studies by Truong on the QCISD/6-311G(d,p) surface[199] and by Truong and Duncan on the BH&HLYP/6-311G(d,p) surface.[200] The rate constants were actually calculated along MEPs that were scaled to give classical barrier heights of 14.0 kcal/mol in the study of Truong[199] and of 14.8 and 14.6 kcal/mol, respectively, in the study of Truong and Duncan.[200] In these studies, the calculated rate constants were compared with the experimental values of Baulch et al.,[39] but when comparing with the more recent experimental values,[33] the calculated rate constants are typically larger (by a factor of ≥ 2 at low temperatures and a factor of <2 at higher temperatures). Interestingly, although the barrier height along the scaled MEP is close to the best estimate value of Pu and Truhlar, the calculated rate constants are quite different than those obtained on the MCG3-SRP

surface. This implies that, although the classical barrier height is an important factor in reaction kinetics, other topological properties of the surface (i.e., the reaction-path curvature, the width of the barrier, etc) can be significant in determining kinetic and dynamic quantities.

Among the analytic surfaces, the surface with saddle point characteristics for the H + CH_4 abstraction closest to the Pu−Truhlar values is the MJG2 surface proposed by Espinosa-Garcia and Corchado.[134] This surface was used in direct dynamics calculations employing VTST/MT, and it was found to underestimate the experimental rate constants proposed by Baulch et al.[39] by ∼30% and to overestimate the experimental rate constants proposed by Sutherland et al.[33] by almost a factor of 2 at low temperatures and ∼50% at higher temperatures. The other surface proposed by Espinosa-Garcia and Corchado (MJ2)[134] and that by Espinosa-Garcia (EG)[150] show similar results even though the classical barrier heights are somewhat smaller at 13.8 and 12.9 kcal/mol, respectively.

7.2. Kinetic Isotope Effects

Pu and Truhlar[138] used the MCCM-SRP surfaces[137] to calculate various kinetic isotope effects for both the forward and reverse abstraction reactions. Three surfaces (MC-QCISD-SRP, MCG3-SRP, and HDFT with a specific reaction parameter MPW60/6-31+G(d,p)) surface were used to calculate deuterium kinetic isotope effects for eight isotopic combinations. The results agree very well with most of the experimental values, in support of the overall accuracy of the proposed surfaces.

The H + CH_4/D + CH_4 kinetic isotope effect was recently calculated by Manthe and co-workers[365] using accurate full-dimensional quantum dynamics calculations on a high-quality interpolated surface.[227] The authors compared their kinetic isotope effects to the recommended experimental values of Kurylo et al.[28] and obtained good agreement, especially when one considers the large uncertainties in the recommended values. However, without giving any explanation, they compared their D + CH_4 rate constants to the raw (uncorrected, unrecommended) data of Kurylo et al.[28] and obtained poor agreement. In light of the questionable treatment of the experimental data by Kurylo et al.,[28] a more interesting comparison may be between the calculations of Manthe and co-workers[365] and the earlier MCG3-SRP direct dynamics calculation employing VTST/MT of Pu and Truhlar.[138] At 400 K, Manthe and co-workers calculated a kinetic isotope effect of 0.48, in reasonable agreement with the earlier 0.58 value.[138] Both values are more reliable than the experiment, and the good agreement provides an encouraging check of both the PESs and the dynamics methods.

Kinetic isotope effects for both the H + CH_4 abstraction reaction and the reverse reaction have been also calculated using VTST/MT by Espinosa-Garcia and Corchado[134] and by Espinosa-Garcia,[150] and the calculated values show a reasonably good agreement with the experimental values.

The study of Pu and Truhlar[138] also looked at the Mu + CH_4 abstraction reaction where muonium (Mu) is a nonconventional isotope of hydrogen with a mass of about one-ninth of the mass of a proton. The calculated muonium kinetic isotope effects show the correct variation with temperature, but the values agree rather poorly with the experimental ones, especially at high temperatures. Some possible reasons for this disagreement were presented and discussed.

7.3. Low-Temperature Tunneling Effects

To explain the experimental observation of Momose et al.[72] that the deuterated reaction $CD_3 + H_2 \rightarrow CD_3H + H$ occurs but the unsubstituted $CH_3 + H_2 \rightarrow CH_4 + H$ does not in solid *para*-H_2 at 5 K, Kurosaki and Takayanagi[205] and Kurosaki[432] reported variational transition state theory calculations with semiclassical tunneling contributions for both reactions. These calculations were carried out at the QCISD-(T)/cc-pvTZ//MP2/cc-pVTZ level of theory, and these studies qualitatively explain the experimental observation.

7.4. Detailed Reaction Dynamics

The observed stripping mechanism for the H + $CH_4 \rightarrow$ H_2 + CH_3 reaction, initially observed by Zare and co-workers,[78] has also been investigated theoretically. In an initial study,[79] the EG analytic surface and the B3LYP/6-31G(d,p) surface were used by Camden et al. in quasiclassical trajectory calculations. These authors found that the B3LYP/6-31G(d,p) surface semiquantitatively reproduces the experimental results while the EG surface does not, and they interpreted these observations as resulting from different opacity functions due to the EG surface having a saddle point closer to the product valley than the B3LYP surface (which in turn is similar to the CCSD(T)/cc-pVTZ surface). Subsequent studies at other collision energies show similar results.[80,81] The saddle point geometry on the B3LYP/6-31G-(d,p) surface is similar to that of the MCCM surfaces above, but the classical barrier height is much smaller at 9.4 kcal/mol. However, in a more recent study, Espinosa-García and co-workers[153] used the EG surface to analyze the effect of the dynamics method by carrying out quasiclassical trajectory and reduced-dimensionality quantum scattering calculations. It was found that only the quantum mechanical calculations reproduced the experimental angular scattering at the high energies of the experiment, so the problem in the initial paper of Camden et al.[79] appears to be due to limitations of the QCT method not the EG surface.

Results of quasiclassical trajectory calculations using the interpolated surface of Bowman and co-workers[230,231] for the H + CD_4 abstraction reaction show good agreement with the experimental rotational distribution of HD summed over all vibrational states for an initial relative kinetic energy of 1.52 eV (35 kcal/mol). Collisions initiated with the symmetric stretching vibration of CH_4 excited were also studied. Camden et al.[84] experimentally found that the reactivity of the H + CH_4 reaction is enhanced by a factor 3.0 ± 1.5 when the C−H antisymmetric stretch mode is excited. Espinosa-García and co-workers performed QCT calculations[152] on the EG surface, and Bowman and co-workers[231] performed QCT calculations on their ab initio surface; there is good agreement between these studies and the experiment in the wide energy range of 1.52−2.20 eV (35−51 kcal/mol). Xie and Bowman[232] also investigated the H + CHD_3 reaction using QCT calculations. A key point in the QCT studies of Bowman and co-workers[231,232] is that they validated a key assumption of the QCT method for studying the effect of C−H stretch excitation on the H + CH_4 and H + CHD_3 dynamics, namely, that the energy in the C−H stretching mode remains localized long enough (even though one is calculating the dynamics by classical mechanics without using good action variables) for the collision to be studied before energy is randomized. They found that exciting the C−H stretch enhances the production of H_2, which they

found to occur by a rebound mechanism, but not the production of HD, which they found to occur by stripping.

As we noted at the end of section 3.6, the experimental state-to-state dynamics studies for this reaction have been performed at high energies, 1−2 eV, while the potential energy surfaces developed for this system were originally designed and tested for thermal conditions, i.e., kinetics studies at low energies (about the classical barrier height, 14.8 kcal/mol ≈ 0.6 eV). A direct comparison between theory and experiment needs to take this into account. Two future prospects, one experimental and another theoretical, can be envisioned. Experimentally, it is necessary to obtain data at lower energy, 0.5−1.0 eV, which represents a true challenge. Such studies at a low energy are important to unequivocally determine the dynamics and the mechanism of the thermal H + CH_4 reaction and to permit directly comparing the reaction mechanism with those of other similar atom + methane reactions[155,157,159,433−439] (e.g., Cl + CH_4, F + CH_4, O(^{3}P) + CH_4, etc.) that take place at low energies. Theoretically, progress can be made in developing or refining surfaces in high-energy regions (i.e., distant from the reaction valleys).

8. Concluding Remarks

The construction of potential energy surfaces for polyatomic systems is reaching levels of accuracy similar to ones attained previously only for triatomic systems. In generating potential energy surfaces and quantifying their accuracy, one wants to test against as much experimental data as possible, including rate constants, activation energies, kinetic isotope effects, and the curvature in the Arrhenius plots (for both the forward and reverse reactions), as well as various detailed reaction dynamics quantities. Differences between the calculated and experimental quantities can result from a less-than-perfect potential energy surface, from a less-than-reliable dynamics method, from possible experimental errors, or from combinations of these, and recent work is beginning to allow a careful analysis of all these factors.

Over more than six decades, the H + CH_4 reaction and its isotopic variants have represented a target against which to test kinetics and dynamics theories and PESs for polyatomic reactions. In the past decade, potential energy surfaces for the CH_5 system as well as other polyatomic reactions have been constructed that reproduce almost exactly many experimental kinetics data and some details of the state-to-state dynamics, although they have not yet been capable of simulating all the fine details of this dynamics. Although constructed by different workers and different methods, these accurate potential energy surfaces have very similar features, which leads us to conclude that the quest for an accurate CH_5 potential energy surface is achieving unprecedented success.

9. Glossary of Acronyms

AM1	Austin model 1
B3LYP	Becke three-parameter Lee−Yang−Parr density functional
BEBO	bond-energy-bond-order
BH&HLYP	Becke half-and-half Lee−Yang−Parr density functional
CASSCF	complete active space self-consistent field
CBS	complete one-electron basis set
CCI	complete CI
CCSD(T)	coupled-cluster theory with single and double excitations and with a quasi-perturbative treatment of connected triple excitations
CI	configuration interaction
CNDO	complete neglect of differential overlap
CVT	canonical variational transition-state theory
CVT/SCT	CVT with SCT
D	deuterium isotope of hydrogen
DFT	density functional theory
EG	analytic surface of Espinosa-García, previously sometimes labeled the PES-2002 surface
ESR	electron spin resonance
FCI	full CI
G2	Gaussian-2 method of Pople and co-workers
G3	Gaussian-3 method of Pople and co-workers
GT	generalized transition state
HDFT	hybrid DFT
HF	Hartree−Fock
INDO	intermediate neglect of differential overlap
IRC	intrinsic reaction coordinate
J1	analytic surface no. 1 of Joseph, Steckler, and Truhlar
J2	analytic surface no. 2 of Joseph, Steckler, and Truhlar
J2A	analytic surface no. 2A of Joseph, Steckler, and Truhlar
J3	analytic surface no. 3 of Joseph, Steckler, and Truhlar
JG1	version 1 of the analytic surface of Jordan and Gilbert
JG2	version 2 of the analytic surface of Jordan and Gilbert
JANAF	joint Army Navy Air Force
LCT	large-curvature tunneling
LEP	London−Eyring−Polanyi
LEPS	London−Eyring−Polanyi−Sato
MCCM	multicoefficient correlation methods
MCG3	multicoefficient G3
MCG3-SRP	MCG3 with SRP
MCMM	multiconfiguration molecular mechanics
MCOMP2	MCCM Colorado MP2
MCOMP2-SPR	MCOMP2 with SRP
MC-QCISD	multicoefficient QCISD
MC-QCISD-SRP	MC-QCISD with SRP
MEP	minimum energy path
MJ2	modified J2
MJG2	modified JG2
MM	molecular mechanics
MO	molecular orbital
MP2	Møller−Plesset second-order perturbation theory (for electronic structure)
MP4	Møller−Plesset fourth-order perturbation theory (for electronic structure)
MP4SDQ	MP4 with single, double, and quadruple substitutions
mPW	modified Perdew−Wang (functional)
mPW1PW91	one-parameter HDFT method based on the mPW exchange functional and PW91 correlation functional (also called mWP1PW, mPW0, and MPW25)
MPW1K	modified Perdew−Wang functional with one parameter for kinetics
MPW58	mPW1PW91 method with the percentage of HF exchange equal to 58%
MPW60	mPW1PW91 method with the percentage of HF exchange equal to 60%
MR	modified R
MT	multidimensional tunneling
MVBC	modified VBC
μOMT	microcanonical optimized multidimensional tunneling

PES	potential energy surface (sometimes called potential energy hypersurface or potential energy function)
PES-2002	old name for the EG surface
photo-LOC	photo law-of-cosines
PMP4	fourth-order Møller−Plesset perturbation theory with spin projection
PNO-CEPA	coupled electron pair approximation based on a configuration interaction method with pseudonatural orbitals
Pol-CI	polarization CI
PW91	Perdew−Wang '91
QCISD	quadratic CI calculations including single and double substitutions
QCISD(T)	QCISD including a noniterative triples contribution
QCT	quasiclassical trajectory
QM/MM	quantum mechanics-molecular mechanics
R	analytic surface of Raff
RCCSD(T)	restricted CCSD(T)
RHF	restricted HF
SCT	small-curvature tunneling
S_N2	bimolecular nucleophilic substitution
SRP	specific reaction parameters or specific range parameters
T	tritium isotope of hydrogen
TST	transition-state theory or generalized TST, which includes VTST
UHF	unrestricted HF
UMP2	unrestricted MP2
URVA	unified reaction valley analysis
VB	valence bond
VBC	analytic surface of Valencich, Bunker, and Chapman
VB/MM	VB and MM
VTST	variational TST
VTST/MT	VTST with MT contributions
ZCT	zero-curvature tunneling
ZPE	zero-point energy

10. Acknowledgments

J.E.-G. is grateful to Junta de Extremadura and Ministerio de Educación y Ciencia (Spain) for the financial support during the last few years. This work was supported in part by the U.S. Department of Energy under Grant No. DE-FG02-86ER13579.

11. References

(1) Truhlar, D. G.; Wyatt, R. E. *Adv. Chem. Phys.* **1977**, *36*, 141.
(2) Mielke, S. L.; Peterson, K. A.; Schwenke, D. W.; Garrett, B. C.; Truhlar, D. G.; Michael, J. V.; Su, M.-C.; Sutherland, J. W. *Phys. Rev. Lett.* **2003**, *91*, 63201.
(3) Truhlar, D. G.; Steckler, R.; Gordon, M. S. *Chem. Rev.* **1987**, *87*, 217.
(4) Fernandez-Ramos, A.; Miller, J. A.; Klippenstein, S. J.; Truhlar, D. G. *Chem. Rev.* **2006**, *106*, 4518.
(5) Liu, Y. P.; Lu, D. H.; Gonzalez-Lafont, A.; Truhlar, D. G.; Garrett, B. C. *J. Am. Chem. Soc.* **1993**, *115*, 7806.
(6) Born, M.; Oppenheimer, R. *Ann. Phys.* **1927**, *84*, 457.
(7) Atkins, P. W.; Friedman, R. S. *Molecular Quantum Mechanics*, 4th ed.; Oxford University Press: New York, 2005.
(8) Cahn, R. S.; Ingold, C. K.; Prelog, V. *Experientia* **1956**, *12*, 81.
(9) Cahn, R. S.; Ingold, C.; Prelog, V. *Angew. Chem., Int. Ed. Engl.* **1966**, *5*, 385.
(10) Wolfgang, R. *Acc. Chem. Res.* **1969**, *2*, 248.
(11) Herschbach, D. R. *Adv. Chem. Phys.* **1966**, *10*, 319.
(12) Schmatz, S.; Clary, D. C. *J. Chem. Phys.* **1998**, *109*, 8200.
(13) Bogdanov, B.; McMahon, T. B. *J. Phys. Chem. A* **2006**, *110*, 1350.
(14) Chattopadhyay, A.; Tasaki, S.; Bersohn, R.; Kawasaki, M. *J. Chem. Phys.* **1991**, *95*, 1033.
(15) Rowland, F. S.; Palino, G. F. *J. Phys. Chem.* **1971**, *75*, 1299.
(16) Weston, R. E., Jr.; Ehrenson, S. *Chem. Phys. Lett.* **1971**, *9*, 351.
(17) Morokuma, K.; Davis, R. E. *J. Am. Chem. Soc.* **1972**, *94*, 1060.
(18) Minyaev, R. M.; Gribanova, T. N.; Minkin, V. I.; Starikov, A. G.; Hoffmann, R. *J. Org. Chem.* **2005**, *70*, 6693.
(19) Berlie, M. R.; LeRoy, D. J. *Can. J. Chem.* **1954**, *32*, 650.
(20) Klein, R.; McNesby, J. R.; Scheer, M. D.; Schoen, L. J. *J. Chem. Phys.* **1959**, *30*, 58.
(21) Fenimore, C. P.; Jones, G. W. *J. Phys. Chem.* **1961**, *65*, 2200.
(22) Biordi, J. C.; Papp, J. F.; Lazzara, C. P. *J. Chem. Phys.* **1974**, *61*, 741.
(23) Biordi, J. C.; Lazzara, C. P.; Papp, J. F. *Symp. (Int.) Combust. (Proc.)*, 15th, 917 (1975).
(24) Biordi, J. C.; Lazzara, C. P.; Papp, J. F. *Combust. Flame* **1976**, *26*, 57.
(25) Jamieson, J. W. S.; Brown, G. R. *Can. J. Chem.* **1964**, *42*, 1638.
(26) Sepehrad, A.; Marshall, R. M.; Purnell, H. *J. Chem. Soc., Faraday Trans.* **1979**, *75*, 835.
(27) Kurylo, M. J.; Timmons, R. B. *J. Chem. Phys.* **1969**, *50*, 5076.
(28) Kurylo, M. J.; Hollinden, G. A.; Timmons, R. B. *J. Chem. Phys.* **1970**, *52*, 1773.
(29) Marquaire, P. M.; Dastidar, A. G.; Manthorne, K. C.; Pacey, P. D. *Can. J. Chem.* **1994**, *72*, 600.
(30) Roth, P.; Just, T. *Ber. Bunsen-Ges. Phys. Chem.* **1975**, *79*, 682.
(31) Rabinowitz, M. J.; Sutherland, J. W.; Patterson, P. M.; Klemm, R. B. *J. Phys. Chem.* **1991**, *95*, 674.
(32) Bryukov, M. G.; Slagle, I. R.; Knyazev, V. D. *J. Phys. Chem. A* **2001**, *105*, 3107.
(33) Sutherland, J. W.; Su, M. C.; Michael, J. V. *Int. J. Chem. Kinet.* **2001**, *33*, 669.
(34) Walker, R. W. *J. Chem. Soc., Ser. A* **1968**, 2391.
(35) Clark, T. C.; Dove, J. E. *Can. J. Chem.* **1973**, *51*, 2147.
(36) Shaw, R. *J. Phys. Chem. Ref. Data* **1978**, *7*, 1179.
(37) Warnatz, J. In *Combustion Chemistry*; Gardiner, W. C., Jr., Ed.; Springer-Verlag: New York, 1984; p 233.
(38) Tsang, W.; Hampson, R. F. *J. Phys. Chem. Ref. Data* **1986**, *15*, 1087.
(39) Baulch, D. L.; Cobos, C. J.; Cox, R. A.; Esser, C.; Frank, P.; Just, T.; Kerr, J. A.; Pilling, M. J.; Troe, J.; Walker, R. W.; Warnatz, J. *J. Phys. Chem. Ref. Data* **1992**, *21*, 411.
(40) Frenklach, M.; Goldenberg, M.; Wang, H.; Bowman, C. T.; Hanson, R. K.; Smith, G. P.; Golden, D. M.; Gardiner, W. C.; Lissianski, V. *GRI-Mech 1.2*; Gas Research Institute: Chicago, IL, 1994.
(41) Kobrinsky, P. C.; Pacey, P. D. *Can. J. Chem.* **1974**, *52*, 3665.
(42) Marshall, R. M.; Shahkar, G. *J. Chem. Soc., Faraday Trans.* **1981**, *77*, 2271.
(43) Möller, W.; Mozzhukhin, E.; Wagner, H. G. *Ber. Bunsen-Ges. Phys. Chem.* **1986**, *90*, 854.
(44) Baeck, H. J.; Shin, K. S.; Yang, H.; Qin, Z.; Lissianski, V.; Gardiner, W. C., Jr. *J. Phys. Chem.* **1995**, *99*, 15925.
(45) Taylor, H. S.; Rosenblum, C. *J. Chem. Phys.* **1938**, *6*, 119.
(46) Anderson, R. D.; Taylor, H. A. *J. Phys. Chem.* **1952**, *56*, 498.
(47) Majury, T. G.; Steacie, E. W. R. *Can. J. Chem.* **1952**, *30*, 800.
(48) Davison, S.; Burton, M. *J. Am. Chem. Soc.* **1952**, *74*, 2307.
(49) Whittle, E.; Steacie, E. W. R. *J. Chem. Phys.* **1953**, *21*, 993.
(50) Majury, T. G.; Steacie, E. W. R. *Discuss. Faraday Soc.* **1953**, 45.
(51) Wijnen, M. H. J.; Steacie, E. W. R. *Discuss. Faraday Soc.* **1953**, 118.
(52) Gesser, H.; Steacie, E. W. R. *Can. J. Chem.* **1956**, *34*, 113.
(53) Shapiro, J. S.; Weston, R. E., Jr. *J. Phys. Chem.* **1972**, *76*, 1669.
(54) Knyazev, V. D.; Bencsura, A.; Stoliarov, S. I.; Slagle, I. R. *J. Phys. Chem.* **1996**, *100*, 11346.
(55) Gray, P.; Herod, A. A.; Jones, A. *Chem. Rev.* **1971**, *71*, 247.
(56) Kerr, J. A.; Parsonage, A. M. J. *Evaluated Kinetic Data on Gas-Phase Hydrogen Transfer Reactions of Methyl Radicals*; Butterworths: London, 1976.
(57) Boyd, R. K. *Chem. Rev.* **1977**, *77*, 93.
(58) Lim, C.; Truhlar, D. G. *J. Chem. Phys.* **1983**, *79*, 3296.
(59) Furue, H.; Pacey, P. D. *J. Phys. Chem.* **1990**, *94*, 1419.
(60) Schatz, G. C.; Wagner, A. F.; Dunning, T. H., Jr. *J. Phys. Chem.* **1984**, *88*, 221.
(61) Rebbert, R. E.; Steacie, E. W. R. *Can. J. Chem.* **1954**, *32*, 113.
(62) Benson, S. W.; Jain, D. V. S. *J. Chem. Phys.* **1959**, *31*, 1008.
(63) Pratt, G.; Rogers, D. *J. Chem. Soc., Faraday Trans. I* **1976**, *72*, 2769.
(64) Rodriguez, A. E.; Pacey, P. D. *J. Phys. Chem.* **1986**, *90*, 6298.
(65) Steacie, E. W. R.; Phillips, N. W. F. *J. Chem. Phys.* **1936**, *4*, 461.
(66) Trenner, N. R.; Morikawa, K.; Taylor, H. S. *J. Chem. Phys.* **1937**, *5*, 203.
(67) Germann, G. J.; Huh, Y. D.; Valentini, J. J. *J. Chem. Phys.* **1992**, *96*, 1957.
(68) Chou, C.-C.; Rowland, F. S. *J. Chem. Phys.* **1969**, *50*, 2763.
(69) Chou, C.-C.; Rowland, F. S. *J. Chem. Phys.* **1969**, *50*, 5133.
(70) Chou, C.-C.; Rowland, F. S. *J. Phys. Chem.* **1971**, *75*, 1283.
(71) Ting, C.-T.; Weston, R. E., Jr. *J. Phys. Chem.* **1973**, *77*, 2257.

(72) Momose, T.; Hoshina, H.; Sogoshi, N.; Katsuki, H.; Wakabayashi, T.; Shida, T. *J. Chem. Phys.* **1998**, *108*, 7334.
(73) Hoshina, H.; Fushitani, M.; Momose, T.; Shida, T. *J. Chem. Phys.* **2004**, *120*, 3706.
(74) Wolfgang, R. *Prog. React. Kinet.* **1965**, *3*, 97.
(75) Wolfgang, R. *Ann. Rev. Phys. Chem.* **1965**, *16*, 15.
(76) Valentini, J. J.; Aker, P. M.; Germann, G. J.; Huh, Y. D. *Faraday Discuss. Chem. Soc.* **1991**, *91*, 173.
(77) Germann, G. J.; Huh, Y. D.; Valentini, J. J. *Chem. Phys. Lett.* **1991**, *183*, 353.
(78) Camden, J. P.; Bechtel, H. A.; Zare, R. N. *Angew. Chem., Int. Ed.* **2003**, *42*, 5227.
(79) Camden, J. P.; Bechtel, H. A.; Brown, D. J. A.; Martin, M. R.; Zare, R. N.; Hu, W.; Lendvay, G.; Troya, D.; Schatz, G. C. *J. Am. Chem. Soc.* **2005**, *127*, 11898.
(80) Camden, J. P.; Hu, W.; Bechtel, H. A.; Brown, D. J. A.; Martin, M. R.; Zare, R. N.; Lendvay, G.; Troya, D.; Schatz, G. C. *J. Phys. Chem. A* **2006**, *110*, 677.
(81) Hu, W.; Lendvay, G.; Troya, D.; Schatz, G. C.; Camden, J. P.; Bechtel, H. A.; Brown, D. J. A.; Martin, M. R.; Zare, R. N. *J. Phys. Chem. A* **2006**, *110*, 3017.
(82) Fernandez-Alonso, F.; Bean, B. D.; Ayers, J. D.; Pomerantz, A. E.; Zare, R. N.; Banares, L.; Aoiz, F. J. *Angew. Chem., Int. Ed.* **2000**, *39*, 2748.
(83) Fernandez-Alonso, F.; Zare, R. N. *Ann. Rev. Phys. Chem.* **2002**, *53*, 67.
(84) Camden, J. P.; Bechtel, H. A.; Brown, D. J. A.; Zare, R. N. *J. Chem. Phys.* **2005**, *123*, 134301.
(85) Camden, J. P.; Bechtel, H. A.; Brown, D. J. A.; Zare, R. N. *J. Chem. Phys.* **2006**, *124*, 34311.
(86) Baldridge, K. K.; Gordon, M. S.; Steckler, R.; Truhlar, D. G. *J. Phys. Chem.* **1989**, *93*, 5107.
(87) Truhlar, D. G.; Gordon, M. S. *Science* **1990**, *249*, 491.
(88) Gonzalez-Lafont, A.; Truong, T. N.; Truhlar, D. G. *J. Phys. Chem.* **1991**, *95*, 4618.
(89) Truhlar, D. G. In *The Reaction Path in Chemistry: Current Approaches and Perspectives*; Heidrich, D., Ed.; Kluwer: Dordrecht, The Netherlands, 1995; p 229.
(90) London, F. *Z. Elektrochem.* **1929**, *35*, 552.
(91) Eyring, H.; Walter, J.; Kimball, G. E. *Quantum Chemistry*; Wiley: New York, 1944.
(92) Truhlar, D. G.; Parr, C. A. *J. Phys. Chem.* **1971**, *75*, 1844.
(93) Raff, L. M. *J. Chem. Phys.* **1974**, *60*, 2220.
(94) Chakraborty, A.; Zhao, Y.; Lin, H.; Truhlar, D. G. *J. Chem. Phys.* **2006**, *124*, 44315.
(95) Gorin, E.; Kauzmann, W.; Walter, J.; Eyring, H. *J. Chem. Phys.* **1939**, *7*, 633.
(96) Polanyi, J. C. *J. Chem. Phys.* **1955**, *23*, 1505.
(97) Polanyi, J. C. *J. Chem. Phys.* **1956**, *24*, 493.
(98) Johnston, H. S.; Parr, C. *J. Am. Chem. Soc.* **1963**, *85*, 2544.
(99) Johnston, H. S. *Adv. Chem. Phys.* **1960**, *3*, 131.
(100) Johnston, H. S.; Goldfinger, P. *J. Chem. Phys.* **1962**, *37*, 700.
(101) Arthur, N. L.; McDonell, J. A. *J. Chem. Phys.* **1972**, *56*, 3100.
(102) Arthur, N. L.; Donchi, K. F.; McDonell, J. A. *J. Chem. Phys.* **1975**, *62*, 1585.
(103) Arthur, N. L.; Donchi, K. F.; McDonell, J. A. *J. Chem. Soc., Faraday Trans.* **1975**, *71*, 2431.
(104) Garrett, B. C.; Truhlar, D. G. *J. Am. Chem. Soc.* **1979**, *101*, 4534.
(105) Kuntz, P. J.; Nemeth, E. M.; Polanyi, J. C.; Wong, W. H. *J. Chem. Phys.* **1970**, *52*, 4654.
(106) Eyring, H.; Polanyi, M. *Z. Phys. Chem.* **1931**, *B12*, 279.
(107) Sato, S. *Bull. Chem. Soc. Jpn.* **1955**, *28*, 450.
(108) Sato, S. *J. Chem. Phys.* **1955**, *23*, 2465.
(109) Kuntz, P. J.; Nemeth, E. M.; Polanyi, J. C.; Rosner, S. D.; Young, C. E. *J. Chem. Phys.* **1966**, *44*, 1168.
(110) Balint-Kurti, G. G. *Adv. Chem. Phys.* **1975**, *30*, 137.
(111) Ellison, F. O. *J. Chem. Phys.* **1964**, *41*, 2198.
(112) Eaker, C. W.; Parr, C. A. *J. Chem. Phys.* **1976**, *64*, 1322.
(113) Bunker, D. L.; Pattengill, M. *Chem. Phys. Lett.* **1969**, *4*, 315.
(114) Bunker, D. L.; Pattengill, M. *J. Chem. Phys.* **1970**, *53*, 3041.
(115) Valencich, T.; Bunker, D. L. *Chem. Phys. Lett.* **1973**, *20*, 50.
(116) Valencich, T.; Bunker, D. L. *J. Chem. Phys.* **1974**, *61*, 21.
(117) Chapman, S.; Bunker, D. L. *J. Chem. Phys.* **1975**, *62*, 2890.
(118) Wall, F. T.; Porter, R. N. *J. Chem. Phys.* **1962**, *36*, 3256.
(119) Agmon, N.; Levine, R. D. *J. Chem. Phys.* **1979**, *71*, 3034.
(120) Garrett, B. C.; Truhlar, D. G. *J. Phys. Chem.* **1979**, *83*, 1052.
(121) Wagner, A. F.; Schatz, G. C.; Bowman, J. M. *J. Chem. Phys.* **1981**, *74*, 4960.
(122) Joseph, T.; Truhlar, D. G.; Garrett, B. C. *J. Chem. Phys.* **1988**, *88*, 6982.
(123) Vande Linde, S. R.; Hase, W. L. *J. Phys. Chem.* **1990**, *94*, 2778.
(124) Raff, L. M.; Stivers, L.; Porter, R. N.; Thompson, D. L.; Sims, L. B. *J. Chem. Phys.* **1970**, *52*, 3449.
(125) Pople, J. A.; Beveridge, D. L.; Dobosh, P. A. *J. Chem. Phys.* **1967**, *47*, 2026.
(126) Steckler, R.; Dykema, K. J.; Brown, F. B.; Hancock, G. C.; Truhlar, D. G.; Valencich, T. *J. Chem. Phys.* **1987**, *87*, 7024.
(127) Huang, J.; Valentini, J. J.; Muckerman, J. T. *J. Chem. Phys.* **1995**, *102*, 5695.
(128) Duchovic, R. J.; Hase, W. L.; Schlegel, H. B. *J. Phys. Chem.* **1984**, *88*, 1339.
(129) Joseph, T.; Steckler, R.; Truhlar, D. G. *J. Chem. Phys.* **1987**, *87*, 7036.
(130) Walch, S. P. *J. Chem. Phys.* 1980, *72*, 4932.
(131) Schatz, G. C.; Walch, S. P.; Wagner, A. F. *J. Chem. Phys.* **1980**, *73*, 4536.
(132) Sana, M.; Leroy, G.; Villaveces, J. L. *Theor. Chim. Acta* **1984**, *65*, 109.
(133) Jordan, M. J. T.; Gilbert, R. G. *J. Chem. Phys.* **1995**, *102*, 5669.
(134) Espinosa-Garcia, J.; Corchado, J. C. *J. Phys. Chem.* **1996**, *100*, 16561.
(135) Yu, H.-G. *Chem. Phys. Lett.* **2000**, *332*, 538.
(136) Kerkeni, B.; Clary, D. C. *J. Chem. Phys.* **2004**, *120*, 2308.
(137) Pu, J.; Truhlar, D. G. *J. Chem. Phys.* **2002**, *116*, 1468.
(138) Pu, J.; Truhlar, D. G. *J. Chem. Phys.* **2002**, *117*, 10675.
(139) Varandas, A. J. C.; Caridade, P. J. S. B.; Zhang, J. Z. H.; Cui, Q.; Han, K. L. *J. Chem. Phys.* **2006**, *125*, 64312.
(140) Pu, J.; Truhlar, D. G. *J. Chem. Phys.* **2002**, *117*, 1479.
(141) Huarte-Larrañaga, F.; Manthe, U. *J. Phys. Chem. A* **2001**, *105*, 2522.
(142) Bowman, J. M.; Wang, D.; Huang, X.; Huarte-Larranaga, F.; Manthe, U. *J. Chem. Phys.* **2001**, *114*, 9683.
(143) Huarte-Larrañaga, F.; Manthe, U. *J. Chem. Phys.* **2000**, *113*, 5115.
(144) Miller, W. H.; Schwartz, S. D.; Tromp, J. W. *J. Chem. Phys.* **1983**, *79*, 4889.
(145) Tromp, J. W.; Miller, W. H. *Faraday Discuss. Chem. Soc.* **1987**, *84*, 441.
(146) Pu, J.; Corchado, J. C.; Truhlar, D. G. *J. Chem. Phys.* **2001**, *115*, 6266.
(147) Allison, T. C.; Truhlar, D. G. In *Modern Methods for Multidimensional Dynamics Computations in Chemistry*; Thompson, D. L., Ed.; World Scientific: Singapore, 1998; p 618.
(148) Tucker, S. C.; Truhlar, D. G. In *New Theoretical Concepts Understanding Organic Reactions*; Bertran, J., Csizmodia, I. G., Ed.; NATO ASI Series C 267; Kluwer Academic Publishers: Dordrecht, The Netherlands, 1989; p 291.
(149) Espinosa-Garcia, J. *J. Chem. Phys.* **1999**, *111*, 9330.
(150) Espinosa-Garcia, J. *J. Chem. Phys.* **2002**, *116*, 10664.
(151) Rangel, C.; Garcia-Bernaldez, J. C.; Espinosa-Garcia, J. *Chem. Phys. Lett.* **2006**, *422*, 581.
(152) Rangel, C.; Corchado, J. C.; Espinosa-Garcia, J. *J. Phys. Chem. A* **2006**, *110*, 10375.
(153) Rangel, C.; Sanson, J.; Corchado, J. C.; Espinosa-Garcia, J.; Nyman, G. *J. Phys. Chem. A* **2006**, *110*, 10715.
(154) Espinosa-Garcia, J.; Sanson, J.; Corchado, J. C. *J. Chem. Phys.* **1998**, *109*, 466.
(155) Espinosa-Garcia, J.; Garcia-Bernaldez, J. C. *Phys. Chem. Chem. Phys.* **2000**, *2*, 2345.
(156) Rangel, C.; Navarrete, M.; Espinosa-Garcia, J. *J. Phys. Chem. A* **2005**, *109*, 1441.
(157) Espinosa-Garcia, J.; Bravo, J. L.; Rangel, C. *J. Phys. Chem. A* **2007**, *111*, 2761.
(158) Corchado, J. C.; Truhlar, D. G.; Espinosa-Garcia, J. *J. Chem. Phys.* **2000**, *112*, 9375.
(159) Rangel, C.; Navarrete, M.; Corchado, J. C.; Espinosa-Garcia, J. *J. Chem. Phys.* **2006**, *124*, 124306.
(160) Espinosa-Garcia, J. *J. Chem. Phys.* **2002**, *117*, 2076.
(161) Rangel, C.; Espinosa-Garcia, J. *J. Chem. Phys.* **2005**, *122*, 134315.
(162) Espinosa-Garcia, J.; Corchado, J. C. *J. Chem. Phys.* **2000**, *112*, 5731.
(163) Rangel, C.; Espinosa-Garcia, J. *J. Phys. Chem. A* **2006**, *110*, 537.
(164) Rangel, C.; Espinosa-Garcia, J. *J. Phys. Chem. A* **2007**, *111*, 5057.
(165) Espinosa-Garcia, J.; Corchado, J. C. *Recent Res. Dev. Phys. Chem.* **1997**, *1*, 165.
(166) Espinosa-Garcia, J. *Trends Chem. Phys.* **2000**, *8*, 49.
(167) Jaquet, R. *Lect. Notes Chem.* **1999**, *71*, 97.
(168) Schatz, G. C. *Lect. Notes Chem.* **2000**, *75*, 15.
(169) Rossi, I.; Truhlar, D. G. *Chem. Phys. Lett.* **1995**, *233*, 231.
(170) Truhlar, D. G.; Brown, F. B.; Steckler, R.; Isaacson, A. D. In *The Theory of Chemical Reaction Dynamics*; Clary, D. C., Ed.; NATO ASI Series C; Reidel: Dordrecht, The Netherlands, 1986; Vol. 170, p 285.
(171) Becke, A. D. *J. Chem. Phys.* **1993**, *98*, 5648.
(172) Møller, C.; Plesset, M. S. *Phys. Rev.* **1934**, *46*, 618.
(173) Head-Gordon, M.; Pople, J. A.; Frisch, M. J. *Chem. Phys. Lett.* **1988**, *153*, 503.
(174) Krishnan, R.; Pople, J. A. *Int. J. Quantum Chem.* **1978**, *14*, 91.
(175) Pople, J. A.; Seeger, R.; Krishnan, R. *Int. J. Quantum Chem. Symp.* **1977**, *11*, 149.

(176) Krishnan, R.; Schlegel, H. B.; Pople, J. A. *J. Chem. Phys.* **1980**, *72*, 4654.
(177) Raghavachari, K.; Pople, J. A. *Int. J. Quantum Chem.* **1981**, *20*, 1067.
(178) Pople, J. A.; Head-Gordon, M.; Raghavachari, K. *J. Chem. Phys.* **1987**, *87*, 5968.
(179) Cizek, J. *Adv. Chem. Phys.* **1969**, *14*, 35.
(180) Pople, J. A.; Krishnan, R.; Schlegel, H. B.; Binkley, J. S. *Int. J. Quantum Chem.* **1978**, *14*, 545.
(181) Bartlett, R. J. *Ann. Rev. Phys. Chem.* **1981**, *32*, 359.
(182) Purvis, G. D., III; Bartlett, R. J. *J. Chem. Phys.* **1981**, *75*, 1284.
(183) Purvis, G. D., III; Bartlett, R. J. *J. Chem. Phys.* **1982**, *76*, 1910.
(184) Scuseria, G. E.; Janssen, C. L.; Schaefer, H. F., III *J. Chem. Phys.* **1988**, *89*, 7382.
(185) Scuseria, G. E.; Schaefer, H. F., III *Chem. Phys. Lett.* **1988**, *152*, 382.
(186) Scuseria, G. E.; Schaefer, H. F., III *J. Chem. Phys.* **1989**, *90*, 3700.
(187) Villaume, S.; Daniel, C.; Strich, A.; Perera, S. A.; Bartlett, R. J. *J. Chem. Phys.* **2005**, *122*, 44313.
(188) Curtiss, L. A.; Raghavachari, K.; Trucks, G. W.; Pople, J. A. *J. Chem. Phys.* **1991**, *94*, 7221.
(189) Curtiss, L. A.; Raghavachari, K.; Redfern, P. C.; Rassolov, V.; Pople, J. A. *J. Chem. Phys.* **1998**, *109*, 7764.
(190) Curtiss, L. A.; Raghavachari, K.; Redfern, P. C.; Pople, J. A. *J. Chem. Phys.* **2000**, *112*, 1125.
(191) Curtiss, L. A.; Redfern, P. C.; Raghavachari, K. *J. Chem. Phys.* **2007**, *126*, 084108/1.
(192) Fast, P. L.; Corchado, J. C.; Sanchez, M. L.; Truhlar, D. G. *J. Phys. Chem. A* **1999**, *103*, 5129.
(193) Fast, P. L.; Sanchez, M. L.; Truhlar, D. G. *Chem. Phys. Lett.* **1999**, *306*, 407.
(194) Tratz, C. M.; Fast, P. L.; Truhlar, D. G. *PhysChemComm* **1999**, *2* (14), 79.
(195) Rodgers, J. M.; Fast, P. L.; Truhlar, D. G. *J. Chem. Phys.* **2000**, *112*, 3141.
(196) Fast, P. L.; Truhlar, D. G. *J. Phys. Chem. A* **2000**, *104*, 6111.
(197) González, C.; McDouall, J. J. W.; Schlegel, H. B. *J. Phys. Chem.* **1990**, *94*, 7467.
(198) Kraka, E.; Gauss, J.; Cremer, D. *J. Chem. Phys.* **1993**, *99*, 5306.
(199) Truong, T. N. *J. Chem. Phys.* **1994**, *100*, 8014.
(200) Truong, T. N.; Duncan, W. *J. Chem. Phys.* **1994**, *101*, 7408.
(201) Dobbs, K. D.; Dixon, D. A. *J. Phys. Chem.* **1994**, *98*, 5290.
(202) Porezag, D.; Pederson, M. R. *J. Chem. Phys.* **1995**, *102*, 9345.
(203) Jursic, B. S. *Chem. Phys. Lett.* **1996**, *256*, 603.
(204) Jursic, B. S. *Theochem* **1998**, *430*, 17.
(205) Kurosaki, Y.; Takayanagi, T. *Chem. Phys. Lett.* **1999**, *299*, 57.
(206) Kurosaki, Y.; Takayanagi, T. *J. Chem. Phys.* **1999**, *110*, 10830.
(207) Patchkovskii, S.; Ziegler, T. *J. Chem. Phys.* **2002**, *116*, 7806.
(208) Fast, P. L.; Schultz, N. E.; Truhlar, D. G. *J. Phys. Chem. A* **2001**, *105*, 4143.
(209) Lynch, B. J.; Truhlar, D. G. *J. Phys. Chem. A* **2003**, *107*, 3898.
(210) Zheng, J.; Zhao, Y.; Truhlar, D. G. *J. Chem. Theory Comput.* **2007**, *3*, 569.
(211) Adamo, C.; Barone, V. *J. Chem. Phys.* **1998**, *108*, 664.
(212) Perdew, J. P. In *Electronic Structure of Solids*; Ziesche, P., Eschrig, H., Eds.; Akademie Verlag: Berlin, 1991; p 11.
(213) Lynch, B. J.; Fast, P. L.; Harris, M.; Truhlar, D. G. *J. Phys. Chem. A* **2000**, *104*, 4811.
(214) Ischtwan, J.; Collins, M. A. *J. Chem. Phys.* **1994**, *100*, 8080.
(215) Jordan, M. J. T.; Thompson, K. C.; Collins, M. A. *J. Chem. Phys.* **1995**, *103*, 9669.
(216) Jordan, M. J. T.; Thompson, K. C.; Collins, M. A. *J. Chem. Phys.* **1995**, *102*, 5647.
(217) Thompson, K. C.; Collins, M. A. *J. Chem. Soc., Faraday Trans.* **1997**, *93*, 871.
(218) Jordan, M. J. T.; Collins, M. A. *J. Chem. Phys.* **1996**, *104*, 4600.
(219) Collins, M. A. *Theor. Chem. Acc.* **2002**, *108*, 313.
(220) Collins, M. A. *Adv. Chem. Phys.* **1996**, *93*, 389.
(221) Thompson, K. C.; Jordan, M. J. T.; Collins, M. A. *J. Chem. Phys.* **1998**, *108*, 8302.
(222) Takata, T.; Taketsugu, T.; Hirao, K.; Gordon, M. S. *J. Chem. Phys.* **1998**, *109*, 4281.
(223) Wu, T.; Manthe, U. *J. Chem. Phys.* **2003**, *119*, 14.
(224) Lancaster, P.; Salkauskas, K. *Curve and Surface Fitting. An Introduction*; Academic: London, 1986.
(225) Farnig, R. In *Algorithms for Approximation*; Mason, J. C., Cox, M. G., Eds.; Clareton Press: Oxford, U.K., 1987; p 194.
(226) Wu, T.; Werner, H.-J.; Manthe, U. *Science* **2004**, *306*, 2227.
(227) Wu, T.; Werner, H.-J.; Manthe, U. *J. Chem. Phys.* **2006**, *124*, 164307.
(228) Huang, X.; Braams, B. J.; Bowman, J. M. *J. Chem. Phys.* **2005**, *122*, 44308.
(229) Xie, Z.; Braams, B. J.; Bowman, J. M. *J. Chem. Phys.* **2005**, *122*, 224307.
(230) Zhang, X.; Braams, B. J.; Bowman, J. M. *J. Chem. Phys.* **2006**, *124*, 21104.
(231) Xie, Z.; Bowman, J. M.; Zhang, X. *J. Chem. Phys.* **2006**, *125*, 133120.
(232) Xie, Z.; Bowman, J. M. *Chem. Phys. Lett.* **2006**, *429*, 355.
(233) Kim, Y.; Corchado, J. C.; Villa, J.; Xing, J.; Truhlar, D. G. *J. Chem. Phys.* **2000**, *112*, 2718.
(234) Albu, T. V.; Corchado, J. C.; Truhlar, D. G. *J. Phys. Chem. A* **2001**, *105*, 8465.
(235) Lin, H.; Pu, J.; Albu, T. V.; Truhlar, D. G. *J. Phys. Chem. A* **2004**, *108*, 4112.
(236) Gao, J.; Thompson, M. A. *Combined Quantum Mechanical and Molecular Mechanical Methods*; American Chemical Society: Washington DC, 1998.
(237) Gao, J.; Truhlar, D. G. *Ann. Rev. Phys. Chem.* **2002**, *53*, 467.
(238) Ellison, F. O. *J. Am. Chem. Soc.* **1963**, *85*, 3540.
(239) Blais, N. C.; Truhlar, D. G. *J. Chem. Phys.* **1973**, *58*, 1090.
(240) Tully, J. C. In *Semiempirical Methods of Electronic Structure Theory, Part A: Techniques*; Segal, G. A., Ed.; Plenum: New York, 1977; p 173.
(241) Kuntz, P. J. In *Atom-Molecule Collision Theory*; Bernstein, R. B., Ed.; Plenum: New York, 1979; p 79.
(242) Faist, M. B.; Muckerman, J. T. *J. Chem. Phys.* **1979**, *71*, 225.
(243) Warshel, A.; Weiss, R. M. *J. Am. Chem. Soc.* **1980**, *102*, 6218.
(244) Warshel, A. *Computer Modeling of Chemical Reactions in Enzymes and Solutions*; John Wiley & Sons: New York, 1991.
(245) Aaqvist, J.; Warshel, A. *Chem. Rev.* **1993**, *93*, 2523.
(246) Aaqvist, J. In *Computational Approaches to Biochemical Reactivity*; Naray-Szabo, G., Warshel, A., Eds.; Understanding Chemical Reactivity; Kluwer Academic: Dordrecht, The Netherlands, 1997; Vol. 19, p 341.
(247) Kolmodin, K.; Hansson, T.; Danielsson, J.; Aqvist, J. *ACS Symp. Ser.* **1999**, *721*, 370.
(248) Chang, Y. T.; Miller, W. H. *J. Phys. Chem.* **1990**, *94*, 5884.
(249) Chang, Y. T.; Minichino, C.; Miller, W. H. *J. Chem. Phys.* **1992**, *96*, 4341.
(250) Jackels, C. F.; Gu, Z.; Truhlar, D. G. *J. Chem. Phys.* **1995**, *102*, 3188.
(251) Nguyen, K. A.; Jackels, C. F.; Truhlar, D. G. *J. Chem. Phys.* **1996**, *104*, 6491.
(252) Chuang, Y.-Y.; Truhlar, D. G. *J. Phys. Chem. A* **1998**, *102*, 242.
(253) Nguyen, K. A.; Rossi, I.; Truhlar, D. G. *J. Chem. Phys.* **1995**, *103*, 5522.
(254) Lin, H.; Zhao, Y.; Tishchenko, O.; Truhlar, D. G. *J. Chem. Theory Comput.* **2006**, *2*, 1237.
(255) Tishchenko, O.; Truhlar, D. G. *J. Phys. Chem. A* **2006**, *110*, 13530.
(256) Tishchenko, O.; Truhlar, D. G. *J. Chem. Theory Comput.* **2007**, *3*, 938.
(257) Truhlar, D. G. *J. Phys. Chem. A* **2002**, *106*, 5048.
(258) Fukui, K. In *The World of Quantum Chemistry*; Daudel, R., Pullman, B., Eds.; Reidel: Dordrecht, The Netherlands, 1974; p 113.
(259) Fukui, K.; Kato, S.; Fujimoto, H. *J. Am. Chem. Soc.* **1975**, *97*, 1.
(260) Fukui, K. *Acc. Chem. Res.* **1981**, *14*, 363.
(261) Marcus, R. A. *J. Chem. Phys.* **1966**, *45*, 4493.
(262) Marcus, R. A. *J. Chem. Phys.* **1968**, *49*, 2610.
(263) Shavitt, I.; Stevens, R. M.; Minn, F.; Karplus, M. *J. Chem. Phys.* **1968**, *48*, 2700.
(264) Truhlar, D. G.; Kuppermann, A. *J. Am. Chem. Soc.* **1971**, *93*, 1840.
(265) Garrett, B. C.; Truhlar, D. G. *J. Phys. Chem.* **1979**, *83*, 1079.
(266) Fukui, K. *J. Phys. Chem.* **1970**, *74*, 4161.
(267) Page, M. *Comput. Phys. Commun.* **1994**, *84*, 115.
(268) Miller, W. H.; Handy, N. C.; Adams, J. E. *J. Chem. Phys.* **1980**, *72*, 99.
(269) Hofacker, L. *Z. Naturforsch., A* **1963**, *18*, 607.
(270) Marcus, R. A. *Discuss. Faraday Soc.* **1967**, *44*, 7.
(271) Isaacson, A. D.; Truhlar, D. G. *J. Chem. Phys.* **1982**, *76*, 1380.
(272) Miller, W. H. In *The Theory of Chemical Reaction Dynamics*; Clary, D. C., Ed.; NATO ASI Series C; Reidel: Dordrecht, The Netherlands, 1986; Vol. 170, p 27.
(273) Melissas, V. S.; Truhlar, D. G.; Garrett, B. C. *J. Chem. Phys.* **1992**, *96*, 5758.
(274) Garrett, B. C.; Redmon, M. J.; Steckler, R.; Truhlar, D. G.; Baldridge, K. K.; Bartol, D.; Schmidt, M. W.; Gordon, M. S. *J. Phys. Chem.* **1988**, *92*, 1476.
(275) Page, M.; McIver, J. W., Jr. *J. Chem. Phys.* **1988**, *88*, 922.
(276) Gonzalez, C.; Schlegel, H. B. *J. Chem. Phys.* **1989**, *90*, 2154.
(277) Gonzalez, C.; Schlegel, H. B. *J. Phys. Chem.* **1990**, *94*, 5523.
(278) Pulay, P. In *Applications of Electronic Structure Theory*; Schaefer, H. F., III, Ed.; Plenum Press: New York, 1977; p 153.
(279) McIver, J. W., Jr.; Komornicki, A. *J. Am. Chem. Soc.* **1972**, *94*, 2625.
(280) McIver, J. W., Jr.; Komornicki, A. *Chem. Phys. Lett.* **1971**, *10*, 303.
(281) Pople, J. A.; Krishnan, R.; Schlegel, H. B.; Binkley, J. S. *Int. J. Quantum Chem. Symp.* **1979**, *13*, 225.

(282) Pople, J. A.; Schlegel, H. B.; Krishnan, R.; Defrees, D. J.; Binkley, J. S.; Frisch, M. J.; Whiteside, R. A.; Hout, R. F.; Hehre, W. J. *Int. J. Quantum Chem. Symp.* **1981**, *15*, 269.
(283) Garratt, J.; Mills, I. M. *J. Chem. Phys.* **1968**, *49*, 1719.
(284) Handy, N. C.; Schaefer, H. F., III *J. Chem. Phys.* **1984**, *81*, 5031.
(285) Hoffmann, M. R.; Fox, D. J.; Gaw, J. F.; Osamura, Y.; Yamaguchi, Y.; Grev, R. S.; Fitzgerald, G.; Schaefer, H. F., III; Knowles, P. J.; Handy, N. C. *J. Chem. Phys.* **1984**, *80*, 2660.
(286) Fischer, S. F.; Hofacker, G. L.; Seiler, R. *J. Chem. Phys.* **1969**, *51*, 3951.
(287) Garrett, B. C.; Truhlar, D. G. *J. Chem. Phys.* **1979**, *70*, 1593.
(288) Taketsugu, T.; Gordon, M. S. *J. Chem. Phys.* **1996**, *104*, 2834.
(289) Konkoli, Z.; Kraka, E.; Cremer, D. *J. Phys. Chem. A* **1997**, *101*, 1742.
(290) Konkoli, Z.; Cremer, D.; Kraka, E. *J. Comput. Chem.* **1997**, *18*, 1282.
(291) Konkoli, Z.; Cremer, D. *Int. J. Quantum Chem.* **1998**, *67*, 1.
(292) Konkoli, Z.; Larsson, J. A.; Cremer, D. *Int. J. Quantum Chem.* **1998**, *67*, 11.
(293) Konkoli, Z.; Cremer, D. *Int. J. Quantum Chem.* **1998**, *67*, 29.
(294) Konkoli, Z.; Larsson, J. A.; Cremer, D. *Int. J. Quantum Chem.* **1998**, *67*, 41.
(295) Okuno, Y. *J. Chem. Phys.* **2000**, *113*, 3130.
(296) Okuno, Y.; Yokoyama, S.; Mashiko, S. *J. Chem. Phys.* **2000**, *113*, 3136.
(297) Natanson, G. *J. Chem. Phys.* **2002**, *117*, 6378.
(298) Billing, G. D. *Chem. Phys.* **2002**, *277*, 325.
(299) Garrett, B. C.; Truhlar, D. G. *J. Chem. Phys.* **1984**, *81*, 309.
(300) Truhlar, D. G.; Garrett, B. C.; Hipes, P. G.; Kuppermann, A. *J. Chem. Phys.* **1984**, *81*, 3542.
(301) Truhlar, D. G.; Isaacson, A. D.; Garrett, B. C. In *Theory of Chemical Reaction Dynamics*; Baer, M., Ed.; CRC Press: Boca Raton, FL, 1985; p 65.
(302) Kreevoy, M. M.; Truhlar, D. G. In *Investigation of Rates and Mechanisms of Reactions*, 4th ed.; Bernasconi, C. F., Ed.; Techniques of Chemistry Series 6; John Wiley & Sons, Inc.: New York, 1986; Part 1, p 13.
(303) Truhlar, D. G.; Garrett, B. C.; Klippenstein, S. J. *J. Phys. Chem.* **1996**, *100*, 12771.
(304) Garrett, B. C.; Truhlar, D. G.; Grev, R. S.; Magnuson, A. W. *J. Phys. Chem.* **1980**, *84*, 1730.
(305) Truhlar, D. G.; Garrett, B. C. *Acc. Chem. Res.* **1980**, *13*, 440.
(306) Fernandez-Ramos, A.; Ellingson, B. A.; Garrett, B. C.; Truhlar, D. G. In *Reviews in Computational Chemistry*; Lipkowitz, K. B., Cundari, T. R., Eds.; Wiley-VCH: Hoboken, NJ, 2007; Vol. 23, p 125.
(307) Glasstone, S.; Laidler, K. J.; Eyring, H. *The Theory of Rate Processes. The Kinetics of Chemical Reactions, Viscosity, Diffusion and Electrochemical Phenomena*; McGraw-Hill: New York, 1941.
(308) Isaacson, A. D. *J. Phys. Chem. A* **2006**, *110*, 379.
(309) Masgrau, L.; Gonzalez-Lafont, A.; Lluch, J. M. *J. Comput. Chem.* **2003**, *24*, 701.
(310) Vansteenkiste, P.; Van Neck, D.; Van Speybroeck, V.; Waroquier, M. *J. Chem. Phys.* **2006**, *124*, 44314.
(311) Vansteenkiste, P.; Van Neck, D.; Van Speybroeck, V.; Waroquier, M. *J. Chem. Phys.* **2006**, *125*, 49902.
(312) Ellingson, B. A.; Pu, J.; Lin, H.; Zhao, Y.; Truhlar, D. G. *J. Phys. Chem. A*, in press.
(313) Lu, D.-h.; Truong, T. N.; Melissas, V. S.; Lynch, G. C.; Liu, Y.-P.; Garrett, B. C.; Steckler, R.; Isaacson, A. D.; Rai, S. N.; Hancock, G. C.; Lauderdale, J. G.; Joseph, T.; Truhlar, D. G. *Comput. Phys. Commun.* **1992**, *71*, 235.
(314) Liu, Y. P.; Lynch, G. C.; Truong, T. N.; Lu, D. H.; Truhlar, D. G.; Garrett, B. C. *J. Am. Chem. Soc.* **1993**, *115*, 2408.
(315) Truong, T. N.; Lu, D.-h.; Lynch, G. C.; Liu, Y.-P.; Melissas, V. S.; Stewart, J. J. P.; Steckler, R.; Garrett, B. C.; Isaacson, A. D.; Gonzalez-Lafont, A.; Rai, S. N.; Hancock, G. C.; Joseph, T.; Truhlar, D. G. *Comput. Phys. Commun.* **1993**, *75*, 143.
(316) Fernandez-Ramos, A.; Truhlar, D. G. *J. Chem. Phys.* **2001**, *114*, 1491.
(317) Garrett, B. C.; Truhlar, D. G. *J. Phys. Chem.* **1979**, *83*, 2921.
(318) Fernandez-Ramos, A.; Martinez-Nunez, E.; Smedarchina, Z.; Vazquez, S. A. *Chem. Phys. Lett.* **2001**, *341*, 351.
(319) Karplus, M.; Porter, R. N.; Sharma, R. D. *J. Chem. Phys.* **1965**, *43*, 3259.
(320) Truhlar, D. G.; Muckerman, J. T. In *Atom-Molecule Collision Theory: A Guide to the Experimentalist*; Bernstein, R. B., Ed.; Plenum Press: New York, 1979; p 505.
(321) Bonnet, L.; Rayez, J. C. *Chem. Phys. Lett.* **1997**, *277*, 183.
(322) Bonnet, L.; Rayez, J.-C. *Chem. Phys. Lett.* **2004**, *397*, 106.
(323) Gonzalez-Martinez, M. L.; Bonnet, L.; Larregaray, P.; Rayez, J. C. *J. Chem. Phys.* **2007**, *126*, 041102/1.
(324) Alimi, R.; Garcia-Vela, A.; Gerber, R. B. *J. Chem. Phys.* **1992**, *96*, 2034.
(325) Eaker, C. W.; Schwenke, D. W. *J. Chem. Phys.* **1995**, *103*, 6984.
(326) Guo, Y.; Thompson, D. L.; Sewell, T. D. *J. Chem. Phys.* **1996**, *104*, 576.
(327) McCormack, D. A.; Lim, K. F. *J. Chem. Phys.* **1997**, *106*, 572.
(328) Schatz, G. C.; Horst, M. T.; Takayanagi, T. In *Modern Methods for Multidimensional Dynamics Computations in Chemistry*; Thompson, D. L., Ed.; World Scientific: Singapore, 1998; p 1.
(329) McCormack, D. A.; Lim, K. F. *Phys. Chem. Chem. Phys.* **1999**, *1*, 1.
(330) Xie, Z.; Bowman, J. M. *J. Phys. Chem. A* **2006**, *110*, 5446.
(331) Kouri, D. J.; Sun, Y.; Mowrey, J. Z.; Zhang, H.; Truhlar, D. G.; Haug, K.; Schwenke, D. W. In *Mathematical Frontiers in Computational Chemical Physics*; Truhlar, D. G., Ed.; Springer-Verlag: New York, 1988; p 207.
(332) Light, J. C.; Walker, R. B. *J. Chem. Phys.* **1976**, *65*, 4272.
(333) Truhlar, D. G.; Schwenke, D. W.; Kouri, D. J. *J. Phys. Chem.* **1990**, *94*, 7346.
(334) Zhang, D. H.; Zhang, J. Z. H. *J. Chem. Phys.* **1994**, *101*, 1146.
(335) Zarur, G.; Rabitz, H. *J. Chem. Phys.* **1974**, *60*, 2057.
(336) Clary, D. C.; Schatz, G. C. *J. Chem. Phys.* **1993**, *99*, 4578.
(337) Palma, J.; Clary, D. C. *J. Chem. Phys.* **2000**, *112*, 1859.
(338) Kerkeni, B.; Clary, D. C. *Phys. Chem. Chem. Phys.* **2006**, *8*, 917.
(339) Yamamoto, T. *J. Chem. Phys.* **1960**, *33*, 281.
(340) Miller, W. H. *J. Chem. Phys.* **1974**, *61*, 1823.
(341) Marcus, R. A. *J. Chem. Phys.* **1966**, *45*, 2138.
(342) Greene, E. F.; Kuppermann, A. *J. Chem. Educ.* **1968**, *45*, 361.
(343) Takayanagi, T. *J. Chem. Phys.* **1996**, *104*, 2237.
(344) Yu, H.-G.; Nyman, G. *J. Chem. Phys.* **1999**, *111*, 3508.
(345) Wang, M. L.; Li, Y.; Zhang, J. Z. H.; Zhang, D. H. *J. Chem. Phys.* **2000**, *113*, 1802.
(346) Wang, M.; Zhang, J. Z. H. *J. Chem. Phys.* **2002**, *116*, 6497.
(347) Wang, M. L.; Zhang, J. Z. H. *J. Chem. Phys.* **2002**, *117*, 10425.
(348) Wang, M. L.; Zhang, J. Z. H. *J. Chem. Phys.* **2002**, *117*, 3081.
(349) Wang, M. L.; Zhang, J. Z. H. *J. Chem. Phys.* **2002**, *117*, 10426.
(350) Wang, D.; Bowman, J. M. *J. Chem. Phys.* **2001**, *115*, 2055.
(351) Li, Y. M.; Zhang, J. Z. H. *J. Theor. Comput. Chem.* **2002**, *1*, 25.
(352) Bowman, J. M. *Theor. Chem. Acc.* **2002**, *108*, 125.
(353) Mortensen, E. M.; Pitzer, K. S. *Chem. Soc. (London) Spec. Publ.* **1962**, (16), 57.
(354) Mortensen, E. M. *J. Chem. Phys.* **1968**, *48*, 4029.
(355) Garrett, B. C.; Truhlar, D. G. *Proc. Natl. Acad. Sci. U.S.A.* **1979**, *76*, 4755.
(356) Bowman, J. M.; Ju, G. Z.; Lee, K. T. *J. Chem. Phys.* **1981**, *75*, 5199.
(357) Palma, J.; Echave, J.; Clary, D. C. *J. Phys. Chem. A* **2002**, *106*, 8256.
(358) Yang, M.; Zhang, D. H.; Lee, S.-Y. *J. Chem. Phys.* **2002**, *117*, 9539.
(359) Kerkeni, B.; Clary, D. C. *J. Phys. Chem. A* **2003**, *107*, 10851.
(360) Kerkeni, B.; Clary, D. C. *J. Phys. Chem. A* **2004**, *108*, 8966.
(361) Kerkeni, B.; Clary, D. C. *Chem. Phys. Lett.* **2006**, *421*, 499.
(362) Szichman, H.; Baer, R. *J. Chem. Phys.* **2002**, *117*, 7614.
(363) Haug, K.; Schwenke, D. W.; Shima, Y.; Truhlar, D. G.; Zhang, J.; Kouri, D. J. *J. Phys. Chem.* **1986**, *90*, 6757.
(364) Huarte-Larrañaga, F.; Manthe, U. *J. Chem. Phys.* **2002**, *116*, 2863.
(365) van Harrevelt, R.; Nyman, G.; Manthe, U. *J. Chem. Phys.* **2007**, *126*, 84303.
(366) Meyer, H. D.; Manthe, U.; Cederbaum, L. S. *Chem. Phys. Lett.* **1990**, *165*, 73.
(367) Manthe, U.; Meyer, H. D.; Cederbaum, L. S. *J. Chem. Phys.* **1992**, *97*, 3199.
(368) Manthe, U. *Chem. Phys.* **2006**, *329*, 168.
(369) Manthe, U. *J. Theor. Comp. Chem.* **2002**, *1*, 153.
(370) Wang, D. *J. Chem. Phys.* **2002**, *117*, 9806.
(371) Wang, D. *J. Chem. Phys.* **2003**, *118*, 1184.
(372) Goodson, D. Z.; Roelse, D. W.; Chiang, W.-T.; Valone, S. M.; Doll, J. D. *J. Am. Chem. Soc.* **2000**, *122*, 9189.
(373) Zhao, Y.; Yamamoto, T.; Miller, W. H. *J. Chem. Phys.* **2004**, *120*, 3100.
(374) Miller, W. H.; Zhao, Y.; Ceotto, M.; Yang, S. *J. Chem. Phys.* **2003**, *119*, 1329.
(375) Eyring, H. *J. Chem. Phys.* **1935**, *3*, 107.
(376) Evans, M. G.; Polanyi, M. *Trans. Faraday Soc.* **1935**, *31*, 875.
(377) Gray, S. K.; Miller, W. H.; Yamaguchi, Y.; Schaefer, H. F., III *J. Am. Chem. Soc.* **1981**, *103*, 1900.
(378) Carrington, T., Jr.; Hubbard, L. M.; Schaefer, H. F., III; Miller, W. H. *J. Chem. Phys.* **1984**, *80*, 4347.
(379) Truhlar, D. G.; Kilpatrick, N. J.; Garrett, B. C. *J. Chem. Phys.* **1983**, *78*, 2438.
(380) Gonzalez-Lafont, A.; Truong, T. N.; Truhlar, D. G. *J. Chem. Phys.* **1991**, *95*, 8875.
(381) Skodje, R. T.; Schwenke, D. W.; Truhlar, D. G.; Garrett, B. C. *J. Phys. Chem.* **1984**, *88*, 628.
(382) Horiuti, J. *Bull. Chem. Soc. Jpn.* **1938**, *13*, 210.
(383) Keck, J. C. *Adv. Chem. Phys.* **1967**, *13*, 85.
(384) Wang, I. S. Y.; Karplus, M. *J. Am. Chem. Soc.* **1973**, *95*, 8160.

(385) Malcolme-Lawes, D. J. *J. Chem. Soc., Faraday Trans. II* **1975**, *71*, 1183.
(386) Leforestier, C. *J. Chem. Phys.* **1978**, *68*, 4406.
(387) Truhlar, D. G.; Duff, J. W.; Blais, N. C.; Tully, J. C.; Garrett, B. C. *J. Chem. Phys.* **1982**, *77*, 764.
(388) Helgaker, T.; Uggerud, E.; Jensen, H. J. A. *Chem. Phys. Lett.* **1990**, *173*, 145.
(389) Car, R.; Parrinello, M. *Phys. Rev. Lett.* **1985**, *55*, 2471.
(390) Tachibana, A.; Fueno, H.; Yamabe, T. *J. Am. Chem. Soc.* **1986**, *108*, 4346.
(391) Doubleday, C., Jr.; McIver, J. W., Jr.; Page, M. *J. Phys. Chem.* **1988**, *92*, 4367.
(392) Field, M. J. *Chem. Phys. Lett.* **1990**, *172*, 83.
(393) Eckart, C. *Phys. Rev.* **1930**, *35*, 1303.
(394) Hartmann, H.; Grein, F.; Zettler-Thieler, P. *Z. Phys. Chem.* **1960**, *23*, 139.
(395) Kaufman, J. J.; Harkins, J. J.; Koski, W. S. *Int. J. Quantum Chem.* **1967**, *1s*, 261.
(396) Lathan, W. A.; Hehre, W. J.; Curtiss, L. A.; Pople, J. A. *J. Am. Chem. Soc.* **1971**, *93*, 6377.
(397) Ehrenson, S.; Newton, M. D. *Chem. Phys. Lett.* **1972**, *13*, 24.
(398) Botschwina, P.; Meyer, W. *Chem. Phys.* **1977**, *20*, 43.
(399) Niblaeus, K.; Roos, B. O.; Siegbahn, P. E. M. *Chem. Phys.* **1977**, *26*, 59.
(400) Siegbahn, P. E. M. *Chem. Phys.* **1977**, *25*, 197.
(401) Cársky, P.; Zahradnik, R. *Int. J. Quantum Chem.* **1979**, *16*, 243.
(402) Wigner, E. *Z. Phys. Chem.* **1932**, *B19*, 203.
(403) Boatz, J. A.; Gordon, M. S. *J. Phys. Chem.* **1989**, *93*, 5774.
(404) Tachibana, A.; Fukui, K. *Theor. Chim. Acta* **1978**, *49*, 321.
(405) Tachibana, A.; Fukui, K. *Theor. Chim. Acta* **1979**, *51*, 189.
(406) Tachibana, A.; Fukui, K. *Theor. Chim. Acta* **1979**, *51*, 275.
(407) Natanson, G. A. *Mol. Phys.* **1982**, *46*, 481.
(408) Shida, N.; Almlof, J. E.; Barbara, P. F. *Theor. Chim. Acta* **1989**, *76*, 7.
(409) Natanson, G. A.; Garrett, B. C.; Truong, T. N.; Joseph, T.; Truhlar, D. G. *J. Chem. Phys.* **1991**, *94*, 7875.
(410) Natanson, G. A. *Chem. Phys. Lett.* **1991**, *178*, 49.
(411) Natanson, G. A. *Chem. Phys. Lett.* **1992**, *190*, 209.
(412) Natanson, G. A. *Chem. Phys. Lett.* **1992**, *190*, 215.
(413) Fast, P. L.; Corchado, J. C.; Truhlar, D. G. *J. Chem. Phys.* **1998**, *109*, 6237.
(414) Jursic, B. S. *Theochem* **1995**, *358*, 139.
(415) Jursic, B. S.; Zdravkovski, Z. *Int. J. Quantum Chem.* **1995**, *56*, 115.
(416) Jursic, B. S. *Chem. Phys. Lett.* **1995**, *244*, 263.
(417) Jursic, B.; Zdravkovski, Z. *J. Chem. Soc., Perkin Trans. II* **1995**, 1223.
(418) Durant, J. L. *Chem. Phys. Lett.* **1996**, *256*, 595.
(419) Jursic, B. S. *Chem. Phys. Lett.* **1996**, *256*, 213.
(420) Jursic, B. S. *J. Chem. Phys.* **1996**, *104*, 4151.
(421) Zhao, Y.; Pu, J.; Lynch, B. J.; Truhlar, D. G. *Phys. Chem. Chem. Phys.* **2004**, *6*, 673.
(422) Zhao, Y.; Truhlar, D. G. *J. Phys. Chem. A* **2004**, *108*, 6908.
(423) Zhao, Y.; Gonzalez-Garcia, N.; Truhlar, D. G. *J. Phys. Chem. A* **2005**, *109*, 2012.
(424) Zhao, Y.; Truhlar, D. G. *J. Phys. Chem. A* **2005**, *109*, 5656.
(425) Zhao, Y.; Schultz, N. E.; Truhlar, D. G. *J. Chem. Theory Comput.* **2006**, *2*, 364.
(426) Zhao, Y.; Truhlar, D. G. *Theor. Chem. Acc.*, available in the Online First section of SpringerLink at http://dx.doi.org/10.1007/s00214-007-0310-x.
(427) Zhao, Y.; Lynch, B. J.; Truhlar, D. G. *J. Phys. Chem. A* **2004**, *108*, 2715.
(428) Zhao, Y.; Lynch, B. J.; Truhlar, D. G. *J. Phys. Chem. A* **2004**, *108*, 4786.
(429) Hancock, G. C.; Mead, C. A.; Truhlar, D. G.; Varandas, A. J. C. *J. Chem. Phys.* **1989**, *91*, 3492.
(430) Dunning, T. H., Jr. *J. Chem. Phys.* **1989**, *90*, 1007.
(431) Corchado, J. C.; Chuang, Y.-Y.; Fast, P. L.; Villà, J.; Hu, W.-P.; Liu, Y.-P.; Lynch, G. C.; Nguyen, K. A.; Jackels, C. F.; Melissas, V. S.; Lynch, B. J.; Rossi, I.; Coitiño, E. L.; Fernandez-Ramos, A.; Pu, J.; Albu, T. V.; Steckler, R.; Garrett, B. C.; Isaacson, A. D.; Truhlar, D. G. *POLYRATE 9.1*; University of Minnesota: Minneapolis, MN, 2002.
(432) Kurosaki, Y. *Nukleonika* **2002**, *47*, S81.
(433) Simpson, W. R.; Rakitizis, T. P.; Kandel, S. A.; Orr-Ewing, A. J.; Zare, R. N. *J. Chem. Phys.* **1995**, *103*, 7313.
(434) Simpson, W. R.; Rakitzis, T. P.; Kandel, S. A.; Lev-On, T.; Zare, R. N. *J. Phys. Chem.* **1996**, *100*, 7938.
(435) Harper, W. W.; Nizkorodov, S. A.; Nesbitt, D. J. *J. Chem. Phys.* **2000**, *113*, 3670.
(436) Harper, W. W.; Nizkorodov, S. A.; Nesbitt, D. J. *Chem. Phys. Lett.* **2001**, *335*, 381.
(437) Shiu, W.; Lin, J. J.; Liu, K.; Wu, M.; Parker, D. H. *J. Chem. Phys.* **2004**, *120*, 117.
(438) Shiu, W.; Lin, J. J.; Liu, K. *Phys. Rev. Lett.* **2004**, *92*, 103201.
(439) Sanson, J.; Corchado, J. C.; Rangel, C.; Espinosa-Garcia, J. *J. Phys. Chem. A* **2006**, *110*, 9568.
(440) Guo, Y.; Harding, L. B.; Wagner, A. F.; Minkoff, M.; Thompson, D. L. *J. Chem. Phys.* **2007**, *126*, 104105.
(441) Dawes, R.; Thompson, D. L.; Guo, Y.; Wagner, A. F.; Minkoff, M. *J. Chem. Phys.* **2007**, *126*, 184108.

CR078026X